5.5 RF SYSTEM

The design of the B Factory RF system is governed by the requirement that the system be as conservative and reliable as possible, despite the increased demands associated with the high luminosity. In this section, we describe the design for the RF system and indicate the basis for our technical choices.

The B Factory RF system must fulfill the following requirements:

- Provide sufficient voltage to maintain acceptable quantum lifetime and suitable bunch length
- Provide sufficient power to compensate for the losses due to synchrotron radiation and losses into higher-order modes (HOMs)
- Provide a suitable low-impedance environment for the beam

All of these requirements are common to every collider and storage ring RF system and do not in themselves drive us into uncharted territory as far as RF system design is concerned. The noteworthy difference in the case of the B Factory is associated with the very large beam current that must be supported—an order of magnitude higher than in present colliders.

The choice of frequency is driven by the need to produce short bunches and the availability of high-power RF sources. To minimize injection jitter, we have also specified that the storage ring RF systems be harmonically related to the 2856-MHz SLAC linac, which serves as the B Factory injector. We selected a frequency of 476 MHz to meet these needs. This choice provides the required 1-cm bunches with moderate voltage and is a convenient subharmonic of the linac frequency. Moreover, klystrons capable of providing in excess of 1 MW of CW power are available, or can be easily modified to work at this frequency. Because the frequency range near 500 MHz is a common choice for storage rings, it is also a good starting point for the design of the RF cavity, as discussed below.

To provide adequate lifetime, the RF system momentum acceptance $\Delta p/p$ (the "bucket height") should be of the order of $10\sigma_E/E$. For our parameters (see Table 4-1), this calls for a bucket height of 0.6% in the HER and 1% in the LER. A more stringent voltage requirement arises from the need to provide short bunches, σ_ℓ = 1 cm, to avoid luminosity losses associated with the beam-beam interaction (for example, excitation of synchrobetatron resonances, as discussed in Section 4.4). This requires a voltage of 18.5 MV for the HER and 9.5 MV for the LER at our chosen frequency of 476 MHz.

The power requirements are most severe for the HER. Here, the energy loss per turn due to the emission of synchrotron radiation is 3.58 MeV. At the nominal operating current of 1.48 A, the total power that must be provided to the beam is 5.3 MW; miscellaneous losses, such as resistive-wall heating and HOM losses, add to this value. If the number of cavities were not a concern, the power could simply be distributed over sufficiently many RF cells that it did not become a technology issue.

Unfortunately, the RF cells contribute considerable impedance to the ring and can lead to either single-bunch or coupled-bunch instabilities, as discussed in Section 4.3.

Although single-bunch instabilities are not predicted to limit the performance of the B Factory collider, HOMs of the RF cavities, driven by the intense beams, are expected to give rise to wakefields that cause potentially severe longitudinal and transverse coupled-bunch instabilities. This aspect could easily limit the performance of the B Factory and must be avoided, or at least mitigated, in the design of the RF system.

In practice, this means that the total impedance presented by the RF cavities should be kept as low as possible. To minimize the HOM impedance, we keep the number of cavities small and we adopt single-cell cavities, rather than multicell structures of the type used in PEP. (In multicell structures, the number of possible modes is multiplied by the number of cells, as compared with the modes of a single cell.) In consequence, the single cells must operate at high accelerating fields to provide the required voltage and must provide high power to the beam. Even with these precautions, the cavity HOMs must be damped substantially to reduce their shunt impedance to acceptably low values, and a number of feedback systems must be employed to combat the effects of the coupled-bunch instabilities.

The B Factory RF system could employ either room-temperature or superconducting cavities. Because about 60% of the RF power is delivered to the beam, only a small reduction of installed RF power could be realized by using superconducting technology (at the cost of increased complexity associated with the required cryogenic systems). Furthermore, the technology of providing a large input power and removing a large HOM power in a superconducting environment is not yet in hand. For these reasons, and because the expertise at SLAC and LBL is mainly in conventional room-temperature RF systems, an approach using copper cavities was chosen.

The filling pattern adopted for our collider design places the beam bunches in every other RF bucket throughout 95% of the circumference, with a 5% gap in the bunch train to avoid trapping ions in the HER beam. Thus, out of the 3492 possible RF buckets in each ring, 1658 are filled with beam. The same filling pattern for both rings minimizes asymmetries in the beam-beam collisions, but it may be desirable to add bunches in the positron beam to equalize transients induced in the two RF systems by the beam gaps.

5.5.1 RF System Choices and Requirements

The design of the RF systems is based on the following input parameters for the HER and LER:

- The high luminosity of 3×10^{33} cm^{-2} s^{-1} requires high beam currents: 1.48 A (HER) and 2.14 A (LER).
- The lattice design and beam current determine the power to be delivered to the beam: 6 MW (HER) and 3 MW (LER).
- The low vertical beta functions of 3 cm (HER) and 1.5 cm (LER) at the interaction point require a bunch length of 1 cm, which, in turn, requires a large overvoltage.

Two frequency regimes, 350 MHz and 500 MHz, were initially considered because 1-MW CW klystrons are commercially available at these frequencies. Cavity designs also exist at both frequencies, namely, PEP, LEP, and APS cavities at 350 MHz, and Daresbury, KEK, and ALS cavities at 500 MHz. Because the required overvoltage to

achieve the design bunch length is reduced at higher frequencies, the higher-frequency regime was selected.

As mentioned above, to allow for stable injection with small phase deviations, 476 MHz, a subharmonic of the SLAC linac frequency, was established as the operating frequency for the RF systems of both rings. Contacts with klystron manufacturers indicate that the existing 508-MHz klystron design can be easily modified to operate at 476 MHz.

The cavity design was strongly influenced by the requirement to load HOMs to a very low shunt impedance for beam stability reasons, while simultaneously maintaining a high shunt impedance for the fundamental mode. The scheme for loading the HOMs is a further development of that employed at Daresbury [Corlett, 1989, and Corlett and Hill, 1989] and the ALS [Jacob et al., 1990], and analyzed by Conciauro and Arcioni [1990]. The technique consists of suitably positioning three waveguides on the wall of the cavity, with the waveguides dimensioned to be below cutoff for the fundamental mode while transmitting all unwanted HOMs into dissipative loads. This method of HOM impedance reduction does not restrict the cavity shape in other respects, leaving the designer free to maximize the shunt impedance of the fundamental mode (using a reentrant cavity shape). Thus, a cavity shape similar to the ALS cavity can be used, as shown in Fig. 5-100. The calculated shunt impedance of this ALS-type cavity is 5.3 MΩ, but, considering all the ports and wall-heating effects, a lower value, say, 3.5 MΩ, is a more reasonably achievable fundamental-mode shunt impedance in an actual cavity.

The chosen RF system configuration requires each cavity to handle a maximum wall loss of about 150 kW at an accelerating gradient of 4.5 MV/m. It also requires the input

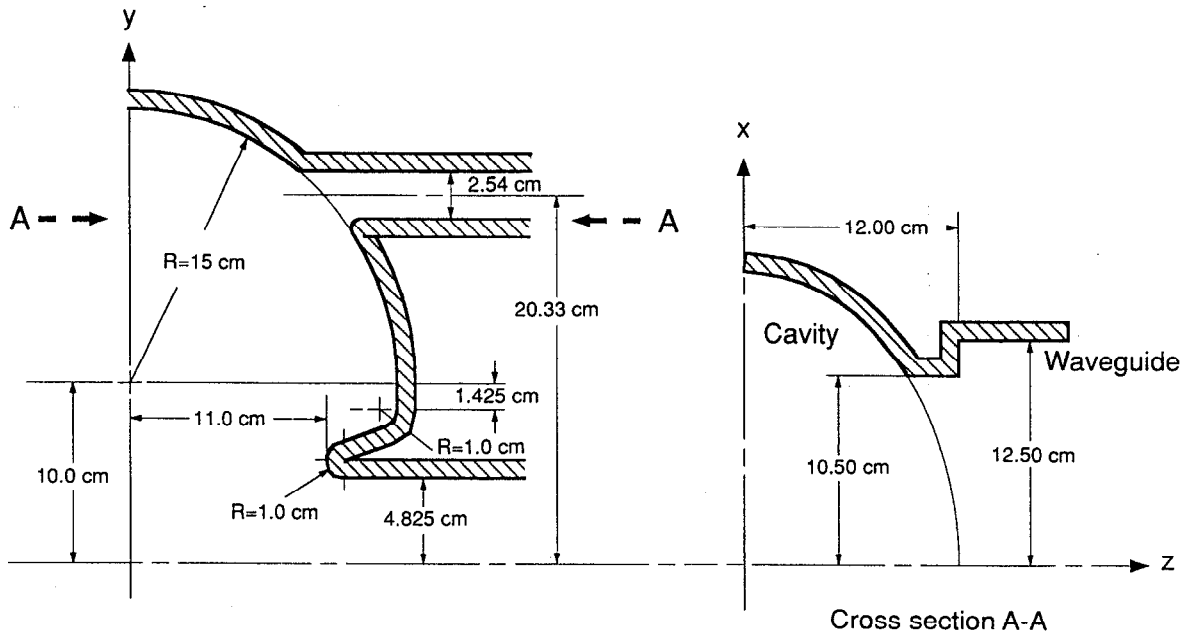

Fig. 5-100. Schematic of a quadrant of the B Factory RF cavity.

window and coupling network for each cavity to carry a power load of almost 500 kW. Both requirements are challenging and will be discussed further in the context of the cavity description. The klystron output power is assumed to be 90% of saturated power to accommodate a capability for overdrive needed by some of the feedback circuits.

Based on the above considerations, the B Factory RF system can meet all requirements with 10 klystron stations, driving 20 cavities, in the HER, and 5 klystron stations, driving 10 cavities, in the LER. The parameters for the RF systems for both rings are summarized in Table 5-29.

5.5.2 Cavity Design

The large synchrotron radiation losses mean that the RF cavities and conventional circuit components, such as windows and couplers, must deliver very high power throughput to the beam. In addition, the large circulating currents make it imperative to keep the HOM impedance as low as possible to avoid uncontrollable coupled-bunch instabilities. Thus, the number of cavities must be a compromise between their power-handling capability and the total beam impedance. The power-handling capability of existing (or reasonably extrapolated) window and coupler technology, and the problem of heat dissipation in the cavity walls and apertures, ultimately limit the power into each cell and thus determine the minimum number of cells that can be used reliably.

5.5.2.1 Choice of Cavity Shape. Preliminary optimization of the cavity shape was done using the URMEL-T code (triangle mesh version). Initially, the mode patterns of open, or "bell-shaped" (Fig. 5-101a), and reentrant (Fig. 5-101b) cavities having the same beam pipe radius and fundamental-mode frequencies were compared. The results clearly demonstrate that, for conventional copper construction, there is no advantage to the open shape as far as the HOM impedances are concerned—in fact quite the opposite. (For superconducting cavities, where the fundamental-mode shunt impedance is very high in any case, there are other advantages to the smooth shape—for example, to reduce the problems of field emission and multipactoring.) With this in mind, we adopted a reentrant cavity design with nose cones, patterned after those used at Daresbury, the Photon Factory, and the ALS.

5.5.2.2 Cavity Parameters. URMEL calculates the transit-time-corrected shunt impedance R_s (= $V^2/2P$) for the basic reentrant geometry to be about 5.3 MΩ, with an unloaded Q of 45,000 and R_s/Q of 116 Ω. In a real cavity, this impedance is degraded by the addition of ports and damping waveguides and by the effect of increased temperature on the conductivity of the copper. Using MAFIA and ARGUS to compare the fundamental-mode properties with and without damping waveguides suggests a loss of about 10–12% in R_s and Q due to these structures, while R_s/Q stays about constant. Experience with other designs suggests a further 10% will be lost by the addition of the tuner, drive, and other ports.

The degradation due to thermal effects is determined by the effective wall temperature for the maximum power of 150 kW dissipated in the cavity. Extrapolation from existing designs (see Table 5-30), and studies using MAFIA and ARGUS outputs in a thermal model with the ANSYS code, suggest the average temperature rise may be as

Table 5-29. RF system parameters for the B Factory high- and low-energy rings.

Parameter	HER	LER
RF frequency, f_{RF} [MHz]	476	
Harmonic number, h	3492	
RF voltage, V [MV]	18.5	9.5
Beam current, I [A]	1.48	2.14
Energy loss/turn [MeV]	3.58	1.24
Synchrotron radiation power, P_{SR} [MW]	5.30	2.65
HOM power (est.) [MW]	0.53	0.93
Cavity wall loss, total [MW]	2.44	1.3
Klystron power, total [MW]	10.00	5.0
Number of klystrons	10	5
Klystron power, P [MW]	1.0	
Number of cavities	20	10
Shunt impedance/cavity,[a] R_s [MΩ]	3.5	
Gap voltage/cavity [MV]	0.93	0.94
Accelerating gradient [MV/m]	4.20	4.3
Wall loss/cavity [kW]	122	130
Coupling factor without beam, β	3.7	3.8
Unloaded Q of cavity	30000	
Synchrotron frequency [kHz]	7.1	7.0
Natural bunch length, σ [cm]	1.0	1.0

[a] $R_s = V^2/2P$

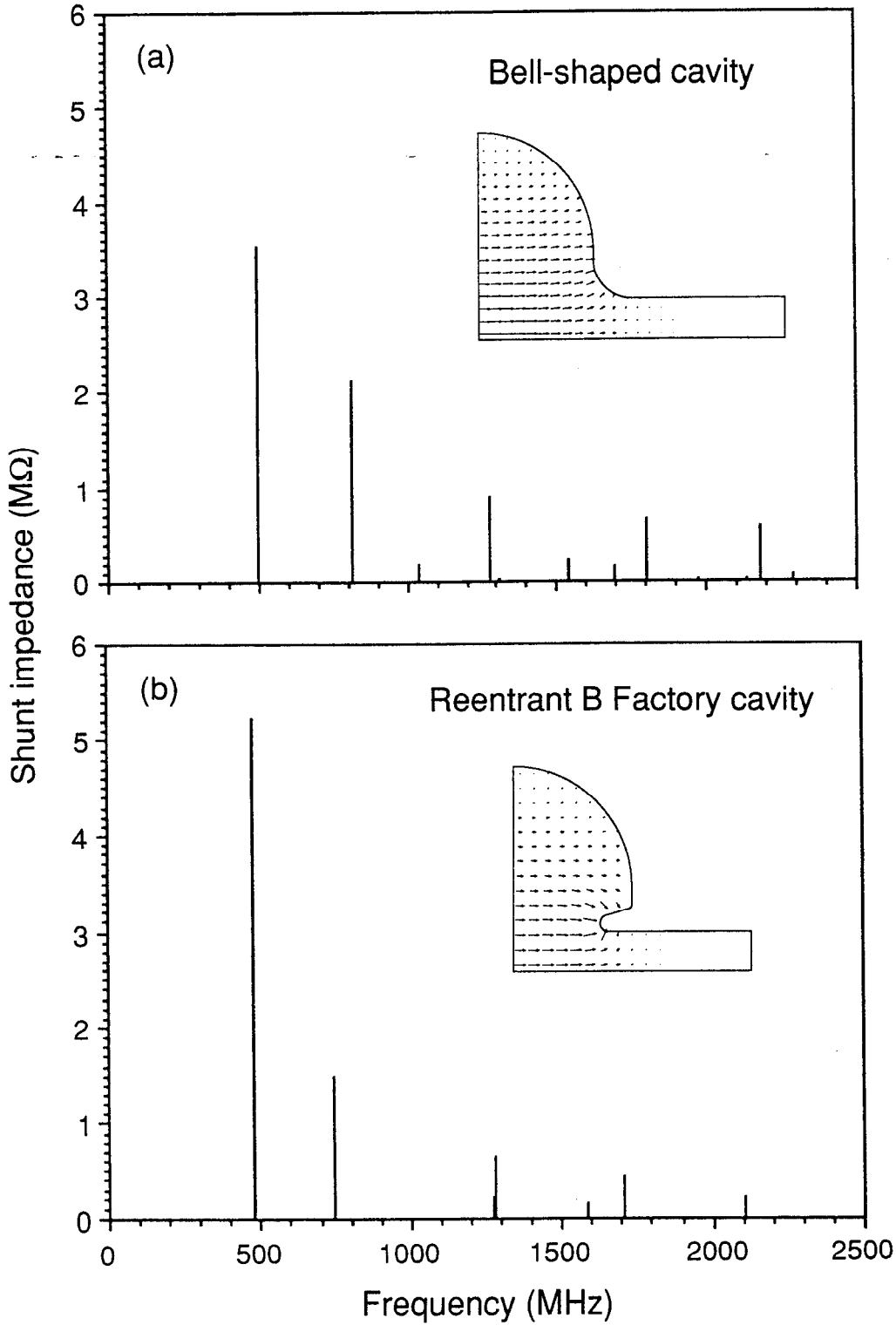

Fig. 5-101. Mode pattern calculated for (a) an open, or "bell-shaped," cavity and (b) a reentrant cavity shape

Table 5-30. Temperature comparison of existing and proposed cavities.

System	Frequency (MHz)	Power (kW/cell)	T_{inlet} (°C)	$\Delta T(H_20)$ (°C)	ΔT(Cu) (°C)	ΔT(total) (°C)	R_s loss (%)
PETRA cavity[a]	500	24	45	10	18	53	23.3
PEP cavity (Al)	350	50	35	10	15	40	23
LEP cavity[b]	350	25	20	9	12	21	4.2
ALS cavity[c]	500	70	40	3	18	41	~9
B Factory cavity	476	150	35	10	31	56	14

[a]Gaede et al., 1980
[b]Henke and Wilson, 1981
[c]Taylor, 1990

much as 56°C. This would give rise to an additional loss of about 14% in R_s and Q. Lowering the input water temperature by the use of chillers could reduce this, but may not be cost-effective. The result of these cumulative losses is to reduce the practical shunt impedance to about 3.5 MΩ, with a Q of about 30,000.

The coupling to the waveguide is such that a good match can be obtained at the nominal operating currents of 1.48 A (HER) and 2.14 A (LER). This requires a coupling factor β of about 3.7 and results in a loaded $Q_L = Q_0/(1 + \beta)$ of approximately 7000. Both loop- and aperture-type couplers were considered. The loop coupler has the advantage that the coupling may be adjusted mechanically by rotating it, but it is a more complicated structure that must be water-cooled because of the very high surface-current density. An aperture coupler, on the other hand, has the advantages of simplicity and lower surface-current density but has a fixed coupling factor. The usual method of achieving a match with an aperture coupler is to use a tuning stub in the waveguide, usually a sliding short-circuit device. Unfortunately, this may cause practical problems. Therefore, a loop-type coupler was ultimately chosen for the B Factory because of the possible variation in beam currents that must be handled.

Either coupling device requires the use of a vacuum window at some point. At lower power levels, previous designs have incorporated ceramic windows in the construction of the coupler (sometimes with disastrous results), either in the coaxial part of the loop or as a disk filling the coupling aperture. Neither of these designs is suitable for very high power applications, where it is necessary to locate the window well away from the harmful heating of the cavity standing-wave fields. These may penetrate into the waveguide near the coupling point, so it is prudent to locate the window a safe distance away in the waveguide. Such a window then need only survive the heating due to the traveling wave that carries power to the cavity. Designs of this type are currently being

developed by commercial sources. Remote location of the vacuum window requires that the waveguide adjacent to the cavity be part of the cavity vacuum system, which may lengthen the conditioning time and increase pumping requirements. The ceramic window must still be protected against multipactoring, which can be done by using a low-secondary-emission surface coating.

5.5.2.3 HOM Damping. The high beam currents, and therefore the potential for very high coupled-bunch instability growth rates, require that special attention be paid to the HOM impedances of the cavities. To reduce the growth rates to a level where they can be controlled by a technically (and economically) feasible feedback system required careful attention to the issue of HOM damping at an early point in the cavity design. Externally applied damping techniques using tuned couplers have not proved effective enough in existing applications to meet the requirements of the B Factory. Damping waveguides were therefore included in the initial design of the cavity. These waveguides are designed to propagate at the HOM frequencies and are positioned to offer the maximum coupling to the most troublesome HOMs, while being below cutoff and offering minimal perturbation at the fundamental-mode frequency.

The effect of the size, shape, and location of these coupling apertures has been studied experimentally on a simple pillbox structure and computationally using the three-dimensional code MAFIA on both the simple pillbox shape and the B Factory cavity shape. MAFIA results for the B Factory cavity have also been verified by comparison with the ARGUS code where possible. The waveguide apertures will be fabricated by electroforming (along with the tuner, drive, and other coupling ports) when the cavity is constructed. Cooling channels will be added to the outside of the cavity, with particular attention paid to the heat concentration around the orifices of these various structures.

Calculation of the damping effect of these waveguides was carried out with MAFIA, making use of the Kroll-Yu method [Kroll and Yu, 1990]. This method involves calculating the frequencies of the cavity modes modified by waveguides having short-circuits placed at various lengths. This technique is necessary because MAFIA is not capable of solving the complex eigenvalue problem that arises when significant losses are introduced into the model. The validity of this method was demonstrated experimentally by using a pillbox-shaped cavity, to which three waveguides were attached. The results for this pillbox are given in Table 5-31, which shows strong damping of all troublesome higher modes to Q values less than 60. These results agree very well with calculations, especially considering that our terminating loads on the waveguides were less than ideal. Calculations for a similar damping scheme applied to the proposed B Factory cavity shape (see Table 5-32) also produced acceptable reduction of the HOM Q values (for example, the Q of the TM011 mode was reduced to 30), with tolerable losses of fundamental-mode impedance and Q (about 12%). If verified by experiment, this HOM damping will result in instability growth rates well within the capability of a reasonable feedback system (see Section 5.6).

The first calculated example of waveguide damping applied to the B Factory cavity shape uses shallow rectangular waveguides with a cutoff frequency of about 600 MHz; this choice allows all of the HOMs to propagate. The first and strongest longitudinal HOM has an unloaded frequency of around 750 MHz, and the cutoff frequency of the damping waveguide must be sufficiently far below this to allow for the frequency drop

Table 5-31. Damping of an aluminum pillbox cavity by three 1 in. ×6 in. waveguides (f_c = 786.8 MHz).

	No waveguides (MAFIA)			Three waveguides				
				MAFIA/Kroll			Experiment	
Mode	Frequency (MHz)	Q	RT^2 (MΩ)	Frequency (MHz)	Q	dQ (%)	Frequency (MHz)	Q
TM010 monopole	617.2	36150	1.66	611	33400	8	609.5	649[b]
TM011 monopole	868.4	29500	0.88	841	17	(large)	836.2	31
TE111 dipole	711.6	42100	1.29 (MΩ/m)[a]	708	39300	7	704.2	676[b]
TM110 dipole	909.6	38400	1.34 (MΩ/m)[a]	906	55	(large)	898.8	37
TM111 dipole	1027.2	28000	6.97 (MΩ/m)[a]	1020	28–35	(large)	(not visible)	
TE211 quadrupole	959.9	38400	–	957	54–58	(large)	(not visible)	
TM211[c] quad	1366.2 (URMEL)	36800	–	–	–	–	1365.8	152

[a] R/kr^2, where r is the beam pipe radius, 0.04825 m [URMEL gives $(R/Q)/(kr_0)^{2m}$].
[b] Waveguide load sees evanescent fields of trapped mode.
[c] Identification uncertain.

caused by external loading. The choice of 600 MHz is very conservative, because it also allows the very weak transverse TE mode at 685 MHz to propagate. The required width of this waveguide, 25 cm, is too large to cut directly into the cavity, so a smaller aperture (21 cm) was used, forming an iris into the waveguide (see Fig. 5-100). This solution may lead to practical problems of cooling the surfaces around the iris, where the current density is high. This can be reduced, to some extent, by smoothly blending the edges of the waveguide and iris to remove sharp corners or by using a slightly ridged waveguide design, which can be narrower for the same cutoff frequency, thus eliminating the need for an iris. First indications regarding the feasibility of the second approach are encouraging: The smooth, ridged waveguide solution has a lower fundamental-mode perturbation (about 7%) than does the square guide with the iris, while still offering good coupling to the HOMs.

Table 5-32. Damping of the copper B Factory cavity by three 1 in. × 10 in. waveguides; f_c = 599.6 MHz.

Mode	No waveguides (MAFIA)				Three waveguides (MAFIA/Kroll)					
	Frequency (MHz)	Q	RT^2 (MΩ)[a]	RT^2/Q (Ω)	Frequency (MHz)	Q	dQ (%)	RT^2 (MΩ)[a]	dR (%)	RT^2/Q (Ω)
TM010 monopole	479.9	40003	4.71	117.73	474.6	35248	–12	4.12	–12	117.00
TM011 monopole	750.0	33270	1.35	40.67	745	30	(large)	–	–	–
TE111 dipole	684.5	54844	0.191 (MΩ/m)[b]	–	680	~65	(large)	–	–	–
TM110 dipole	794.3	57762	18.3 (MΩ/m)[b]	–	~795	~73	(large)	–	–	–

[a]MAFIA shunt impedance (transit time corrected)
[b]R/kr^2, where r is the beam pipe radius, 0.04825 m

Evanescent penetration of the cavity fundamental mode into the damping waveguides and other apertures gives rise to the possibility of multipactoring. Increasing the number of ports may therefore require a longer conditioning time before the cavity can take full power, and, in some places, the use of low-secondary-emission coatings may be appropriate. A full-power test of a model cavity will be conducted to prove the effectiveness of the damping and cooling schemes under realistic conditions.

5.5.2.4 Mechanical Design. The cavity geometry, including the size and shape of the HOM loading waveguide holes, will be optimized during the final design phase for the B Factory, but proof-of-concept thermal calculations have been carried out with parameters that are considered realistic, and in some cases overly pessimistic. The results clearly indicate that the general design is workable and that, with detailed engineering, a practical cavity will evolve from our present design.

The cooling scheme chosen for the RF cavity is patterned after the ALS cavity; this basically involves two concentric shells, with the space between them serving as the cooling passage. Fins protrude from the surfaces of the shells into the water and thus channel the flow. Based on a bulk temperature rise of 10°C, with 150 kW of power dissipated in the walls, the cooling passage must be able to transport 57 gpm (= 3.6 kg/s) of water without an excessive pressure drop. Because of the relatively large size of the cavity and cooling channels, this is not a difficult criterion. We have calculated the temperature rise and thermal stress due to a thermal load distribution that arises from the tangential magnetic field at the surface of the cavity. The surface temperature, assuming a bulk water temperature of 45°C, is shown in Fig 5-102. Also calculated were the thermal stresses and the stresses induced by atmospheric pressure loading: The maximum combined stress was 3850 psi. The stress analysis showed that the cavity was mechanically strong enough to withstand the combined atmospheric and water pressure load for reasonable pressure drops through the cavity. Note that the water temperature of 45°C is the design value for the outlet water temperature. Figure 5-102 shows that even with this conservative choice of water temperature and with little effort made to mitigate the heating of the nose cone, the present cavity design is a good starting point for further optimization.

Because of the ports for the HOM loading waveguides, there will be concentrations of wall currents, and hence increased thermal loads, around the periphery of the ports. We have conservatively calculated the thermal loads in these locations. (We believe the results to be pessimistic, as they come out of three-dimensional electromagnetic codes that utilize rectangular blocks of material to model the cavity. Such codes therefore model extremely sharp corners and breaks in the wall currents.) Calculations are under way to analyze the stresses and temperature profiles in this region. The present model treats the intersection of the rectangular waveguide with a plane representing the cavity wall. This simple model is a reasonable approximation near the corner because the radius of curvature is large compared with the wall thickness.

The resultant temperature distribution, with an assumed bulk water temperature of 40°C, is shown in Fig. 5-103. The two hot spots correspond to the two local maxima in thermal loading. The hottest spot, at 129°C, corresponds to a thermal load of 50 W/cm^2. The reasons for this are twofold: First, the acute angle formed by the waveguide and cavity wall creates a long thermal path for the heat to travel, and second, the model is

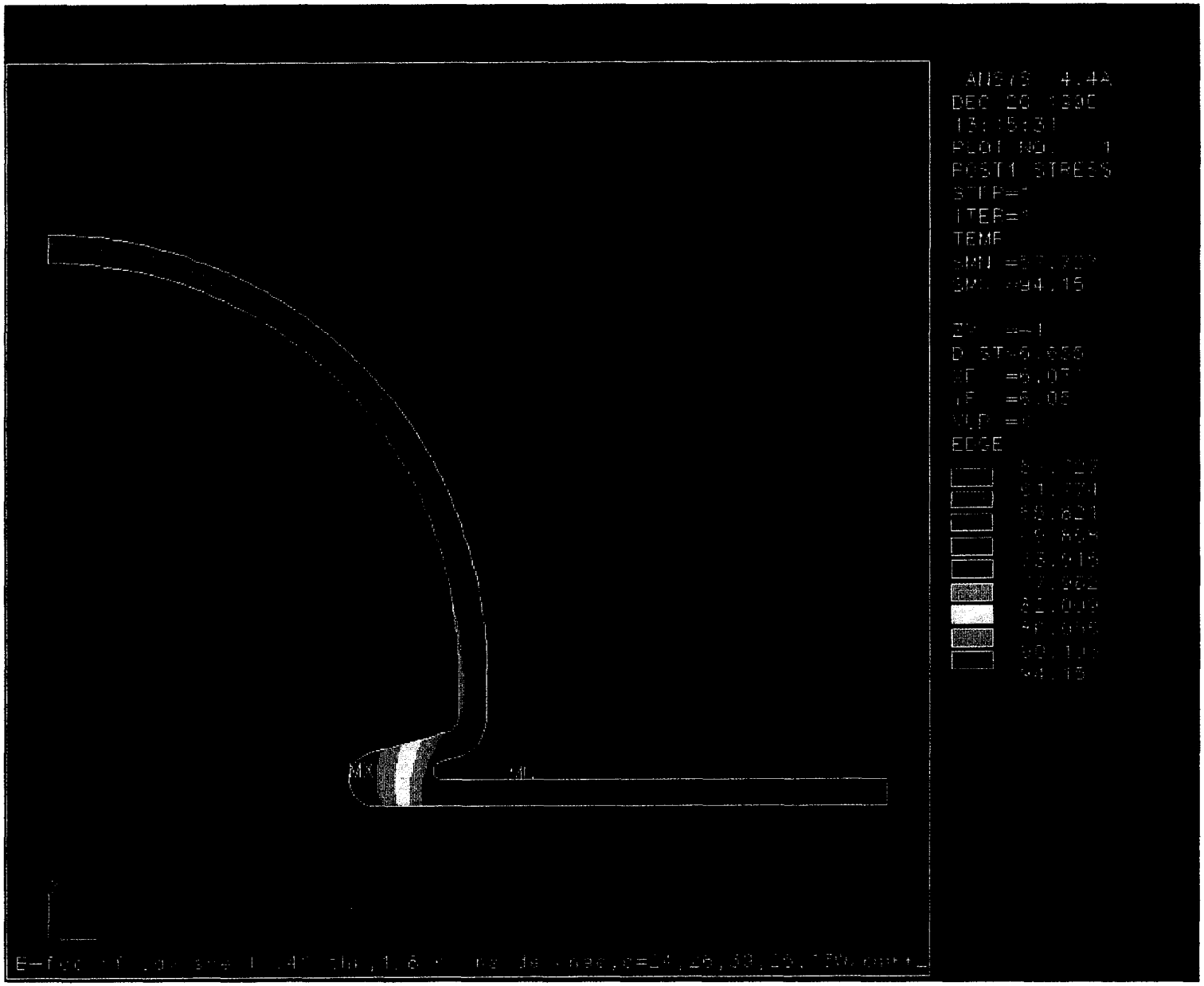

Fig. 5-102. Computed temperature profile for the B Factory RF cavity, due to the thermal load from the tangential magnetic field at 150-kW wall dissipation.

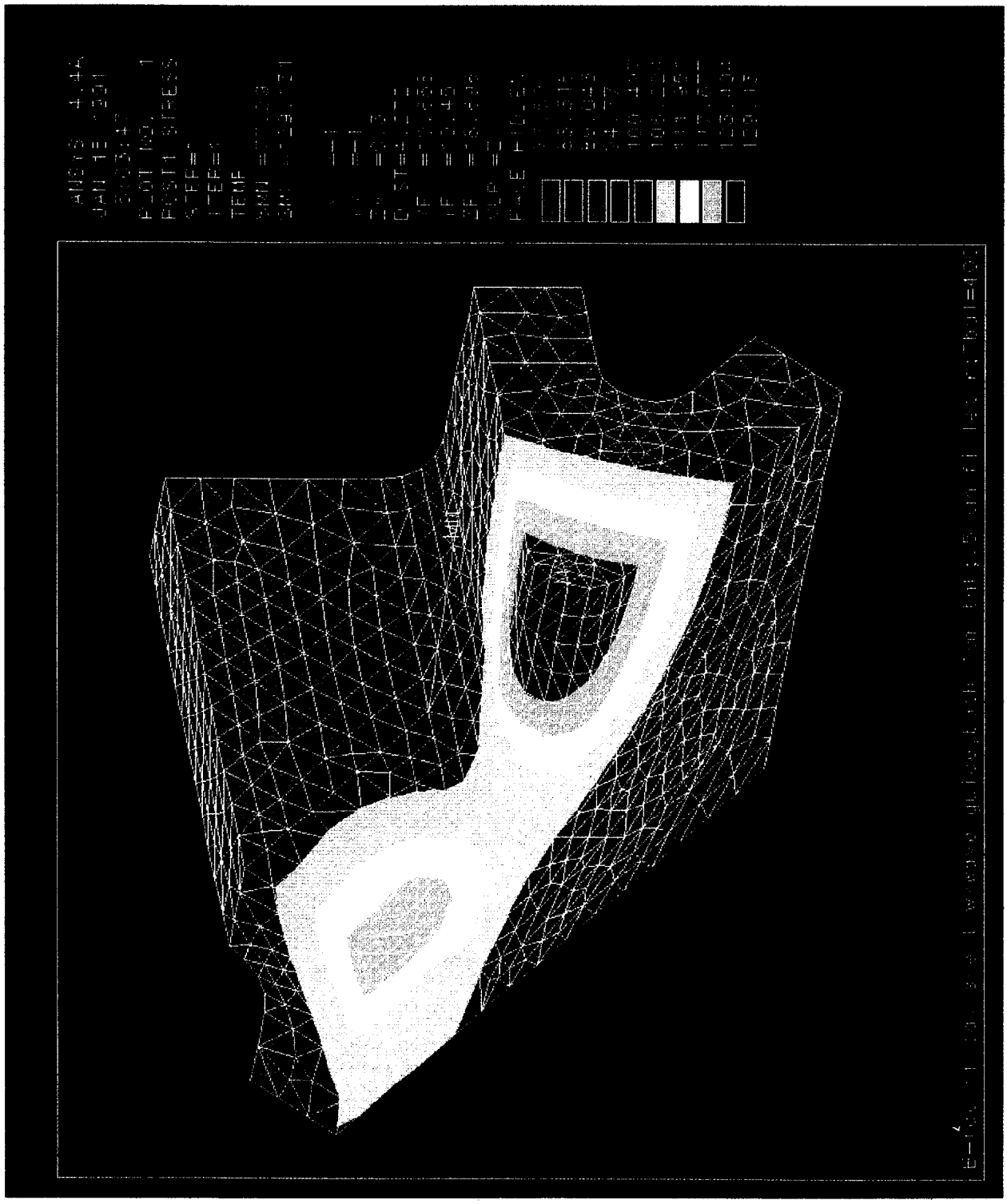

Fig. 5-103. Computed temperature profile in the region of the HOM-loading waveguide ports at 150-kW wall dissipation.

terminated at this point and no heat is allowed to flow across a model boundary. Adjusting the angle of the waveguide-cavity intersection to be 90° (whereby the waveguide extends from the cavity radially) will eliminate the first of these causes. The second can be addressed simply by extending the model. The hotspot located on the vertical wall corresponds to the maximum heat deposition of 80 W/cm^2. Available methods of reducing the temperature in this area include cooling channels, bored cooling passages in the copper, and a reduction in the wall thickness (if it is mechanically feasible). It would also be possible, though not desirable, to add a separate cooling circuit in this region, thereby reducing the bulk water temperature used to cool the region by 5–10°C. Here again, the simulations have revealed the scope of the problem and have shown that the present cavity design is a good starting point for further optimization. In summary, we expect that, following a detailed analysis of the final cavity design, the wall heating problem will yield to present-day cooling technology.

5.5.2.5 Cavity Tuning. The tuning of the cavity will be accomplished with a PEP-style tuner, that is, a 10-cm-diameter plunger with about 10 cm of travel (see Fig. 5-104). Estimates predict a 1.1-MHz tuning range, which is sufficient to cover a temperature-related detuning of 400 kHz per 50°C, as well as a 130-kHz detuning to compensate for beam loading, or a 240-kHz detuning to "park" an idling cavity. This type of tuner uses carbon brushes to prevent HOM power from entering the space within the bellows. The handling of the higher power, compared with the PEP case, will be further evaluated.

5.5.2.6 Input Coupler. An input coupling network using loop coupling from a 6-in. coaxial line is planned. It may be necessary to go to a 9-in. coaxial line if field calculations or multipactoring evaluations indicate an advantage for the larger size. The coupling factor can be varied between 3 and 8 by rotating the loop (a coupling factor of 8.3 would be needed in the high-current, 3-A upgrade case). The coupling network will

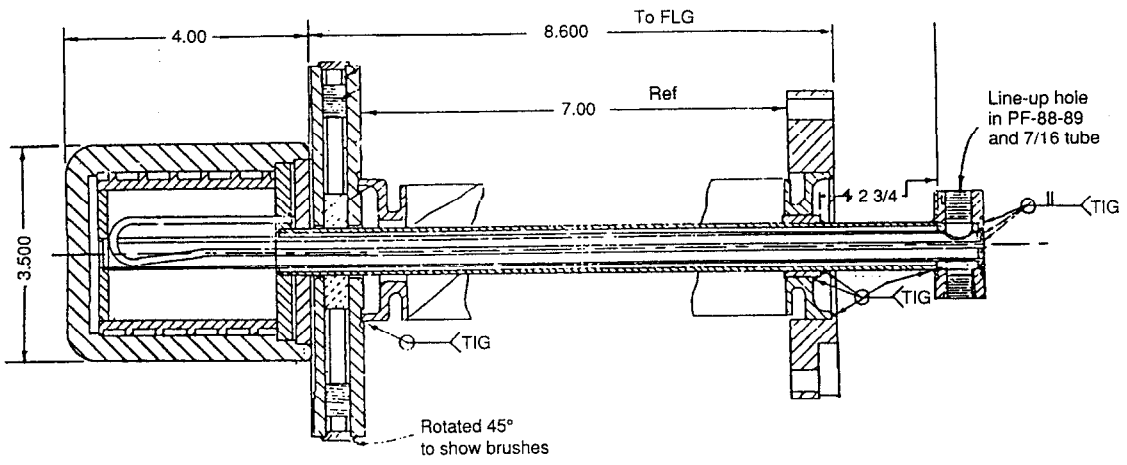

Fig. 5-104. Cross-sectional view of an all-copper PEP cavity tuner.

have to transmit up to 500 kW of RF power. The design provides for vacuum pumping ports at the input coupling network.

5.5.2.7 Input Window. The window must also transmit up to 500 kW of CW RF power. Four configurations are possible (see Fig. 5-105):

- *Coaxial window*: These are used in European and Japanese 1- to 1.2-MW klystrons as output windows, with air cooling on one side. The characteristic impedance is 50 Ω, thus presenting lower voltage across the ceramic, compared with the 300-Ω characteristic impedance of the waveguide. However, the coaxial window is mechanically more difficult to realize than the other types of windows.
- *Ceramic cylinder at the coaxial-line-to-waveguide transition.* This design has been used extensively at SLAC (500 kW per klystron, 300 kW per 5-cell cavity), at LEP (125 kW per cavity), and at CESR (400 kW per cavity under continuous operation, window failure observed at 970 kW, trickle cooling with trichloroethane and trifluoroethane).
- *Ceramic disk in waveguide.* This approach is commercially available and specified at 500 kW per cavity CW, but not yet tested at this power level. This design, using alumina or beryllia disks, is very promising and will be studied carefully for the B Factory.
- *Ceramic cylinder in the waveguide with aperture coupling.* This method is used for the ALS cavity, designed to operate at 70 kW. No operating and power handling experience has been gained yet. Because the ceramic is fairly close to the cavity, it may cause difficulties in the presence of beam-induced fields.

We expect to design a ceramic cylinder or ceramic disk window and also to purchase a commercially available window with a ceramic disk in a waveguide. We will make calculations to determine the field pattern and field stress areas to help in the choice of a promising window design. After a window design is selected, tests are planned in which two such windows will be mounted back-to-back, with adjustable vacuum between them, then run at 500 kW into a load. Extensive monitoring will be provided for these tests in the form of infrared detectors, arc detectors, voltage standing-wave detectors, etc.

5.5.3 RF Station

Each RF station will consist of one klystron powering two cavities; a block diagram is shown in Fig. 5-106. The power is distributed through a WR1800 waveguide and a Magic Tee. Reflected power from the cavities is combined in the Magic Tee and directed back toward the circulator; only imbalance power shows up at the load at the fourth port of the Magic Tee. A 300-kW load at this port is sufficient.

A circulator is required to absorb either the reflected power or the considerable beam-induced power; its presence serves to guarantee stable klystron operation under such conditions. Circulators with 1 MW of CW power capability, both forward and reflected, have been produced in connection with recently developed 1-MW klystrons, and they are

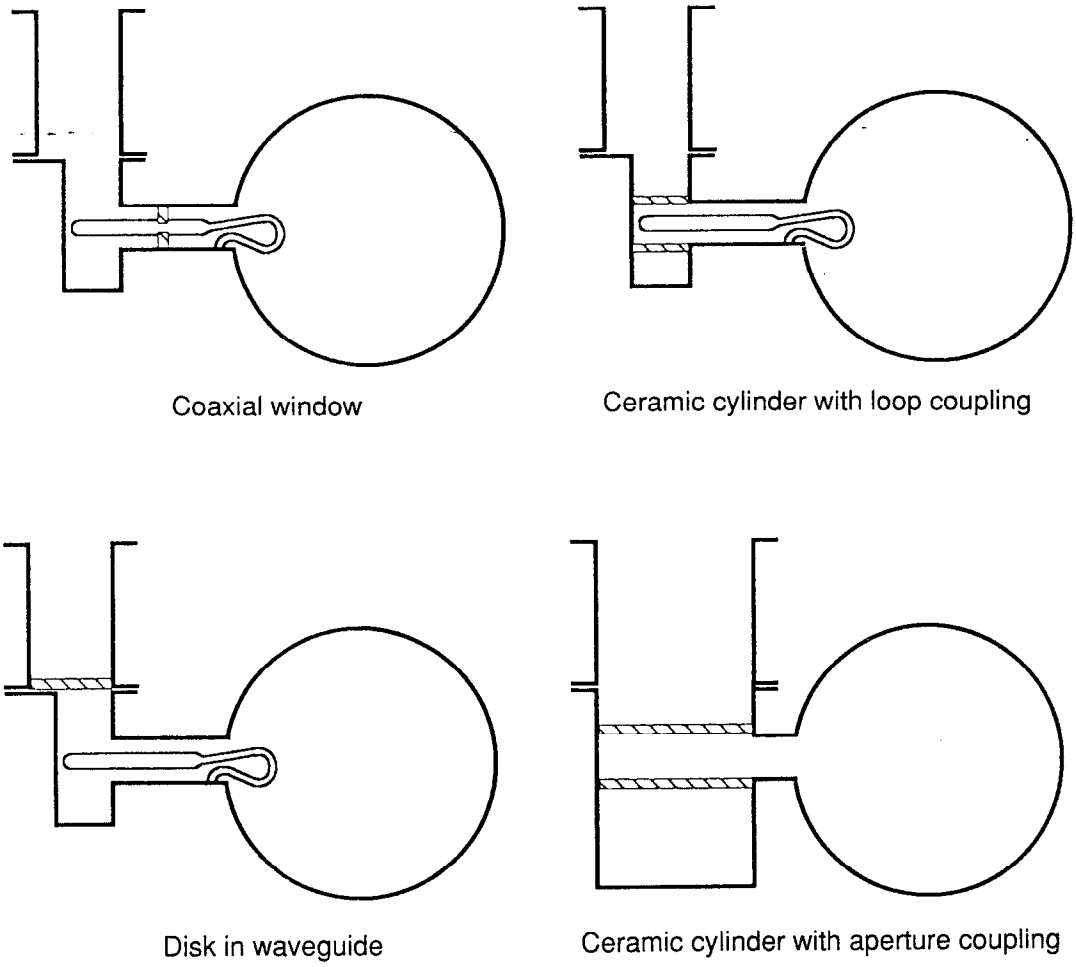

Fig. 5-105. Schematics of four window and coupling network configurations.

commercially available. Reflected power is of the order of 125 kW when there is no beam in the cavities, but beam-induced power can be as high as 1 MW in the case of the klystron tripping off at full beam, and this must be absorbed by the circulator load. The 1-MW condition need only be tolerated for the time it takes to detune the cavities, which is about 1–2 seconds. A 1-MW load at the circulator is planned. Loads with this power-handling capability are now used on klystron test stands.

The klystron is of the modulating-anode type, with an output of greater than 1 MW. A 476-MHz version can be developed in a straightforward manner by scaling from klystrons that are commercially available from several different manufacturers.

A high-voltage power supply provides 80 kV and 20 A, unregulated, with some filtering to a 1% ripple at 720 Hz. This high-voltage ripple causes a 15° phase ripple in the klystron, but this can be regulated out in the low-level RF system. To allow soft turn-

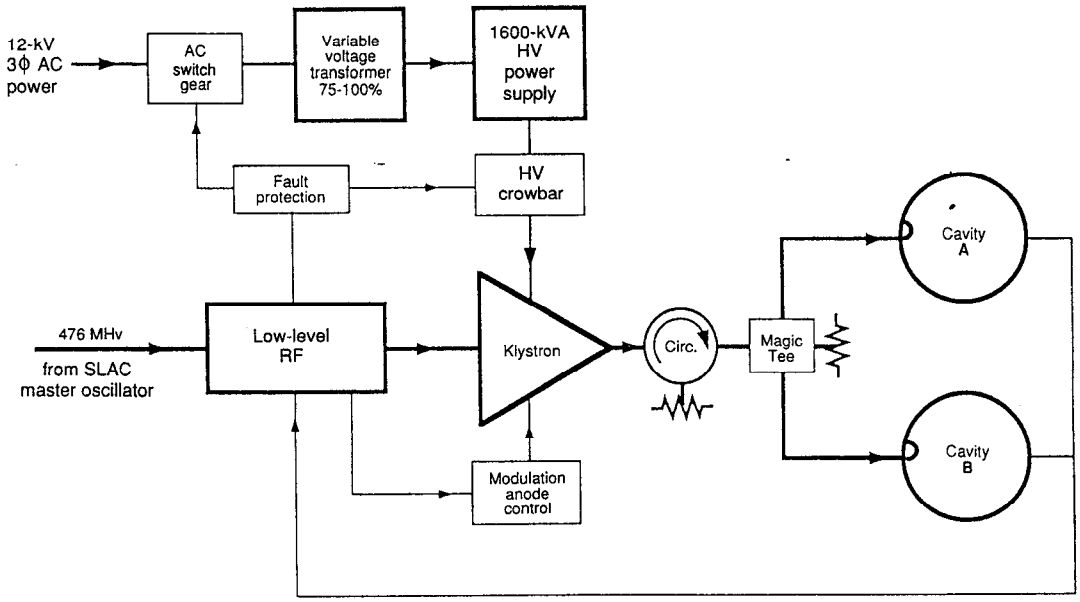

Fig. 5-106. Block diagram of a single B Factory RF station.

on of the klystron, a variable input transformer, 75–100%, is used. Standard fault-protection circuitry, with a crowbar and RF drive removal, is planned to protect the klystron.

5.5.4 Low-Level Controls

The low-level RF system consists of six types of feedback loops, along with the usual controls, interlocks, and protection systems. The various low-level RF system feedback loops are described functionally below and depicted schematically in Fig. 5-107. During the detailed design phase, the stability of the whole system will be calculated and simulated.

Tuning Loop. Two loops of this type, one per cavity, keep the cavities tuned by compensating for either detuning by the beam or temperature effects. Each loop measures phase across its cavity and moves the corresponding tuner. Bandwidth is limited by the stepping motor response to 1 Hz.

RF Feedback Loop. This feedback loop is required to reduce the cavity impedance for the first few coupled-bunch modes, which will interact with the cavity strongly owing to the detuning of the cavity away from 476 MHz. This loop also aids in regulating the cavity reaction to the 5% gap in the beam. Two types of feedback loops are under study. The first is a voltage-follower approach in which the cavity voltage is sampled, shifted to the proper phase, summed with the reference drive signal, and then fed to the klystron

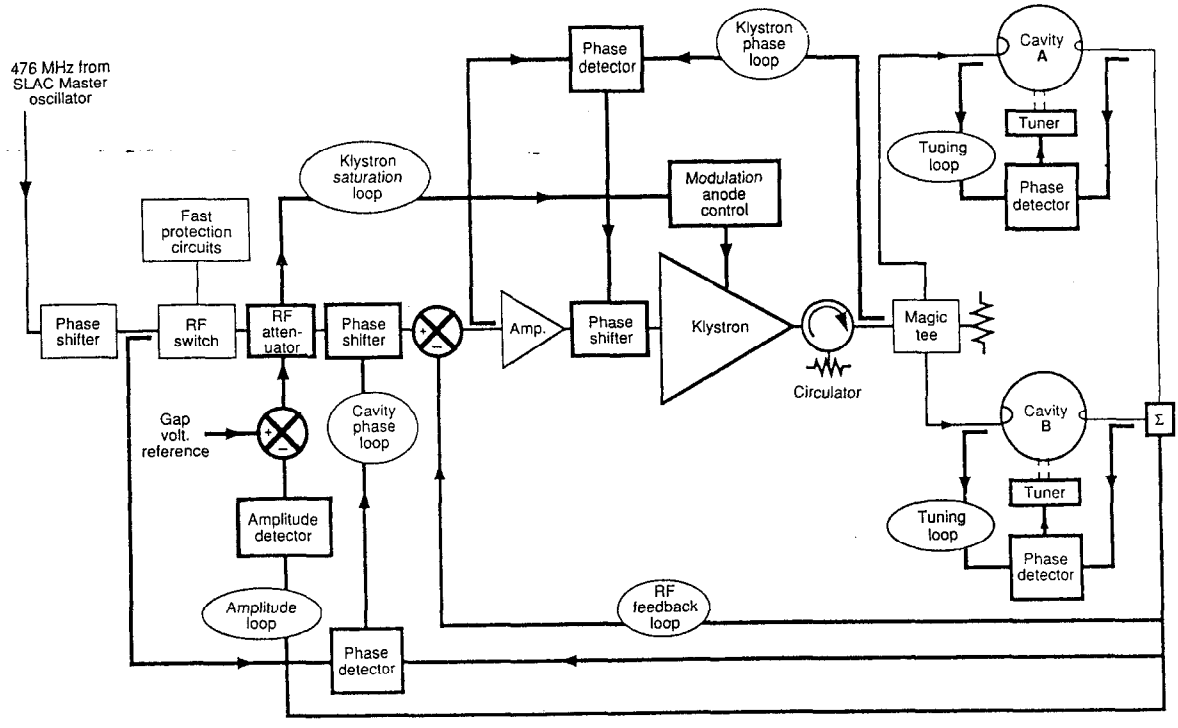

Fig. 5-107. Block diagram of the low-level RF feedback loops.

with the proper amount of gain. The bandwidth of this type of feedback is limited by the total amount of loop delay. Open-loop simulations indicate that a unity-gain bandwidth of 1.1 MHz can be achieved for a system delay of 300 ns. If the delay is 500 ns, the bandwidth is reduced to 700 kHz. A second approach involves sampling the cavity field, picking out only the harmonics of the revolution frequency with a comb filter, delaying the signal to a total delay of one revolution period (7.3μs) before summing with the reference signal and driving the klystron with the correct amount of loop gain. While this RF feedback loop reduces the impedance that drives coupled-bunch modes, additional feedback of bunch phase will be needed to stabilize the beam motion. These phase signals will be supplied by the longitudinal feedback phase detection and applied to the klystron input. Each of these two feedback schemes will be analyzed in detail to establish the one with the best performance. Studies will include merging the control loops into the storage ring simulation code now used for development of the longitudinal feedback system. Actual performance tests can also be done on the existing PEP RF stations.

Klystron Phase Loop. This is implemented to reduce the phase ripple of 15° associated with the 1%, 720-Hz ripple on the klystron high-voltage power supply. Bandwidth of this loop can be as much as 10 kHz.

Cavity Phase Loop. This loop keeps the phase of the vector sum of the fields in two cavities constant, compared with a reference signal (shifted by a station phase shifter) from the SLAC master oscillator. This will be a relatively slow loop, with a bandwidth of about 1 kHz limited by the synchrotron frequency of the beam.

Cavity Amplitude Loop. In a similar fashion to the phase loop, the amplitude loop keeps the gap voltage constant by measuring the magnitude of the cavity field and comparing it to a reference voltage. The loop then adjusts a variable attenuator in the RF reference to the RF feedback loop to keep the gap voltage constant. Bandwidth of this loop will also be of the order of 1 kHz.

Klystron Saturation Loop. To keep the klystron operating efficiently, this loop adjusts the modulation anode for operation at about 90% of saturation. (The klystron will need to be operated at about 90% of saturation to ensure reserve power for RF feedback.) The loop response time should be slow, of the order of seconds. The klystrons will be specified to provide the required power under these operating conditions.

If an RF station trips off, the circulating beam will induce a field in the cavities comparable to the normal operating field. This will not only produce similar wall losses in the cavities, it will also generate 1 MW of power traveling towards the circulator to be absorbed by its load. This will be a temporary condition, because the low-level RF system will move the tuners to a predetermined "park" position corresponding to tuning the cavities about 240 kHz below the nominal frequency of 476 MHz. This tuner position will reduce beam-induced power, while still operating the cavity at a point on the resonance curve that produces Robinson damping. After detuning, the power to be absorbed by the circulator load will be reduced to about 280 kW in the LER and 110 kW in the HER. A monitor will measure the beam-induced power and dump the beam should a potentially dangerous power level be reached. This could happen if, with klystron drive removed, a cavity were accidentally tuned to resonate at 476 MHz.

5.5.5 General Layout

There are three RF buildings available at the PEP site, located in regions 4, 8, and 12 (Fig. 5-108). Each building can accommodate up to six RF stations, for a total of 18. For the initial operation of the B Factory, fifteen stations will be installed, six each in regions 4 and 8, and three in region 12. The RF building layout shown in Fig. 5-109 indicates how the 476-MHz klystrons could be arranged. A profile view of an RF building and a section of the tunnel is shown in Fig. 5-110.

5.5.6 Expandability

Ultimately, we envision one backup station for each B Factory ring — to ensure a full complement of stations for the required luminosity, even if one RF station is down. As discussed in Section 5.5.4, the cavities of an inoperative station would see considerable beam-induced power, and would have to be tuned off-resonance to reduce that power to

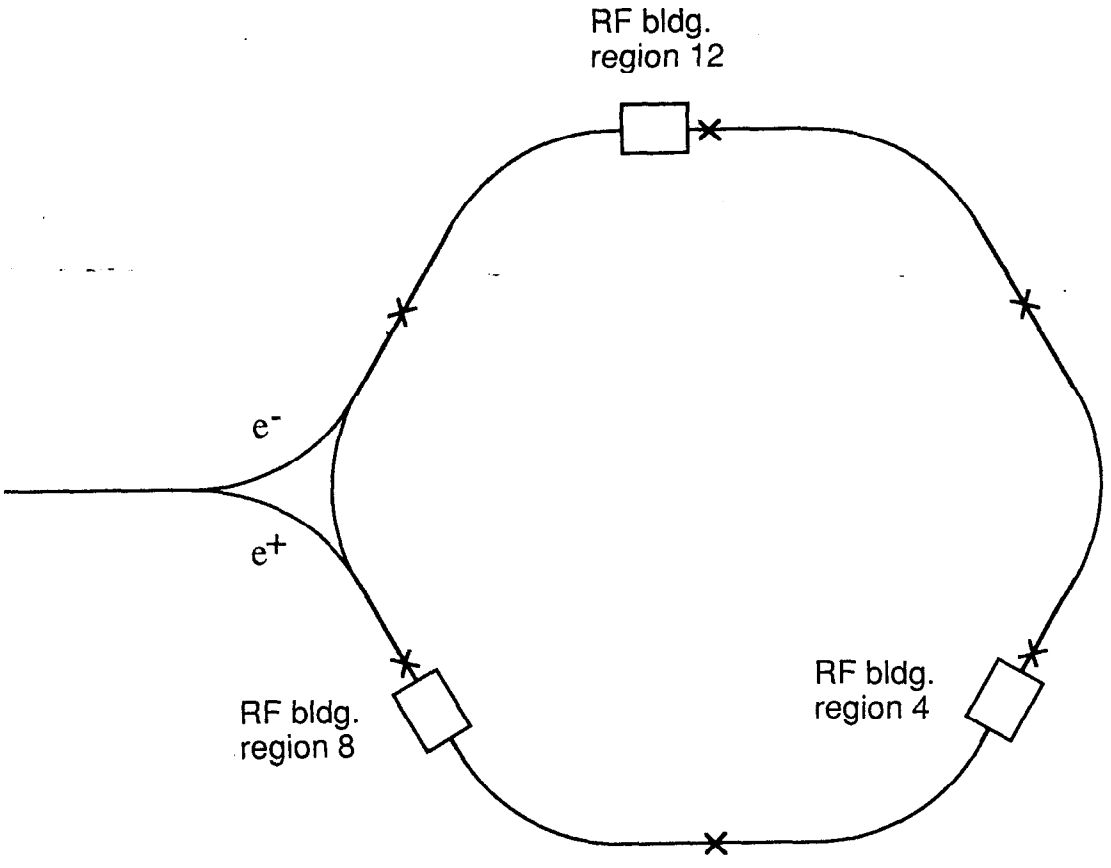

Fig. 5-108. Layout of the B Factory, showing the locations of RF buildings.

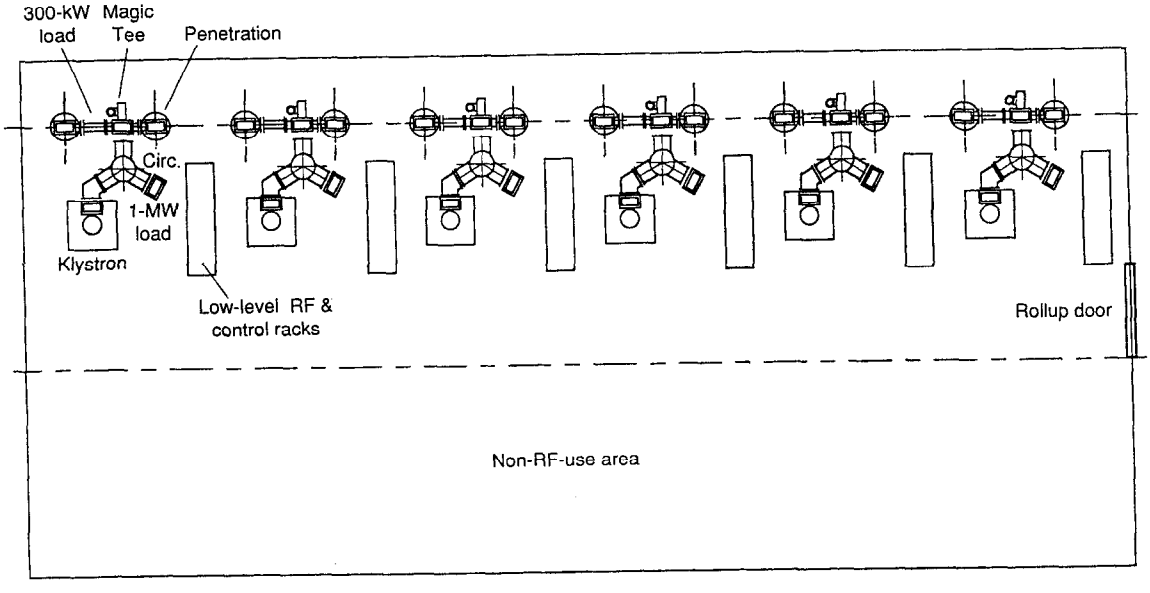

Fig. 5-109. Plan view of an existing RF building, showing the arrangement of six RF stations.

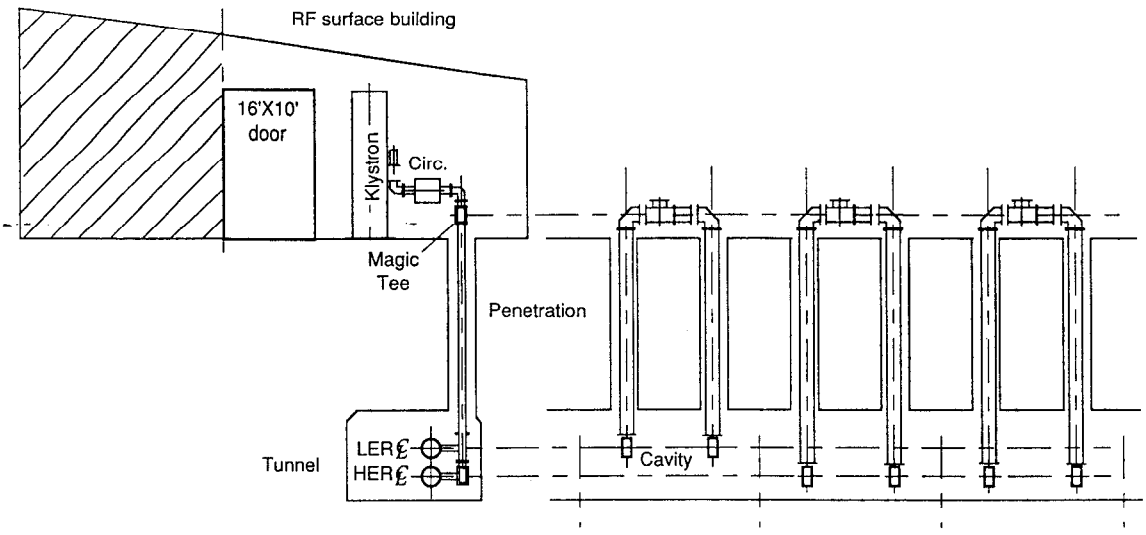

Fig. 5-110. Cross-sectional view showing an RF station and a section of the PEP tunnel.

manageable levels. It will not be possible to change a klystron while a beam is circulating, but maintenance or repair work on the low-level RF modules could be performed when a station is in the off position.

If the B Factory current were increased to 3 A in each ring, additional RF stations would be installed; the number of stations would rise to 15 in the HER and 6 in the LER, and the number of cavities would increase to 30 in the HER and 12 in the LER. The wall loss in each cavity in this scenario would decrease. The coupling factor for each cavity would have to be increased to 8.3, because more power must be delivered to the beam. An additional surface building would also be required to house the three RF stations that could not be accommodated in the present RF buildings.

5.5.7 Summary

Considerable effort has gone into the choice and design of the B Factory cavities. A cavity shape with nose cones provides a maximum shunt impedance at the cavity fundamental mode, while HOMs are heavily damped by three HOM loading waveguides. The 150 kW of wall dissipation requires a careful design of the cooling of the cavity. A drive network with a window capable of delivering 500 kW of RF power to the cavity must also be developed. We believe the proposed designs to be within the realm of present-day technology, but further simulations, as well as actual tests under full power, will be conducted to verify their performance.

We chose an RF system design that uses two single-cell cavities with each 1-MW klystron. This combination can provide the required gap voltage and deliver the needed power to the beam, using the relatively small number of 20 cavities in the HER and 10 in the LER. The low-level RF system, besides providing conventional control and feedback, will also be required to help in the damping of beam-induced instabilities with

direct RF feedback loops. The stability of such loops needs further investigation and performance tests. The planned RF system has the advantage of using existing conventional facilities and can be implemented without any structural changes. All components of the system can be used in a future upgrade to a 3-A machine, with only minor adjustments and the addition of a small number of RF stations.

5.6 FEEDBACK SYSTEMS

As pointed out in the discussion of beam instabilities (see Section 4.3), the high beam currents in the B Factory rings can provide strong excitation of any resonator to which they can couple. The voltages that arise drive coupled-bunch instabilities, and active feedback systems are required to prevent the growth of longitudinal and transverse bunch oscillations. In practice, it is the high-Q resonators associated with the parasitic higher-order modes (HOMs) of the RF cavities that are the main culprits, hence the considerable effort to damp these modes, as described in Section 5.5.

To control the oscillations, the corrective kicks that the feedback system applies to the bunches must be at least as large as the induced resonator voltages minus the effective "voltage" due to the radiation damping. Because the induced voltages are proportional to the shunt impedances of the resonators, the technique of passive damping of HOMs in the RF cavities greatly reduces the feedback voltages required. On the other hand, a single HOM that has been broadened in frequency by damping can potentially cause instability in perhaps 100 coupled-bunch modes of the beam. Therefore, one expects many beam modes to require feedback stabilization.

In most operating accelerator rings, coupled-bunch damping has been applied selectively to the few observed unstable modes. The traditional method has been to extract the beam signal and feed it back at these few unstable mode frequencies. For the B Factory, damping must be provided to suppress many modes, and the systems must be designed in advance, before details of the particular modes that are unstable are known. For both these reasons, we have decided to damp bunch motions with systems that feed the signals detected from each oscillating bunch back to that same bunch. Such *bunch-by-bunch* feedback has the additional advantages of suppressing other disturbances, such as motions driven by the beam-beam interaction, and it is very effective in damping transients introduced by the injection of a small fraction of the stored beam. Systems of this type are now operating at PETRA [Heins et al., 1989].

Although we must deal with a relatively short bunch spacing of 4.2 ns, the electronics required for the prompt processing of such signals is now available. It is also worth noting that, for many-mode operation, the bandwidth required in the power amplifier and kicker would be the same for either mode-filtered or bunch-by-bunch feedback, namely,

$$\Delta f \geq \frac{1}{2} B_0 f_0 = \frac{1}{2}(1746)(136.7\ \text{kHz}) = 119\ \text{MHz} \tag{5-33}$$

It is this bandwidth that makes the power capability costly and emphasizes the importance of an efficient kicker design.

While instabilities driven by HOMs of the cavities are to be controlled by the bunch-by-bunch feedback, there are three longitudinal coupled-bunch modes in each B Factory ring that are driven even more strongly by the off-resonance response of the principal, accelerating RF mode. For these unstable coupled-bunch modes, the RF cavity itself is the most efficient kicker to employ for feedback. Accordingly, narrow-band signals to suppress each of these modes will be fed to the beam through the bandpass of the RF amplifiers.

5.6.1 Longitudinal Damping

The damping applied by the bunch-by-bunch feedback must be capable of opposing the shunt impedance of the strongest cavity HOM, at 750 MHz. As noted in Section 5.5, strong reduction of the Q of this HOM by passive damping has already been demonstrated. Although we have observed a reduction to $Q \approx 30$, we have specified a more conservative value of $Q = 70$ for the feedback system design described here. The various parameters that define the task of the longitudinal feedback system are given in Table 5-33 for both rings. In what follows, the HER will be used to illustrate the feedback system design and expected performance; extension of the design to the LER is straightforward.

The required system gain and kick amplitude are determined by the excitation of the strongest longitudinal resonance, a mode near 750 MHz having phase amplitude $\Delta\phi_0 =$ 0.03 rad (at the RF frequency of 476 MHz). For short bunches this voltage is

$$V = j I_0 R_s \frac{\omega_{res}}{\omega_{RF}} \Delta\phi_0 \qquad (5\text{-}34)$$

where $R_s = 20\ (R/Q)Q = (20)\ (41)\ (70) = 57$ kΩ for the HER. From Eq. 5-34 and the parameters of Table 5-33, we find that the damping voltage must be at least 4 kV/turn. Although radiation damping will provide about one-third of the required damping, we ignored this contribution in our design. That is, the contribution from radiation damping is considered a safety factor, and we have designed the feedback kickers to be capable of 4 kV/turn in the HER (or 2.9 kV/turn in the LER).

Table 5-33. Parameters used for feedback system design.

	HER	LER
Average current, I_0 [A]	1.48	2.14
Number of cavities	20	10
Strongest HOM frequency [MHz]	750	
R/Q per cavity [Ω]	41	
Q	70	
Maximum mode amplitude [ps/rad]	10/0.03	
Injection scheme	1/5 bunch at 60 pps	
Assumed injection errors [$(\delta E/E)$/ps]	0.002/100	

Errors in the energy and/or timing of the injected beam will combine to produce a phase error that is about 14 times as large as the 0.03-rad excitation considered from the 750-MHz HOM. However, the small quantity of charge injected with this large deviation can excite the resonators to only about 3.4 kV. Therefore, if the low-level circuits of the feedback system are designed to limit the kicker output to 4 kV in response to phase excursions greater than 0.03 rad, transients and growth at injection will still be controlled. This action is clearly illustrated by our numerical simulations, shown later in this section.

5.6.1.1 RF Feedback. For the B Factory, the usual practice of detuning the frequency of the cavity accelerating mode to compensate beam loading stabilizes the coupled-bunch mode $m = 0$ (Robinson damping), but leads to difficulties. This is because the detuning must be quite large to account for the beam loading, with the result that the detuned fundamental mode drives bunch modes $m = -1$, -2, and -3 more strongly than can be counteracted by the damping provided by the bunch-by-bunch feedback system. To deal with this, these few particular modes will be damped by signals at the appropriate mode frequencies that are extracted from the detected beam phase signals and fed back through the RF amplifiers and cavities. To ensure that mode $m = -1$ can be damped in this manner, narrow-band active damping circuits around the cavities and drivers will be used to suppress the shunt impedance 130 kHz (that is, f_0) away from 476 MHz. This suppression will be sufficient to reduce the potential growth rate to less than the synchrotron frequency. The effective impedances with and without this suppression are given in Table 5-34. Also listed are the effects of the amplified phase signals for the mode amplitude of 0.03 rad.

5.6.1.2 System Overview and Principle of Operation. The bunch-by-bunch feedback system will measure the instantaneous phase of each bunch with respect to the ring master oscillator and provide a correction voltage for each bunch via a kicker structure. The large number of bunches (1658) and the interbunch time interval of only 4.2 ns require a wideband processing system, with the front-end and power-amplifier stages operating at a 238-MHz clock rate. The processing of the phase information from each bunch can be performed at a lower rate. Our feedback system design therefore employs common wideband front-end and power-amplifier stages, with many processor channels operating in parallel, at a slower rate, to generate the correction signal for each bunch.

Table 5-34. Damping of the m = –1 coupled-bunch mode.

	HER	LER
Effective R [MΩ]	5.85	10.0
Reduced R for $1/t = f_s$ [MΩ]	3.7	1.22
Reduction by active damping system [MΩ]	3.6	1.2
Feedback kick [kV/turn]	162	79

We decided upon a digital signal-processing approach to convert the bunch-phase information into a correction signal. This digital-filter approach permits the use of a matched-filter feedback algorithm and takes advantage of recent commercial activity in the digital signal processing (DSP) field. The programmable nature of this scheme provides flexibility and allows us to implement compactly a nonlinear (soft-limiting) feedback system. It is also possible to program several operating modes into such a system—for example, to distinguish injected bunches from stored bunches, should this be necessary or desirable.

There are two possible approaches to the measurement of longitudinal motion: (i) direct measurement of the phase of each bunch and (ii) measurement of the transverse displacement of each bunch in a region of the storage ring with nonzero dispersion. The second approach requires signal processing to separate the betatron motion from the transverse displacement due to longitudinal motion, and can give problems with synchro-betatron coupling. Furthermore, this approach does not relax any of the timing or bandwidth constraints compared with a phase-measurement–based system. Therefore, we selected the direct phase-measurement approach for our design, which means that the phase of each bunch is our control variable.

5.6.1.3 System Design. Figure 5-111 presents a block diagram of the B Factory longitudinal feedback system, showing its essential elements. The bunch phase signal is derived from a beam pickup structure, which generates a short coherent tone burst for each bunch passage. The phase of this burst is compared with a master oscillator

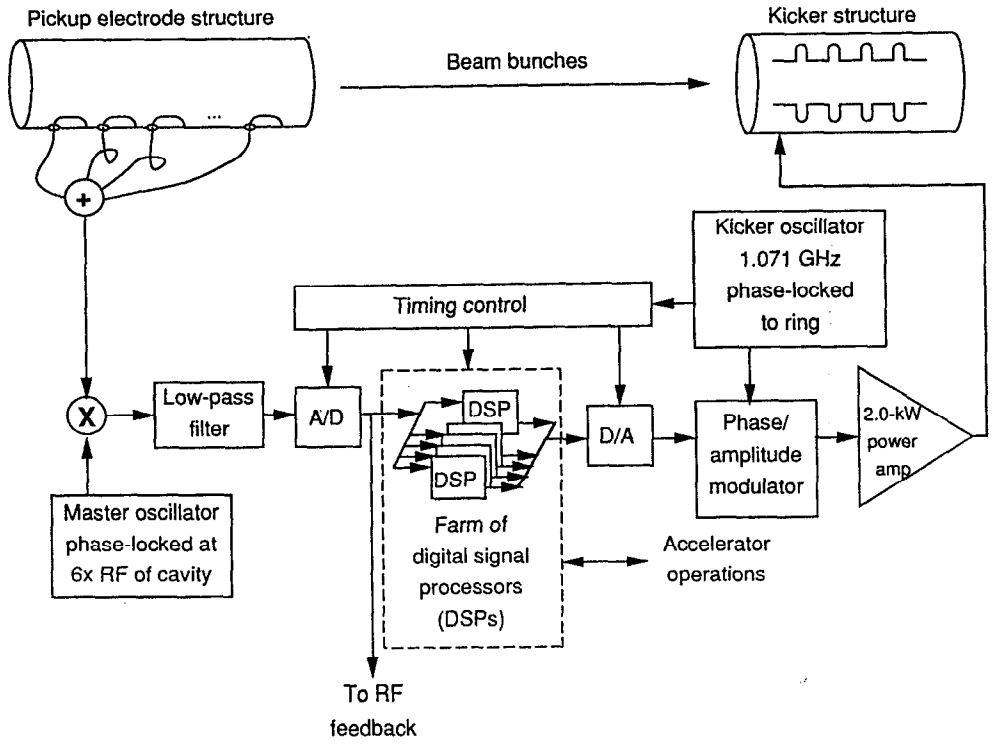

Fig. 5-111. Block diagram of the B Factory longitudinal feedback system.

synchronized to the ring RF system, and the phase-error signal is digitized at the bunch crossing rate. Digital processing of the phase-error signals is performed in an array of microprocessors (the DSP farm). This approach allows parallel processing of the phase-error signals and thus reduces the processing rate needed in each DSP block. The computed correction signals are recombined into a wideband correction signal and converted back to analog form. Finally, the feedback loop is closed via a power amplifier and a kicker structure that applies the correction voltage to each bunch. The constituents of the various functional units in Fig. 5-111 are described below.

Beam Pickup. The beam pickup generates a short (less than 4 ns) tone burst at the sixth-harmonic of the ring RF (that is, at 2856 MHz). We use a periodic coupler structure that generates a burst, rather than a tuned resonant structure, to avoid coupling between adjacent bunches. The burst of RF carrying the signature of the arrival time of the bunch can be generated in several different ways, using stripline pickups, power dividers and combiners, or delay lines. To simulate such a burst in the laboratory, we have performed measurements in which a narrow pulse is launched into a transmission line, coupled to an array of directional couplers evenly distributed along it, with all the coupler outputs added with a power combiner. As an alternative approach, we have also built another passive structure with periodically coupled microstrips. The advantage of this latter approach is that it minimizes the number of RF connections and, for the case of a beam-coupled structure, it would also minimize the number of vacuum feedthroughs.

As depicted in Fig. 5-112, we envision a pickup electrode structure made out of four transmission lines coupled to the beam through slots. The slot width can be adjusted to

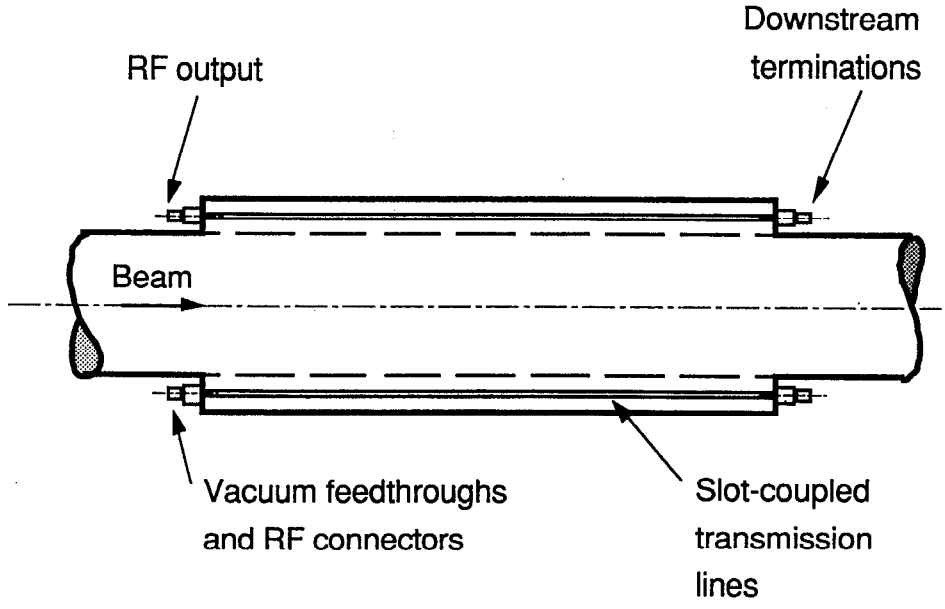

Fig. 5-112. Structure of a pickup electrode. Four transmission lines are coupled to the beam through slots. The pitch of the slots along the beam trajectory determines the tone burst frequency.

control the power coupled to the transmission lines, and the slot periodicity along the beam axis determines the frequency of the output waveform. As mentioned, we plan to operate at 2856 MHz and with 8–10 RF periods in the burst, so the structure length will be nearly 1 m.

Phase Detector. Phase detection is implemented in a double-balanced mixer. A master oscillator, phase-locked to the ring RF, generates a stable 2856-MHz signal for the phase reference. A filter on the output of the mixer eliminates the 2ω term and limits the bandwidth of the signal for noise reduction.

The choice of a 2856-MHz operating frequency is a trade-off between sensitivity and dynamic range. It allows a phase-processing range of ±15° at the 476-MHz frequency of the RF system, with a phase measurement resolution of better than 0.5°. This value is adequate for the linear damping range of the system, but it is important that the phase detector limit cleanly for excursions greater than ±15°, because such a condition is likely at injection. Another attribute required in this block is an automatic gain control (AGC) loop to allow the system to operate over a wide range of beam currents. This loop will control an attenuator between the beam pickup and subsequent processing electronics.

Phase Digitizer. The digitizer converts the phase-error signal from the mixer into an 8-bit signal. It operates at the 238-MHz beam crossing rate and provides a unique measurement at each bunch crossing. Components are available commercially to implement this digitizer.

DSP Farm. The DSP farm includes wideband multiplexing and demultiplexing circuits to convert the sequential 238-MHz data stream into several slower parallel streams. An array of commercial DSPs receives these signals. These processors (which are all identical and execute identical programs) treat each bunch as an individual oscillator and combine information from several sequential crossings of a particular bunch to compute a correction signal on each turn. We intend to use a finite-impulse response (FIR) matched filter for the feedback algorithm. This filter generates the required 90° phase shift and also provides some noise reduction (processing gain) on the raw error signals.

The DSP farm implements the limiting functions mentioned earlier and handles the special out-of-range conditions generated during injection. Before finalizing the design, we will also examine the performance of alternative feedback algorithms, especially a two-coefficient infinite-impulse response (IIR) filter, suggested recently by F. Pedersen. This more compact filter algorithm has the potential to reduce the size of the DSP farm by a factor of ten, but it might have the disadvantage of being less sensitive to the phase signal and more sensitive to electronics systematics and noise.

The analog-to-digital (A/D) phase digitizer produces a digitized sample every 4.2 ns, and the kicker requires a correction signal at this same 4.2-ns interval. Each physical DSP node receives data for several bunches from the A/D and transmits the corresponding correction signals to the digital-to-analog converter (DAC) within the 7.33-μs revolution period of the beam. The design of this system presents a high-speed distribution problem of the scatter-gather type, which can be solved in several ways. Here, we outline one solution as an example. In Fig. 5-113, a demultiplexer follows the

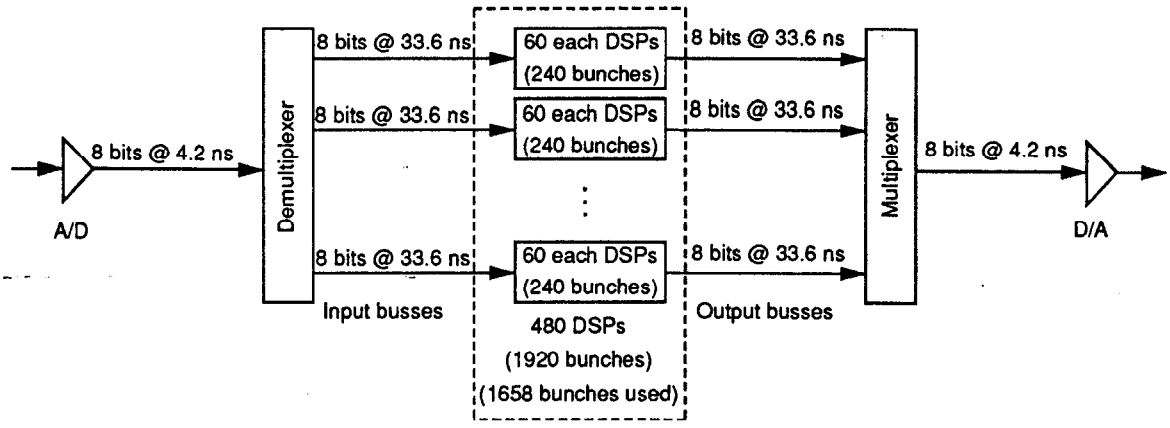

Fig. 5-113. Schematic of one scheme for digital signal distribution for the longitudinal feedback. The bandwidth of the input and output streams is far greater than the throughput of a single DSP. The input stream must therefore be scattered to many DSPs, whose outputs must then be gathered to form the output stream.

A/D and scatters groups of eight sequential samples onto eight 8-bit parallel input busses. A multiplexer precedes the DAC and gathers groups of eight sequential responses from eight 8-bit parallel output busses. On the parallel busses, data move at the rate of one byte every 33.6 ns. Each physical DSP node connects to one input and one output bus and accommodates four bunches. With this architecture, each processor executes at most 80 multiply-accumulate instructions and four groups of I/O and clipping operations per bunch revolution period. Available commercial processors meet this performance requirement.

We anticipate packaging four to eight DSP processors on a VME or VXI module. The digital signal processing for the longitudinal feedback system would then comprise 50 to 100 modules that would be mounted in 3–5 crates. Such a hardware assembly would occupy a standard 19-in. rack and would consume approximately 1–5 kW of power.

Output D/A and Amplifier. This block converts (at a 238-MHz rate) the correction signal stream from the output multiplexer into an analog level suitable for driving subsequent stages. It is an 8-bit system.

Power Amplifier. The longitudinal feedback system uses commercial RF power amplifiers and modulators to provide the signal for the output kickers. The operating frequency is 1.071 GHz at a power level of 2.0 kW. The power amplifiers will be configured in a modular fashion. This allows a soft-failure mode, that is, operation at reduced power levels, should components fail.

Beam Kicker. The beam kicker converts the output signal from the power amplifier into a longitudinal E field to correct the energy of each bunch. A periodic coupler provides the bandwidth required to prevent bunch-to-bunch coupling, along with a small voltage gain. To reduce the broadband power required, four separate kickers are used in

the HER to deliver the 4-kV (maximum) acceleration to the bunches. As illustrated in Fig. 5-114, each kicker will consist of an array of four quarter-wavelength drift tubes, joined in series by half-wavelength delay lines (at the operating frequency of 1.071 GHz). The kicker is constructed as a transmission line (with a characteristic impedance of 25 Ω) made up of several segments in series and parallel. The transmission line is divided into two 50-Ω lines at the ends; these connect through vacuum feedthroughs to the driver at the downstream end and terminating loads upstream. Transitions between the drift tubes and the delay lines between them must be well-matched to avoid reflections that will introduce losses and spurious responses. Initial modeling of series-electrode structures has verified the expected bandwidth; evaluation of the strength and some details of the response is under way.

Each kicker presents to the beam an impedance band that is about 250 MHz wide, with a maximum value of 400 Ω. Such an impedance is too broadband to drive coupled-bunch instabilities and contributes negligibly to the broadband impedance of the ring as well. The power this impedance extracts from the beam, about 800 W per kicker, is dissipated in the terminating loads.

To deliver a different voltage to each passing bunch, the allowed kicker length is limited by the combination of its filling time, the transit time of the passing bunch, and the rise time of the driving amplifier. The characteristics for each four-element kicker unit are summarized in Table 5-35. There are four of these kickers. The use of four units in the HER provides redundancy and a safety margin; the LER uses three identical units.

The 2.0-kW power amplifier required at the 1.071-GHz operating frequency is available from several commercial vendors. These solid-state amplifiers are modular, and typically include low-level drive electronics and power supplies.

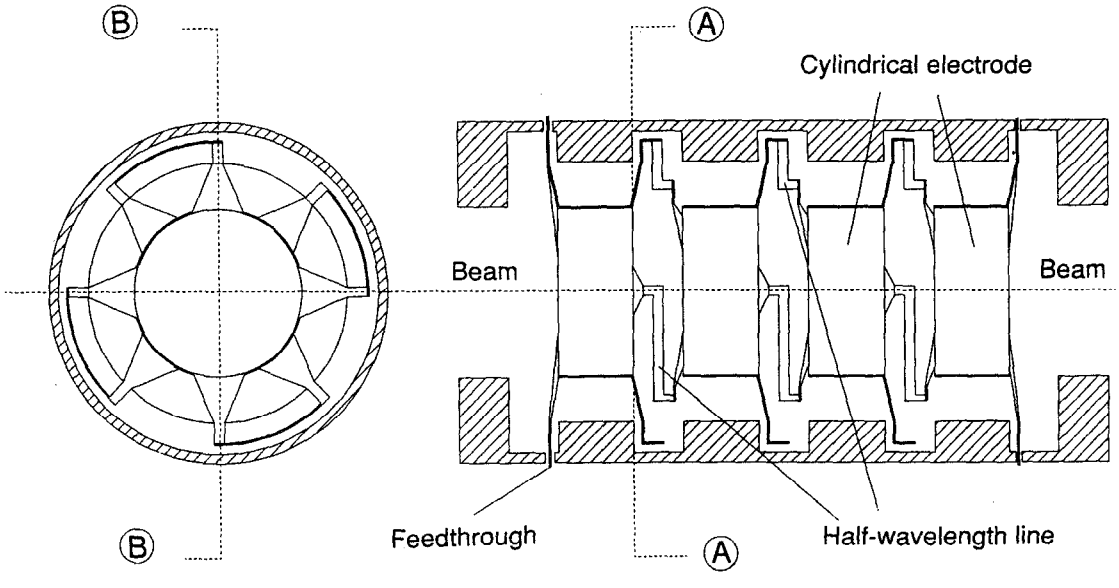

Fig. 5-114. Beam kicker for longitudinal feedback.

Table 5-35. Characteristics of longitudinal feedback kicker units.

Length [cm]	32
Frequency [GHz]	1.071
Kicker bandpass [MHz]	241
Driver bandwidth [MHz]	357
Shunt impedance [Ω]	1600
Power for 1 kV/unit [W]	313
Driver power rating [W]	500

5.6.1.4 System Summary. Table 5-36 provides a summary of the technical specifications proposed for the longitudinal feedback system. Laboratory measurements of a prototype feedback front-end processing system are already under way, and our initial results are quite encouraging. The prototype system has been shown to detect the phase of simulated bunches with a resolution better than the required 0.5° and thus demonstrates the level of performance needed for use at the B Factory.

5.6.1.5 Overview of the Simulation. We have studied the behavior of the proposed longitudinal bunch-by-bunch feedback system with a computer model of the HER. The simulation includes a ring model, along with an electronic model of the bunch-by-bunch feedback system shown in Fig. 5-101. The simulation code calculates the longitudinal motion of the bunches in the ring and their interactions with the RF cavities. It determines the bunch phase at the pickup electrode structure, adds the appropriate kick

Table 5-36. Longitudinal feedback system specifications

RF frequency [MHz]	476
Bunch interval [ns]	4.2
Beam pickup central frequency [MHz]	2856
Phase detector dynamic range (at 476 MHz)	±15°
Phase detector resolution (at 476 MHz)	0.5°
Bunch-to-bunch signal isolation [dB]	>26
Kicker structure operating frequency [GHz]	1.071
Output power [kW]	2.0

from the kicker structure (as determined by the electronic model), and propagates the bunches through the ring and cavities.

The electronic model includes

- The transfer function of the feedback system
- The feedback algorithm that processes the signals from the pickup electrode structure before sending them to the longitudinal kicker
- The properties of the phase detector, the low-pass filter, the front-end A/D, the DSP farm, and the kicker
- Parameters to simulate input noise, gain and offset errors, bandwidth limitations, and the effects of the limited dynamic range of the analog components

The model of the DSP farm emulates a 20-tap FIR filter. The coefficients ξ_j of the taps comprise a sinusoid with a longitudinal oscillation period of 19.3 turns, that is,

$$\xi_j = A_{\mathrm{DSP}} \sin\left(2\pi \frac{j-1}{19.3}\right)$$
$$j \in \{1, \cdots, n_{\mathrm{samples}}\} \tag{5-35}$$

Given measures $x_i(k)$ of the phase of bunch i on successive turns as input, the result of the DSP algorithm is the output

$$y_i(k) = \sum_{j=1}^{n_{\mathrm{samples}}} \xi_j x_i(k-j) \tag{5-36}$$

This result is clipped to an 8-bit signed integer, which is used to inform the kicker of the proper phase of the kicker oscillator for that bunch on that turn. The kicker model is implemented as a phase-modulated RF kicker with a nominal 4-kV maximum output amplitude.

The simulation model assumes that the measurement of bunch phase is independent of bunch charge. This corresponds to the case where the front-end circuits include an AGC loop or where a separate measurement of bunch charge is available for normalization. A propagation delay of at least one turn (7.33 μs) is enforced in the feedback transfer function.

5.6.1.6 Ring Simulation. In the ring simulation code, the bunch phases ϕ_i are taken with respect to the zero crossing of the RF waveform. We assume that a discrete kick is given to each bunch at a single point in the ring; that is, the system is modeled as though there were a discrete change in energy at a single point on each turn. This simplification is justified, because the synchrotron frequency is small compared with the revolution frequency. The motion of bunch i on one turn is divided into two parts:

- Propagation around the ring, outside the kick point:

$$\begin{aligned} \phi_i &\rightarrow \phi_i + T_0\dot{\phi}_i \\ \dot{\phi}_i &\rightarrow \dot{\phi}_i \end{aligned} \tag{5-37}$$

- The kick given to the bunch at the kick location:

$$\begin{aligned} \phi_i &\rightarrow \phi_i \\ \dot{\phi}_i &\rightarrow \dot{\phi}_i + \Delta\dot{\phi}_i \end{aligned} \tag{5-38}$$

The kick given to bunch i includes several components, corresponding to the various contributions that produce an energy change in bunch i on one turn:

- The RF generator voltage in the cavity at the time bunch i passes through. We represent this as $\hat{V}_g \sin \phi_i + V^{\text{cav.fbk}}$, where the second term corresponds to the RF cavity feedback needed to control beam loading at the fundamental.
- The wakefields (both the fundamental mode and HOMs) ringing in the cavity.
- The synchrotron radiation loss per turn, U_0, which actually occurs throughout the ring, but is lumped into the kick in the simulation.
- The voltage V_i^{fdbk} applied to bunch i by the bunch-by-bunch feedback system.

The equation for the total kick is:

$$\Delta\dot{\phi}_i = -\frac{\alpha\omega_{\text{RF}}}{E_0/e}\left[\hat{V}_g \sin\phi_i + V^{\text{cav.fbk}} - \frac{U_0}{e} + V^{\text{wake}} + V_i^{\text{fdbk}}\right] - \frac{2T_0}{\tau_E}\dot{\phi}_i \tag{5-39}$$

where α is the momentum compaction factor, E_0 is the nominal energy for a particle on the design orbit, ω_{RF} is the RF frequency, T_0 is the revolution period, and τ_E is the longitudinal radiation damping time.

Cavity Wakefield. In computing V^{wake}, we keep track of the (complex) wake voltage in each cavity mode k. This voltage gets a discontinuous increment each time a bunch passes through the cavity, and it rotates in phase and attenuates (since ω_k is complex) between bunch passages. Note that according to the fundamental theorem of beam loading, a bunch sees half the wake voltage it induces during its present passage.

Cavity Feedback. Because the beam loading in the fundamental cavity mode is very heavy, RF cavity feedback will be necessary to compensate it. The response at coupled-bunch frequencies that fall within the bandwidth of the fundamental mode will require special feedback. In simulations to date, we have assumed that the compensation is perfect, that is, that $V^{\text{cav.fbk}}$ exactly cancels the fundamental mode of the wakefield in the cavity. In reality, the situation is more complicated (involving the cavity phase loop, amplitude loop, tuning loop, localized impedance reduction, and bunch motion feedback), and the compensation will not be perfect. We are now studying an improved

representation that includes the response of the cavity, the feedback of the phases of nearby beam modes, and the effect of the gap in the bunch train.

5.6.1.7 Simulation Parameters. We start a given simulation run with specified initial conditions ϕ_i and $\dot{\phi}_i$ for each bunch. A typical initial condition we have studied is that of an injected bunch with a relatively large offset from the average synchronous phase, while the remaining bunches are close to the synchronous phase. All bunches, including the injected bunch, begin at the nominal energy, and the charge in all bunches is taken to be equal and to remain constant. (Although not yet implemented, the simulation is structured such that it will be straightforward in the future to include the addition of charge to bunches during injection.)

When the simulation begins, there are no wakefields present in the cavities. As noted above, the present simulations then assume that the wakefield at the fundamental (accelerating) mode is fully compensated; that is, only the effect of the HOM wakefields is included. The present simulations include only the single dominant HOM at 750 MHz, whose properties are included in Table 5-33.

Parameters used in the simulation results shown below are as follows:

- Bunch charge $N_b = 4 \times 10^{10}$
- 1658 bunches (corresponding to a harmonic number of 3492, with every other bucket filled, except in a 5% gap)
- Total current of 1.48 A
- R/Q = 33 Ω per cavity for the single strongest HOM (which is assumed to be damped to $Q = 70$)
- 20 RF cavities
- Starting phase for bunch #5 is $\phi_5 = 0.2915$ rad (that is, a 0.1-rad offset from the synchronous phase of $\phi_s = 0.1915$ rad); the remaining bunches start at the synchronous phase
- $U_0 = 3.52$ MeV/turn
- $\alpha = 0.00241$
- $\hat{V}_g = 18.5$ MV

(In some cases, these parameters are slightly different from those finally adopted for the B Factory, but the simulation results reported below are not strongly influenced by these minor differences.)

5.6.1.8 Simulation Results. We show an example with *no* bunch-by-bunch feedback in Fig. 5-115, which is a plot of the maximum bunch offset ϕ_i reached in 3000 turns for the first 100 bunches after the gap. (Note that the time between injection pulses is 1/60 second, which corresponds to about 2300 turns.) We see that the disturbance due to the offset of a given bunch does not propagate very far back in the bunch train during this time, even *without* a feedback system. However, in the absence of a feedback system, the disturbance would continue to grow and would ultimately propagate further in the bunch train.

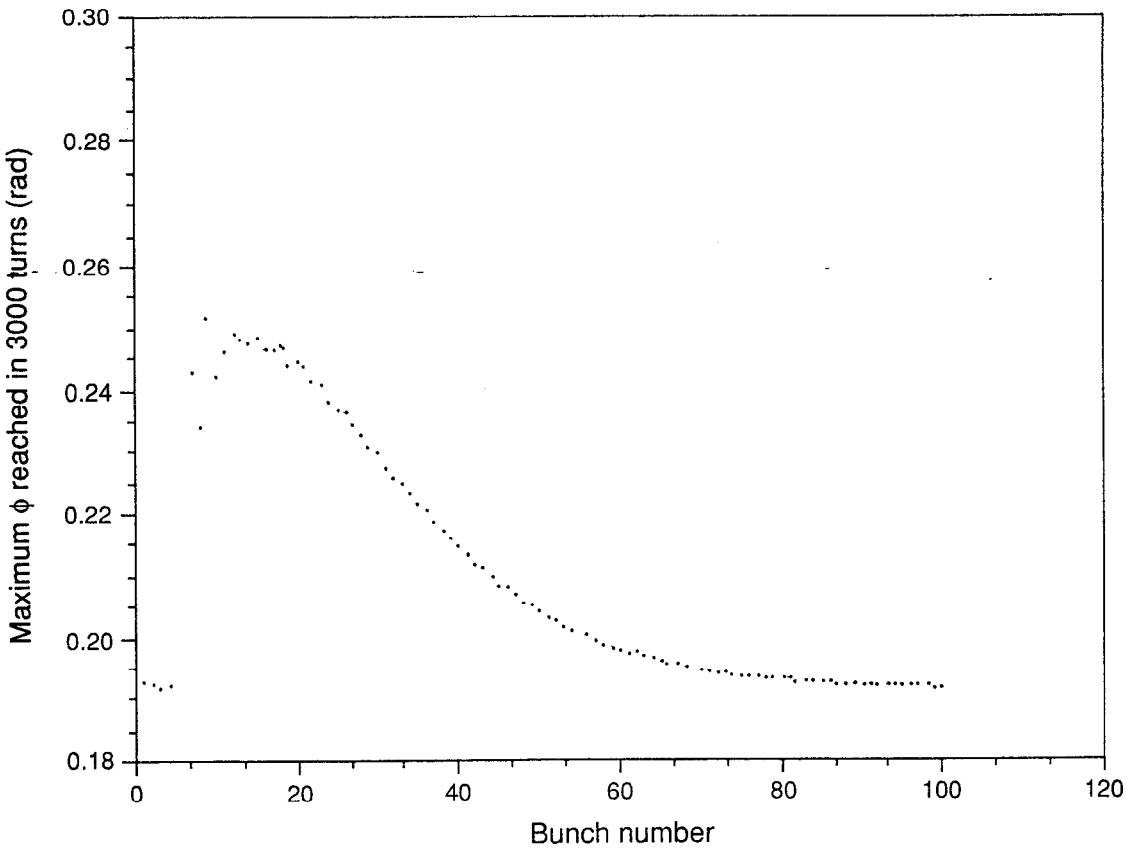

Fig. 5-115. Plot of the maximum bunch offset reached in 3000 turns for the first 100 bunches after the gap, in the absence of feedback.

Next we consider results that include the effects of bunch-by-bunch feedback. In these simulations, the kicker output is limited to 4 kV/turn. Only the first ten bunches after the gap are included, because the coupled-bunch excitation does not extend beyond a very few bunches with the feedback system turned on. These simulations were again run for 3000 turns. To observe the characteristic behavior in fewer turns, the feedback gain in the results described below is increased to correspond to reaching the 4-kV maximum kicker amplitude at a phase offset of 5 mrad rather than 30 mrad.

Figure 5-116 shows the longitudinal phases of the injected bunch (#5) and the bunch immediately following (#6), vs turn number. The envelope of the phase of the injected bunch damps linearly even though the kicker saturates, and the phase of the following bunch grows quickly to its maximum value near 400 turns and then slowly damps. The system limits the excitation of the bunch following the injected bunch and strongly suppresses the excitation of subsequent bunches.

Figure 5-117 exhibits the input and output of the DSP model for bunches #5 and #6 shortly after injection. We see that the DSP output saturates for bunch #5, but maintains the proper 90° phase lag. Benign saturation behavior of this type is difficult to realize with conventional analog approaches.

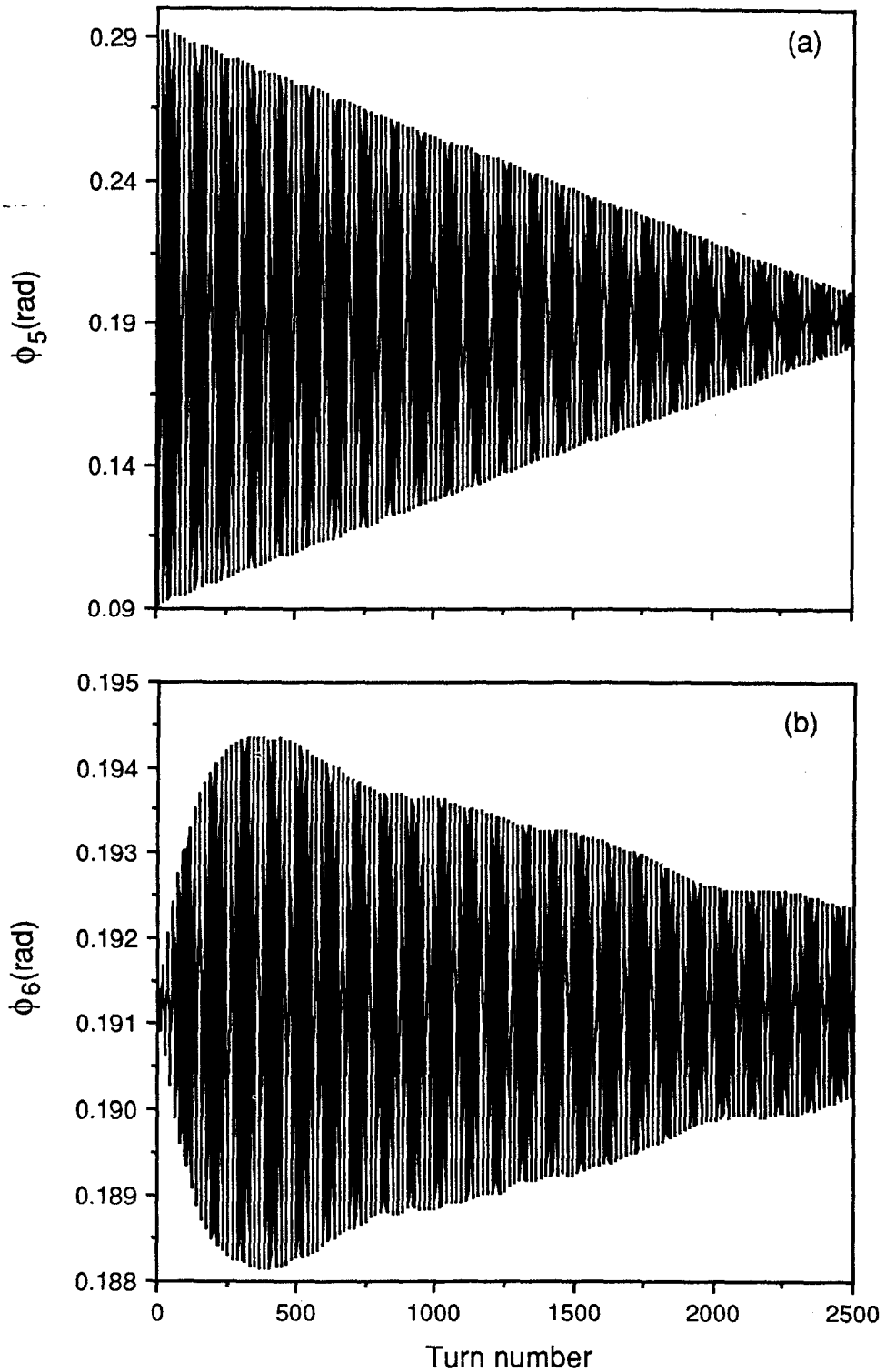

Fig. 5-116. Plots of the longitudinal phases of (a) the injected bunch (#5) and (b) the bunch immediately following (#6), vs turn number, in the presence of a longitudinal feedback system. Note the expanded vertical scale for (b).

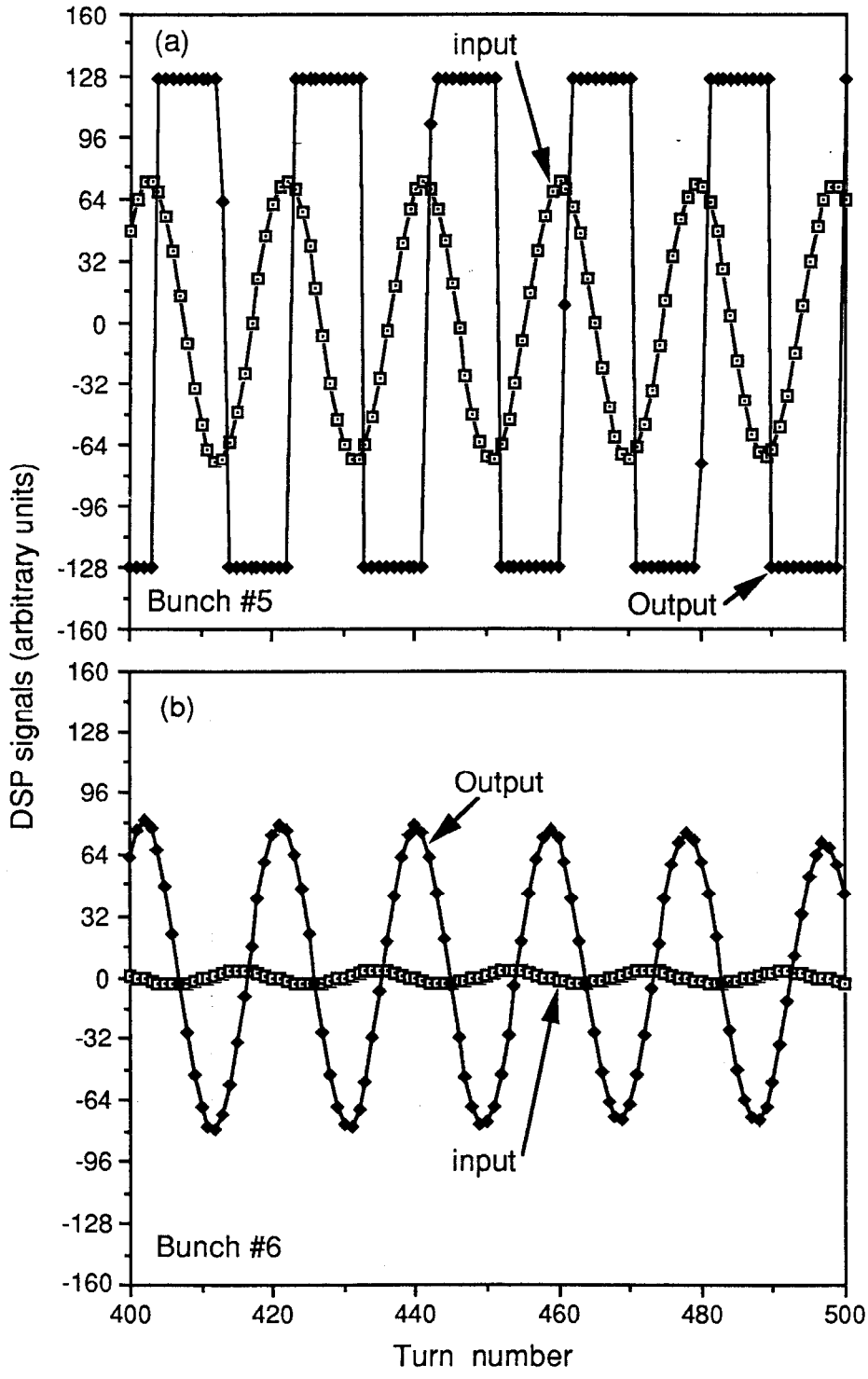

Fig. 5-117. Plots of the input and output of the DSP model for (a) bunch #5 and (b) bunch #6, shortly after the injection of bunch #5.

Figure 5-118a shows the amplitude of the phase-space error vs turn number for the injected bunch (#5). (The phase-space error is defined as the result of adding the error in phase and the error in energy in quadrature, expressed in radians.) We see the amplitude decreasing linearly during the time when the kicker limits at ±4 kV per turn. After coming out of saturation, the amplitude of the injected bunch falls exponentially. The amplitude of the following bunch (#6) is plotted on the same scale. Figure 5-118b shows the behavior of the injected bunch as it leaves the regime of kicker saturation. The decrease in amplitude changes from linear to exponential. Note that the transition from saturation does not perturb the following bunch. Figure 5-118c shows the phase-space error amplitudes for the two bunches immediately following the injected bunch. With bunch-to-bunch coupling in the electronics set to zero, the rates of rise agree with calculations.

Figure 5-119a compares the amplitude of the injected bunch for two values of gain in the DSP model. The lower gain corresponds to our specified value of 4 kV at a phase offset of 30 mrad. The higher gain, used for the simulations that produced Figs. 5-116 through 5-118, corresponds to 4 kV at a 5-mrad offset. Figure 5-119b shows the amplitude of the following bunch at each gain value. Lower gain results in larger excursions of amplitude and slower recovery, as expected. The only penalty of higher gain is a smaller linear regime.

Figure 5-120 shows the amplitudes of the injected bunch (#5) and the two following bunches, with a 10% bunch-to-bunch coupling in the front-end electronics and a 3% coupling in the kicker. In this case, bunch #6 suffers a much greater excursion from equilibrium, but still damps. Bunch #7 suffers only slightly. We conclude from this that our system design is tolerant of a reasonable amount of bunch-to-bunch coupling in the analog components.

5.6.1.9 Conclusions of Simulation Study. In this simulation study of the B Factory longitudinal bunch-by-bunch feedback, we have determined that the system proposed is a reasonable point of departure for a more detailed design effort. We have found that 4 kV/turn is sufficient to damp both an injected bunch and the perturbed stored beam, in the presence of the expected HOM strength. We have set an upper bound on the number of DSPs required for bunch-by-bunch longitudinal feedback, and we have shown that the system performance is insensitive to nonidealities in the electronics. The simulation tools that have been developed for these studies can be adapted to further investigations.

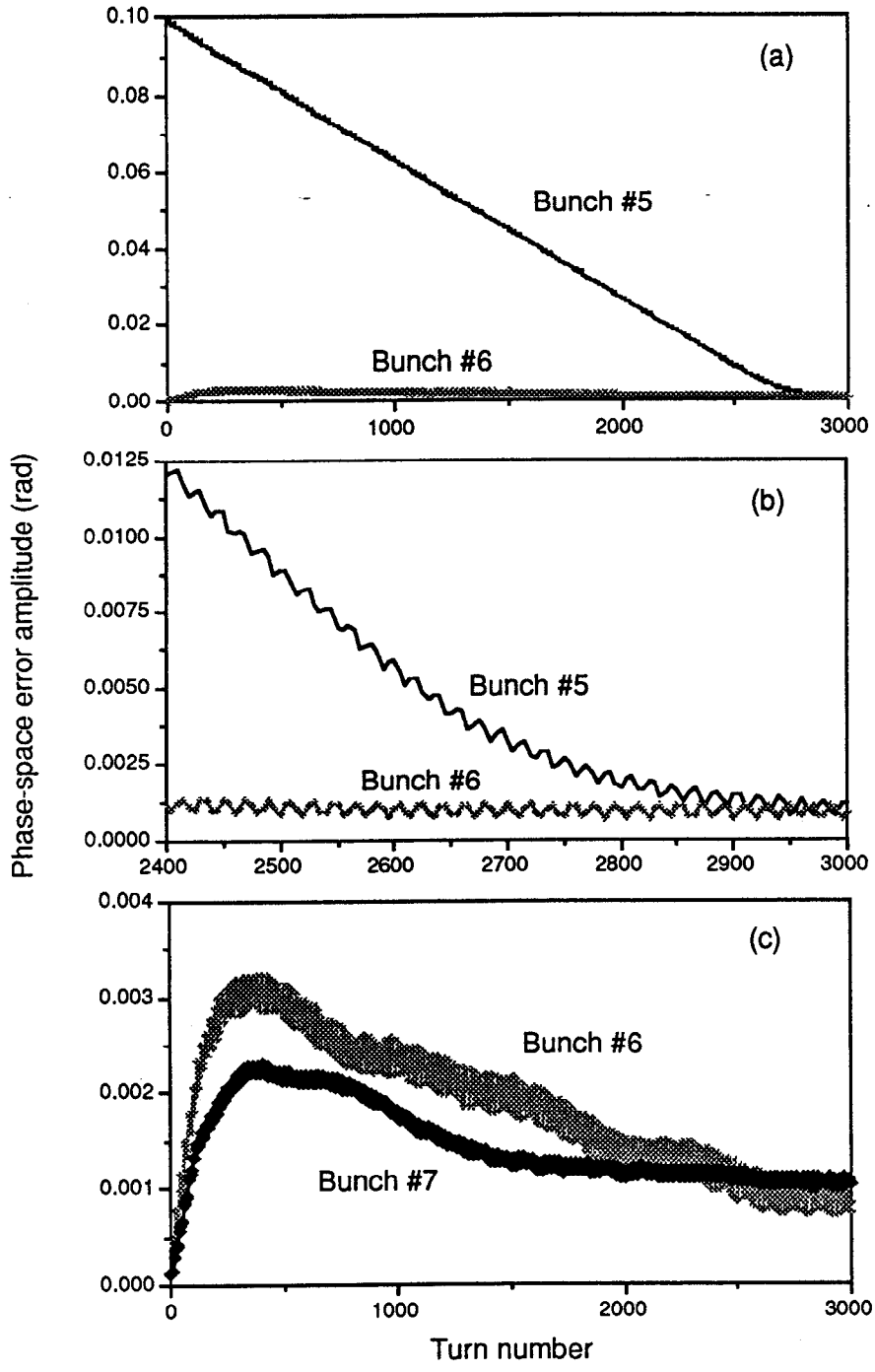

Fig. 5-118. Plots of the phase-space error amplitudes for (a) bunches #5 and #6 for the first 3000 turns, (b) bunches #5 and #6 in the region where the kicker comes out of saturation, and (c) bunches #6 and #7 for the first 3000 turns. In (b) we see that the trailing bunch is undisturbed as the kicker comes out of saturation. The rise times shown in (c) agree with calculated values when no bunch-to-bunch coupling in the electronics is assumed.

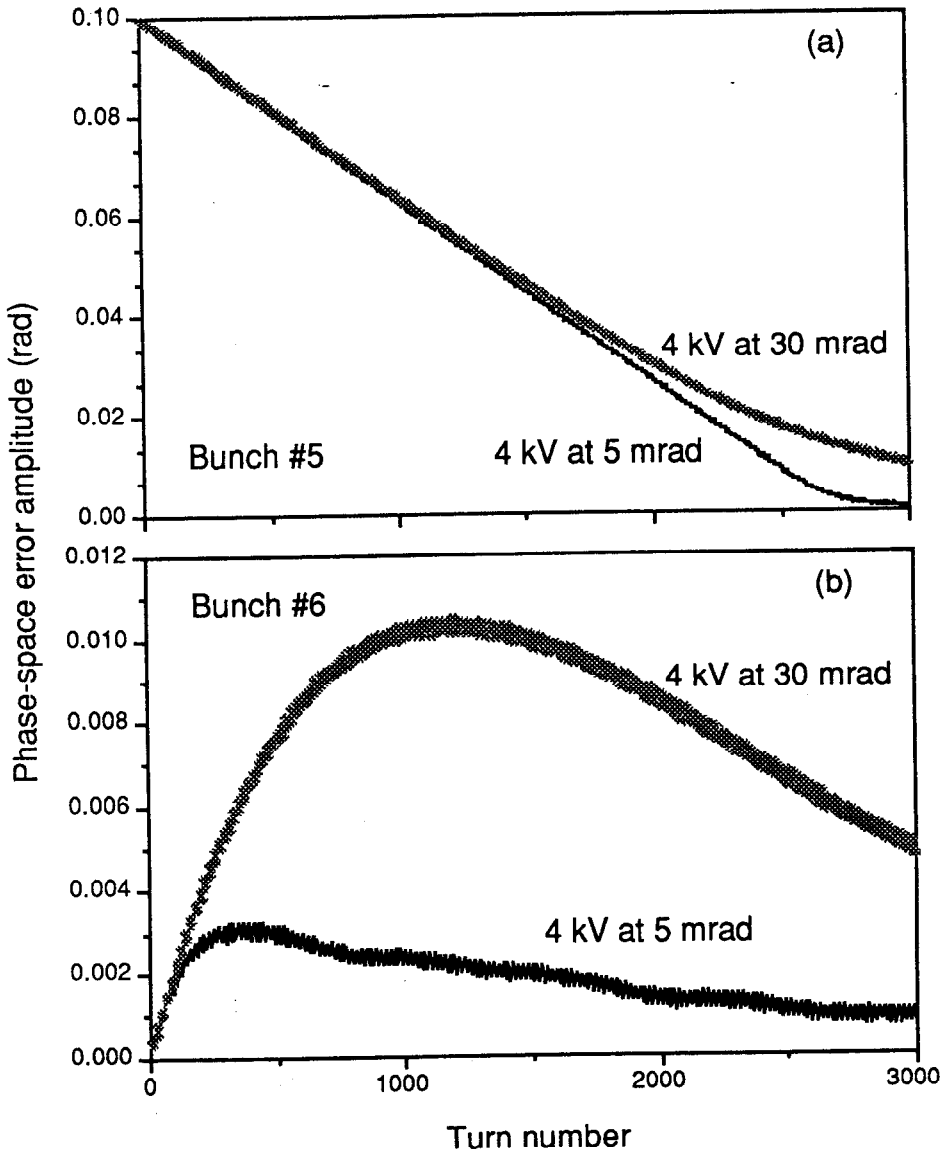

Fig. 5-119. Plots of the phase-space error amplitude for (a) the injected bunch and (b) the following bunch, for two values of the gain: 4 kV at phase offsets of 30 and 5 mrad. The higher gain was used for the simulation results shown in Figs. 5-116 through 5-118. The lower gain corresponds to the actual B Factory hardware specifications.

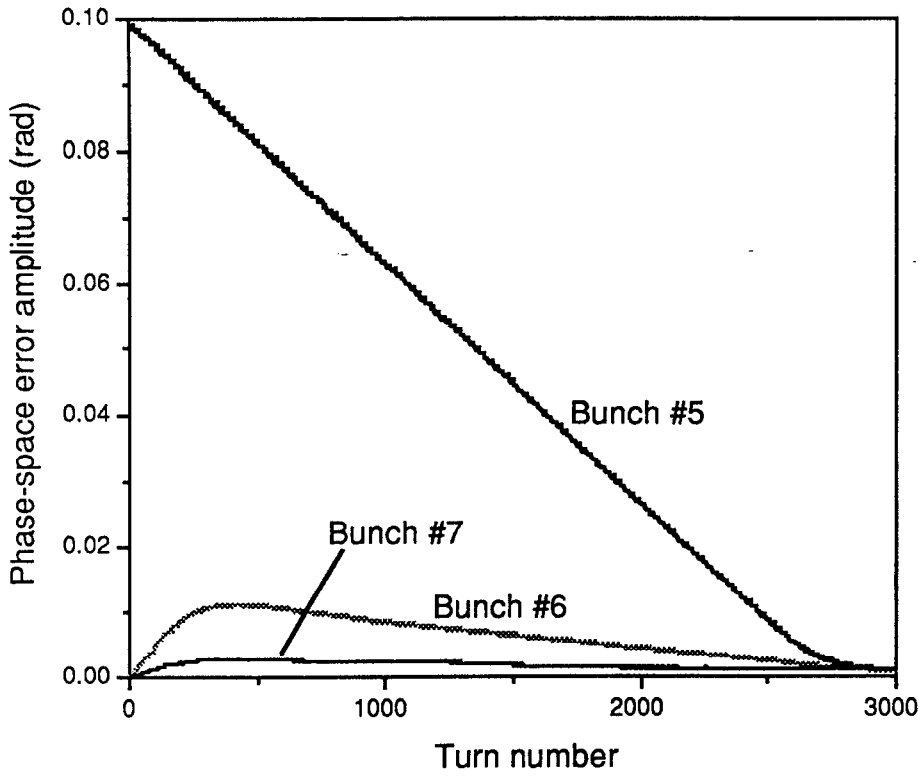

Fig. 5-120. Plot of the phase-space error amplitude for the injected bunch (#5) and the two following bunches, with a 10% bunch-to-bunch coupling in the front-end electronics and a 3% coupling in the kicker.

5.6.2 Transverse Damping

The feedback systems to stabilize transverse coupled-bunch oscillations are similar in principle and architecture to the longitudinal system. Detection of transverse excursions is simpler, and optimization of the kicker calls for a lower operating frequency. The strongest resonance and other parameters for the transverse cases are given in Table 5-37. Again the value $Q = 70$ has been taken for the damped HOM.

For the HER, the highest shunt impedance, $R_\perp$ is 20 $(R_\perp/Q)Q$ = (20) (640) (70) = 900 kΩ/m. The transverse impulse induced in this impedance by the 1-mm oscillation amplitude Δx is

$$V_\perp = j\, 2I_0\, R_\perp \Delta x = 2.8 \text{ kV/turn} \qquad (5\text{-}40)$$

If the kickers that oppose this were located at a point in the ring where the beta function is larger than at the cavities, the required kicker strength would be reduced. Such a reduction has not been utilized at this point in the design development; the kickers are therefore designed to provide up to 2.8 kV/turn at the bunch repetition rate.

Table 5-37. Parameters used for transverse feedback design.

	HER	LER
Average current, I_0 [A]	1.48	2.14
Approximate betatron tune	20	37
Number of cavities	20	10
HOM frequency [MHz]	1060	
R/Q per cavity [Ω/m]	640	
Q	70	
Maximum oscillation amplitude at cavities [mm]	1	
Injection scheme	1/5 bunch each 1/60 s	
Injection error [mm]	10	

As for the longitudinal case, the injection of a small charge with larger amplitude produces a modest excitation of the cavities, in this case 1.1 kV transversely. The resulting transient will be controlled by the bunch-by-bunch feedback system with amplitude-limiting of its output.

The signal processing required for the transverse feedback system is similar to that proposed for the longitudinal system. As shown in Fig. 5-121, a beam pickup structure (utilizing button or stripline electrodes, or possibly a slotted coupler as in the longitudinal design) is used to generate horizontal and vertical position signals. The horizontal and vertical signals are detected and a fast A/D system converts the position information at the 238-MHz bunch rate. The signal processing required to compute the transverse correction voltages is less complex than in the longitudinal case, requiring fewer DSP modules. We anticipate using much of the same processing hardware as for the longitudinal system, and the systems can share a common timing and control path. An output multiplexer combines the correction voltage signals from the DSP farm and a fast D/A converts the information to an analog correction signal. The feedback loop is closed via commercial power amplifiers and modulators, operating in the 180- to 270-MHz band, which drive horizontal and vertical beam kicker structures.

Each transverse kicker unit consists of a pair of stripline electrodes; each electrode is a segment of a cylinder that covers one-third of the perimeter of a 10-cm-diameter aperture. These electrodes have a length of 31.5 cm (one-quarter wavelength at 238 MHz) and have a characteristic impedance $Z_\perp = 50\ \Omega$. The kicker must handle mode frequencies in the range 114–235 MHz. We find the transverse shunt impedance using

$$R_\perp = 2Z_\perp \left(g_\perp \frac{l}{b} \frac{\sin kl}{kl} \right)^2 \tag{5-41}$$

with $g_\perp \approx (4/\pi) \sin 60°$; at the midpoint of the frequency range, this is 2.95 kΩ.

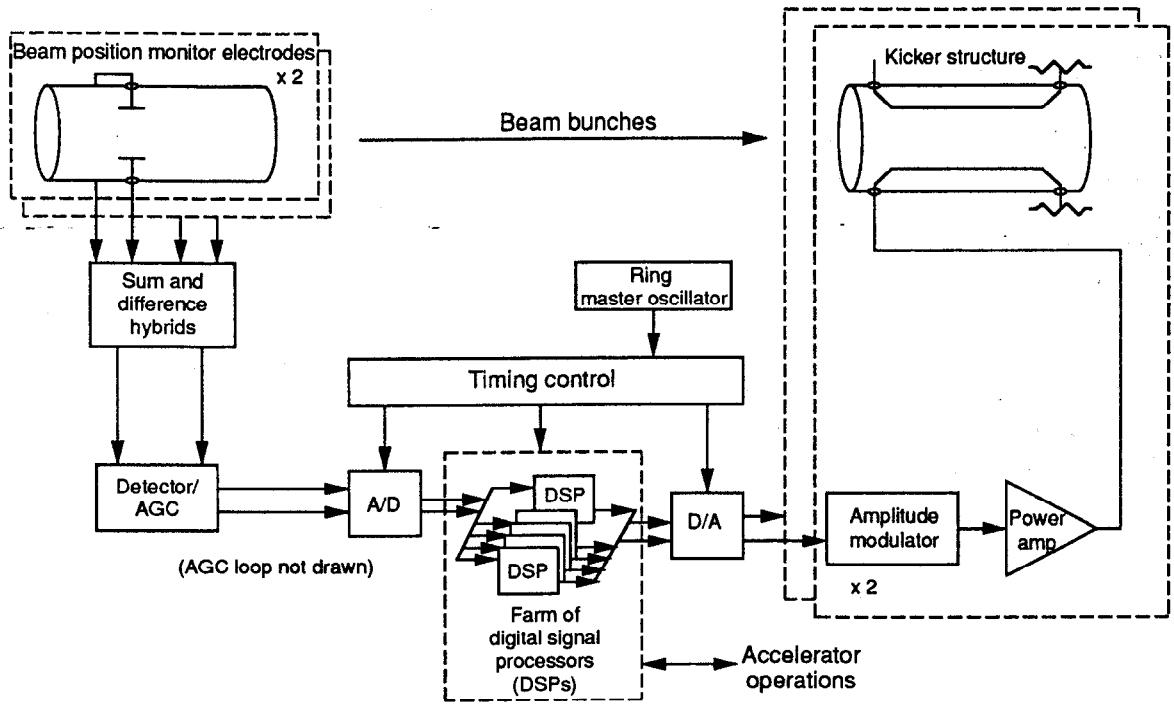

Fig. 5-121. Block diagram of the transverse feedback system.

In the HER, two units will be used, each requiring power $V^2/2R_\perp$. With $V = 1.4$ kV, the power is 332 W per kicker; a 400-W driver is specified. Good isolation between kicks to successive bunches requires that the driver cover the approximate bandwidth of 180–270 MHz. The required complement of transverse kickers is given in Table 5-38.

Table 5-38. Transverse kickers and drivers.

	HER	LER
Number of kickers	2	1
Power per kicker [W]	332	678
Driver rating [W]	400	800

5.6.3 Conclusions

The proposed detection and processing system has been shown to damp excitations from off-energy injected bunches and from the excitation of HOM resonances in the accelerating cavities. Laboratory measurements of prototype front-end detection and digitizing circuitry have demonstrated performance consistent with B Factory requirements. The simulation tools we have developed and the simulation results already obtained provide a solid base for the detailed system design and optimization of the longitudinal and transverse damping systems. Finally, and most importantly, the feedback system output power requirements are relatively modest, and the electronics systems are based on existing commercial technology. We conclude, therefore, that B Factory feedback systems based on the approach outlined here are entirely feasible.

5.7 INSTRUMENTATION AND ELECTRONICS

Most storage rings are equipped with a standard package of instrumentation and electronics designed to speed up injection, optimize the lattice parameters, monitor the beams orbits, and improve the luminosity. The two rings of the B Factory will be no exception, and a full set of diagnostic tools is planned for each ring.

The injection transfer lines will be monitored with instrumentation similar to that currently used at PEP, namely, stripline position monitors, current monitors (resonant toroids), wire scanners, and injection screens (with TV transmission). Also similar to current PEP hardware will be the tune measurement system (with the addition of an X-Y pinger), a direct current transformer, stoppers and scrapers, and profile monitors (UV telescope, vertical beam profile x-ray imaging system, and, for single-bunch operation, a streak camera). However, because of the very high bunch frequency, there will be some systems quite different from those now in operation at PEP. These are

- Beam position monitors (BPMs; button type)
- Bunch-by-bunch current monitor system (for injection control)
- Feedback system to maintain the beams in collision

The last three of these systems, the third of which is altogether new and unique to the operation of the B Factory, are described below.

5.7.1 Beam Position Monitors

The term "beam position monitor" can refer to a piece of vacuum chamber fitted with pickup electrodes, processing electronics and the associated cable plant, or even a special computer code designed to interpret the data produced by this system. We are concerned here only with the processing electronics; the pickup electrodes are described in Section 5.2, and the computer control system that will handle the data processing is covered in Section 5.8.

The position monitors now in place in each half sextant of PEP have their four electrode signals multiplexed onto a single transmission line by means of an arrangement of coaxial relays. The pulses from a single bunch of the stored beam are isolated by a gate, and their amplitude is measured in a relatively narrow bandwidth, with a synchronous detector operating at the revolution frequency of the ring (136 kHz). A sequential detection of the four pickup electrodes at each monitor yields the complete closed orbit in about 30 seconds. However, because of the above-mentioned relays, the four signals are not simultaneously available, and the beam position cannot be obtained for a single turn, as is desirable during commissioning or for certain machine physics experiments.

In contrast with PEP, the high bunch frequency of the B Factory makes it difficult to isolate one bunch (the bunch spacing is 4.2 ns), and the most straightforward approach to a closed-orbit measurement is to detect the fundamental frequency of the train, that is, 238 MHz. All channels of the processing electronics must then be calibrated at this

frequency. On the other hand, it is impractical to distribute such a calibration signal to all the multiplexer relays; consequently, the B Factory will employ a different type of multiplexer, and each monitor will be fitted with a matched set of four cables. Besides eliminating the need for the distribution of a calibration signal, this cable plant will also allow the measurement of single-turn trajectories in a snapshot manner, since now the four electrode signals are simultaneously available for each beam pass.

Each ring of the B Factory includes 144 BPMs; their instrumentation will be divided into 12 identical subsystems. Figure 5-122 depicts the general configuration of the cable plant for one-twelfth of a single ring. Advantage will be taken of the existing instrumentation and controls (I&C) alcoves at ground level, thus avoiding electronics in the tunnel and saving the cost of constructing radiation-proof alcoves. This plan entails a 200-ft increase in the length of each monitor cable and requires a careful trimming of its electrical length, as well as a periodic check of the differential attenuation of each set. One type of coaxial line appropriate for this application is a solid-copper, semirigid cable with an outside diameter of 0.375 in. and a low-density foam dielectric. This type of cable has been shown to resist radiation better than cables with solid polyethylene insulation. The specified attenuation is 2 dB/100 ft at 250 MHz; it remains stable as long as moisture is kept from contaminating the foam dielectric.

The RF multiplexer will be based on PIN diode switches, with which SLAC has had successful experience during the past eight years. (Recent advances in the development of GaAs switches make this alternative very attractive as well. The technology actually used will depend on evaluations during the final design phase.) For the processing electronics themselves, the design for the BPMs of the Advanced Light Source at LBL will be adapted, with the operating frequency changed from 500 to 238 MHz. The ALS package includes one intelligent local controller for each BPM. Four such packages will be required for each half-sextant of each B Factory ring.

In addition, it is worth mentioning that, in contrast to the present position monitor system at PEP, the B Factory design does not require any timing signals for its operation. Even in the single-turn mode, digitization will be initiated with beam-derived triggers, as they are at SLC. This has the effect of confining triggers and timing logic to the main control room, where they will be dedicated to the injection system.

5.7.2 Bunch-by-Bunch Current Monitor

There are two compelling reasons for wishing to operate each ring with an equal population in all its bunches (with the exception of an unpopulated gap for ion clearing). First, one can imagine that the optimization of the beam-beam tune shift will be difficult in the event of nonuniform bunch currents (even though it is desirable to operate with different total currents in the individual rings). Second, equal bunch currents make it easier to control the stability of individual bunches.

This requirement places additional demands on the injection system (see Chapter 6) and suggests that a means of monitoring the intensity of individual bunches is necessary. The two key components of this monitoring system are a fast analog-to-digital converter and a programmable trigger delay generator (see Fig. 5-123). The ADC is a 500-megasample/s track-and-hold circuit, followed by an 8-bit flash converter; both units are

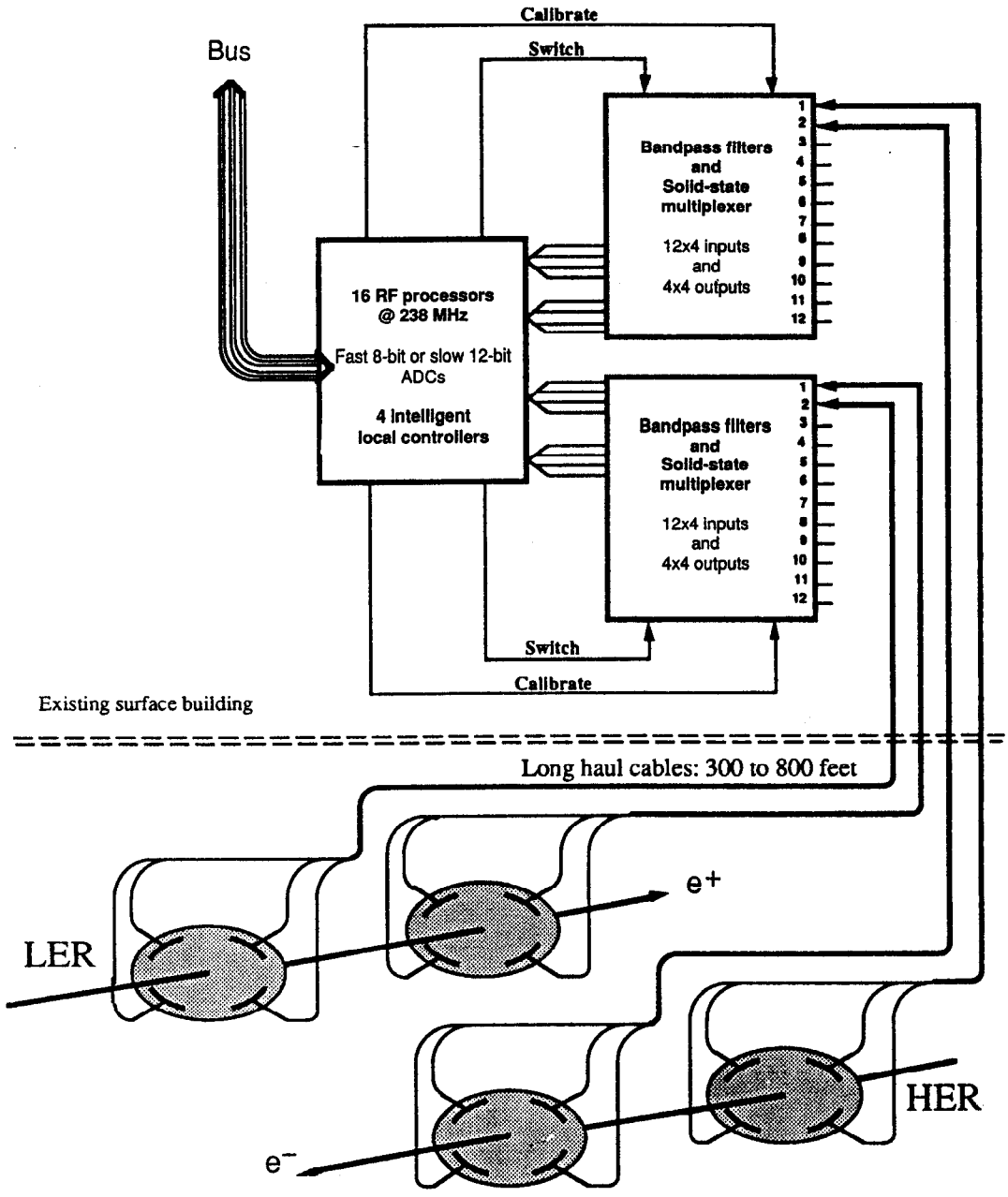

Fig. 5-122. Schematic of a single BPM subsystem, to be installed in existing I&C alcoves. For each ring, the multiplexer addresses two BPMs at a time, thus allowing single-turn measurements for commissioning or for machine physics studies.

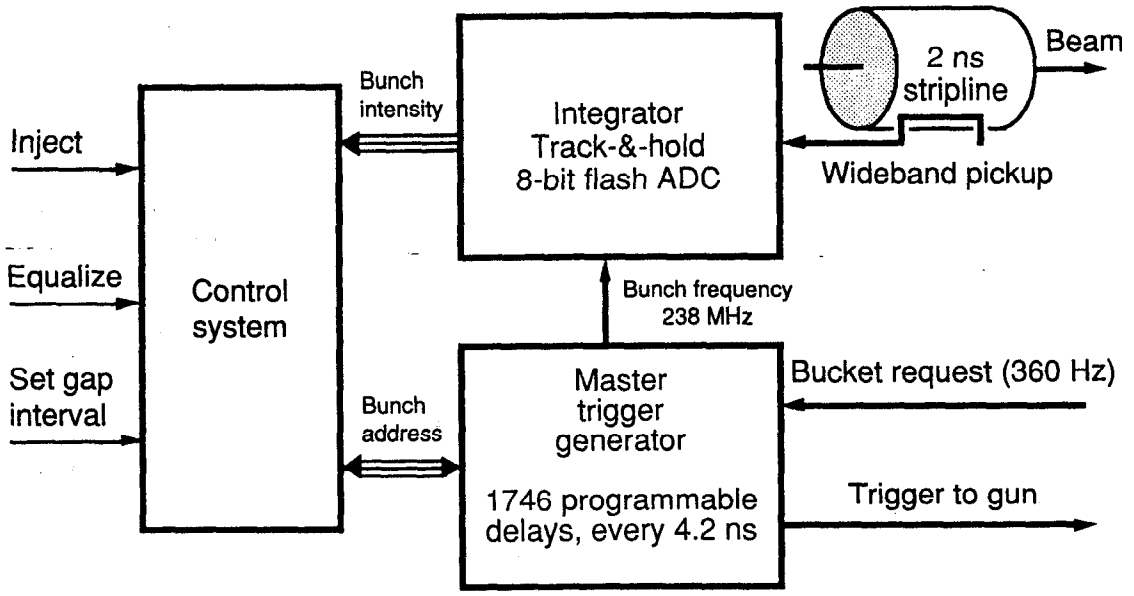

Fig. 5-123. Block diagram of the bunch-by-bunch current monitor. The injector trigger delay is programmed as a function of the bunch address.

now commercially available and sold as a single circuit board. We have evaluated this product in conjunction with the feedback system front end (see Section 5.6). This circuit can be implemented in a straightforward fashion with 100K-series emitter-coupled logic. With both bunch intensity and bunch address data, the control system should be able to devise any injection pattern and monitor its orderly development by interrupting the gun trigger at the proper time and shifting its delay to aim at the next desired bucket. The master trigger generator of PEP will be redesigned to accommodate not only the new requirements of input-output address data, but also the new RF frequency.

For the bunch intensity measurement, we expect a resolution of about 1%. (Injection is planned in steps of 20% up to 80% of full intensity, followed by 5% steps; the residual imbalance in bunch population will be kept below the 5% level.) We anticipate injection trigger jitter of about 50 ps, comparable to that at PEP; this amounts to a phase error of less than 10° at the RF frequency.

5.7.3 Feedback System to Maintain the Beams in Collision

As part of the design effort for the B Factory, we have studied means of monitoring and controlling the beams in collision. Indeed, residual orbit shifts in both rings will have to be corrected with a pair of steering dipoles on each side of the interaction point, for each beam and in both planes. Figure 5-124 depicts an open-loop method of setting these steering dipoles. The hardware normally used for the measurement of the betatron tunes is connected so as to excite one beam and detect the response of the other to this excitation. We expect a strong coupling of the beams when they are colliding; however, this method does not lend itself to automatic control.

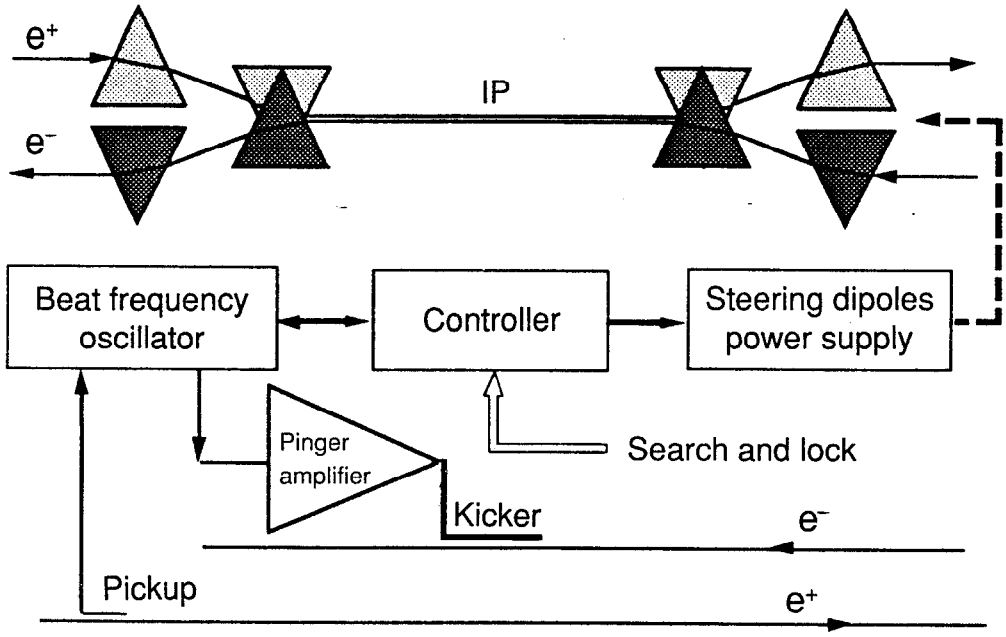

Fig. 5-124. Block diagram of a system for bringing beams into collision, based on the measurement of one beam's response to excitation of the other.

Alternately, the scheme illustrated in Fig. 5-125, involving a rapid count of Bhabha events, could be implemented. Owing to the high luminosity of the B Factory and its relatively low beam energies (the cross section for Bhabha scattering is proportional to $1/E^2$), it should be possible to monitor changes of the order of 1% in luminosity in a few minutes (for instance, at $\mathcal{L} = 10^{31}$ cm^{-2} s^{-1} and a beam energy of 14 GeV, the count rate of the PEP luminosity monitor is of the order of 30 counts per second). We envision a system whereby the beams are brought into collision with the help of a raster scan excitation of the set of dipoles for one beam. After freezing the dipole settings, the system control is then turned over to a surveillance program. After the detection of a small drop in luminosity, a "miniscan" is initiated and the dipoles are reset to optimize the collision rate.

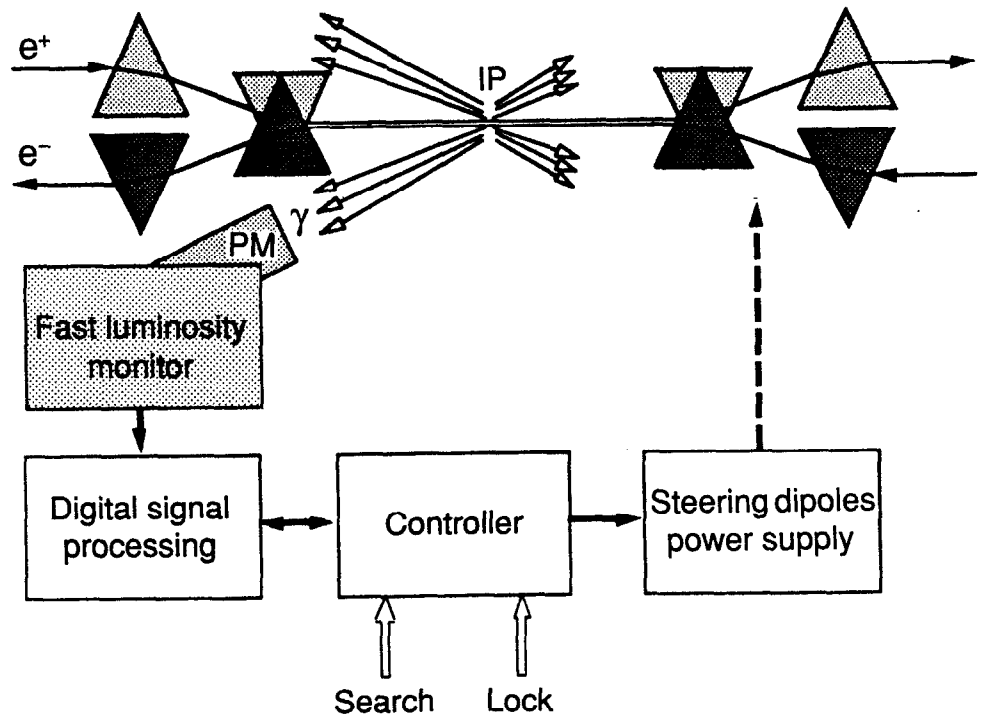

Fig. 5-125. Block diagram of a system for keeping the beams in collision, based on luminosity monitoring.

5.8 CONTROL SYSTEM

The control system for the B Factory comprises two separate systems, one for the linac injector and the other for the storage rings. The two systems are separate but closely integrated, owing to their common architecture and their hardware links.

Since the SLC linac will be used as the B Factory injector, the control system currently running the SLC facility will be retained essentially unchanged. The two injection lines (for electrons and positrons) will be operated through the SLC control system, using an SLC control console located in the B Factory control room.

The SLC control system distributes control functions among a supervisory mainframe, remote consoles for human interface, and remote microcomputers for actual hardware control. A more detailed discussion of the SLC control system can be found in Phinney [1985] and Phinney and Shoaee [1987].

The control system for the HER and LER will be new, but its design is patterned after the SLC control system (see Figs. 5-126 and 5-127). It consists of a multitiered distributed intelligence system. Supervisory control is provided by a pair of mainframes. Normally, one is used for on-line control and the other for software development and off-line monitoring. However, the second computer can be used as a backup should the primary mainframe go down. This redundancy has proved useful with the SLC and will be even more important in a facility serving as a particle "factory." Multiple workstation consoles, networked to the mainframe, provide the interface that allows operators and machine physicists to control and monitor the machine. Also connected to the mainframe are a group of microcomputers, linked by a separate, dedicated high-speed network. These microcomputers will be responsible for the actual machine-control and data-acquisition functions. The microcomputers will be logically organized on a geographical, rather than a functional, basis, thus reducing cabling costs and simplifying the software design, given the database structure described below.

The control systems for the injector and the storage rings are linked in two ways. First, the supervisory mainframes of both systems are networked to allow database exchange, hence streamlining coordination of the operating conditions of the two machines. Second, certain time-critical information will be passed directly from injector microcomputers to storage ring microcomputers via data paths already established for the SLC control system.

The storage ring control system will control and/or monitor the power supplies, vacuum system, RF system, beam position and luminosity monitors, machine protection system, and personnel protection system (status only). Based on experience at PEP, we expect this system to handle approximately 30,000 signals. The control of these functions will be governed by a run-time database in much the same way that the SLC control system now operates. The database will contain all the information needed to describe the machine, including control connections, device characteristics (for example, magnetization polynomial fits), and present configuration (for example, magnetic fields). This allows all devices of similar types to be controlled by the same software utilities, with references to different entries in the database. The database, managed by a standard relational database package, will be maintained by B Factory operations staff.

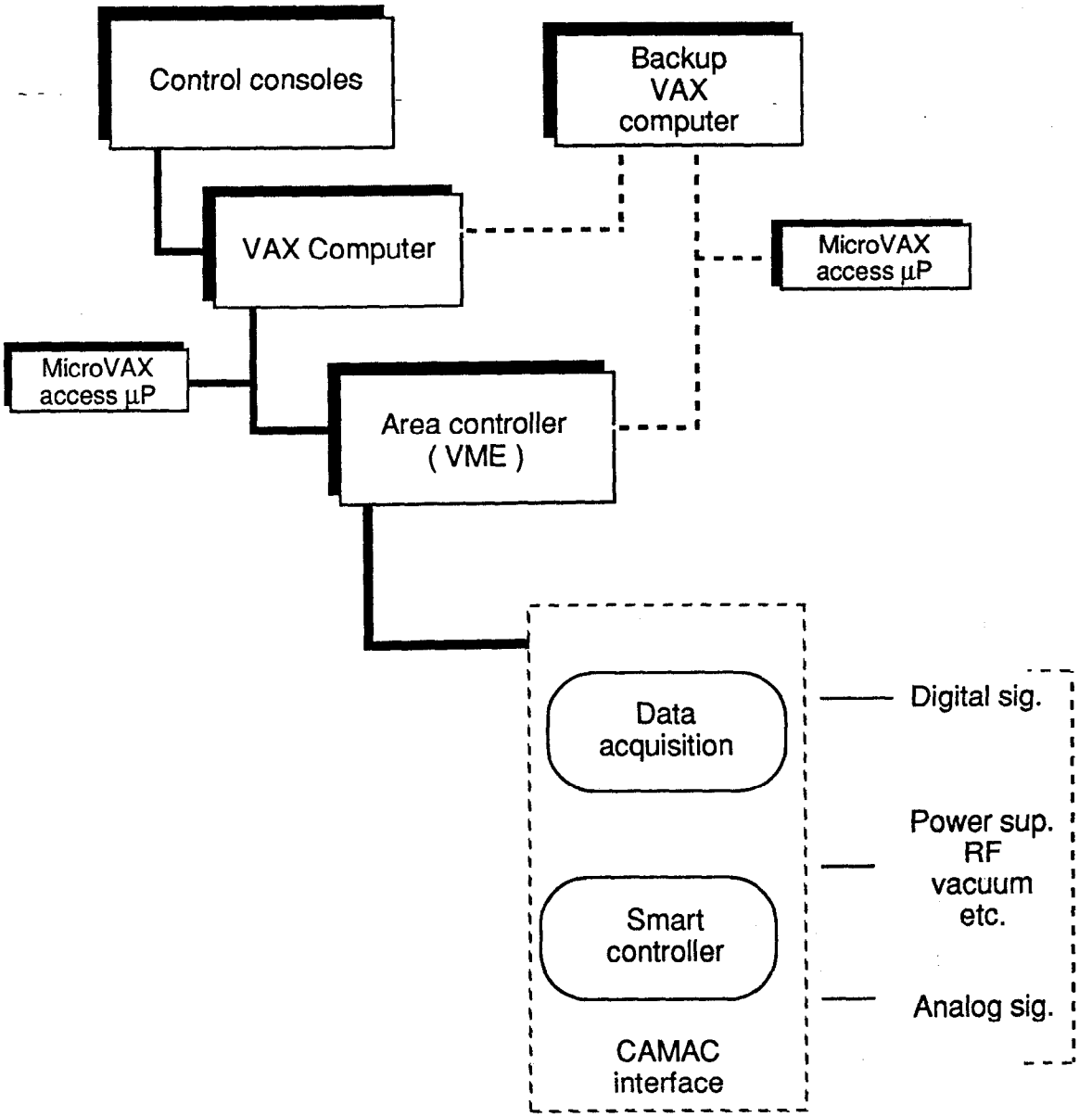

Fig. 5-126. Architecture of the B Factory distributed control system.

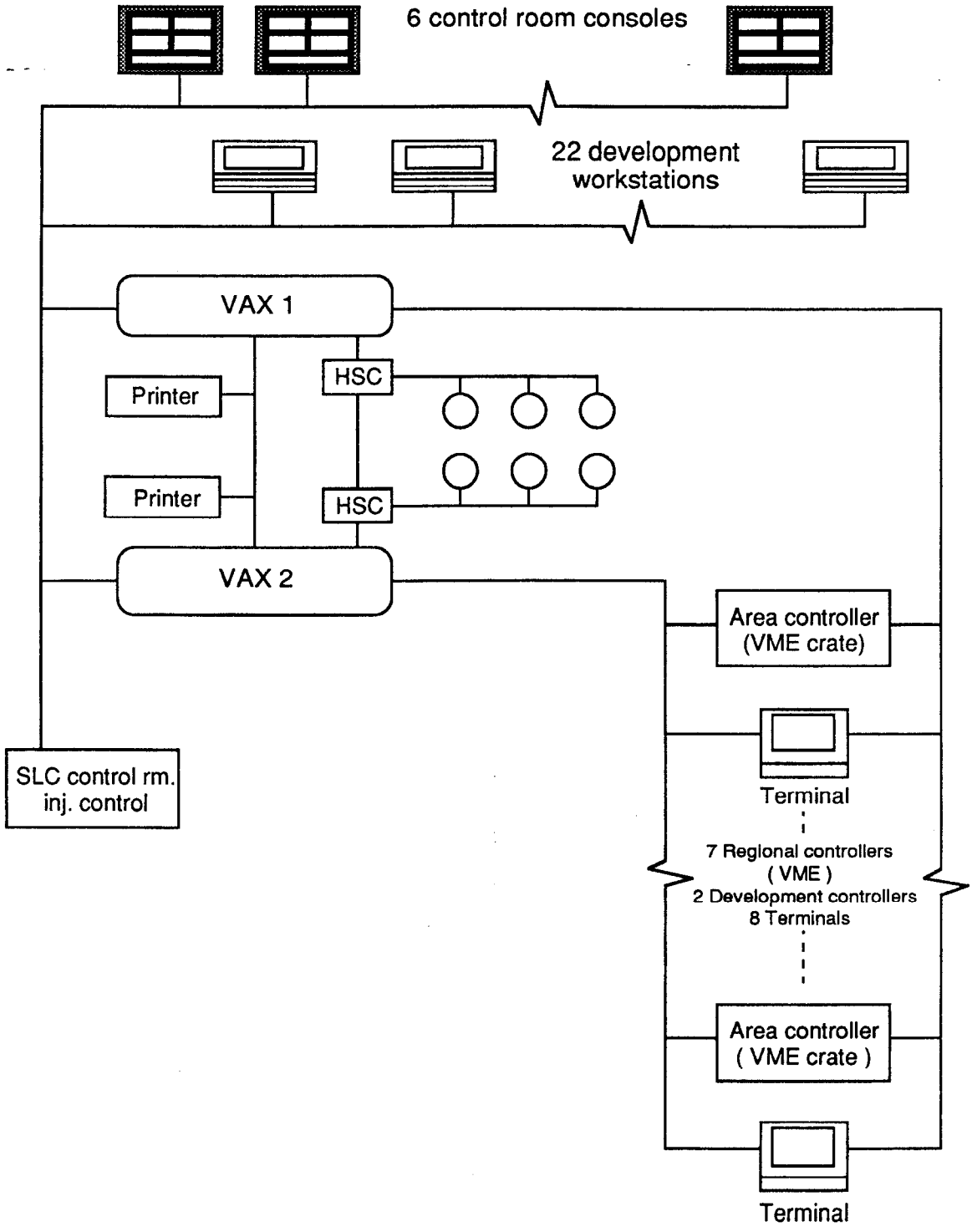

Fig. 5-127. Schematic layout for the B Factory control center.

The database-driven architecture of the control system will also facilitate the use of monitoring and analysis tools already available within the SLC control system. These include historical data regarding machine conditions and correlation analyses of multiple machine parameters. These tools have proved very important in the commissioning and running of the SLC.

5.8.1 Control Center

5.8.1.1 Consoles and User Interface. The control consoles in the control room will be developed in keeping with the philosophy that the operator interfaces must be easy and convenient to use, and must contain graphically presented information rather than a profusion of unprocessed data (see Fig. 5-128). Overview large-screen display systems having color and symbolic representations will be used to monitor machine operating parameters, operational processes and procedures, machine subfunctions, and safety systems.

These facilities will be implemented using industry standard X-Windows graphics systems, so as to separate software packages from the underlying hardware platforms. The hardware will support popular user-interface devices (track-ball, mouse, digitizing pad, etc.) and standard network and connectivity protocols, and will incorporate the flexibility needed to allow future, software-independent development.

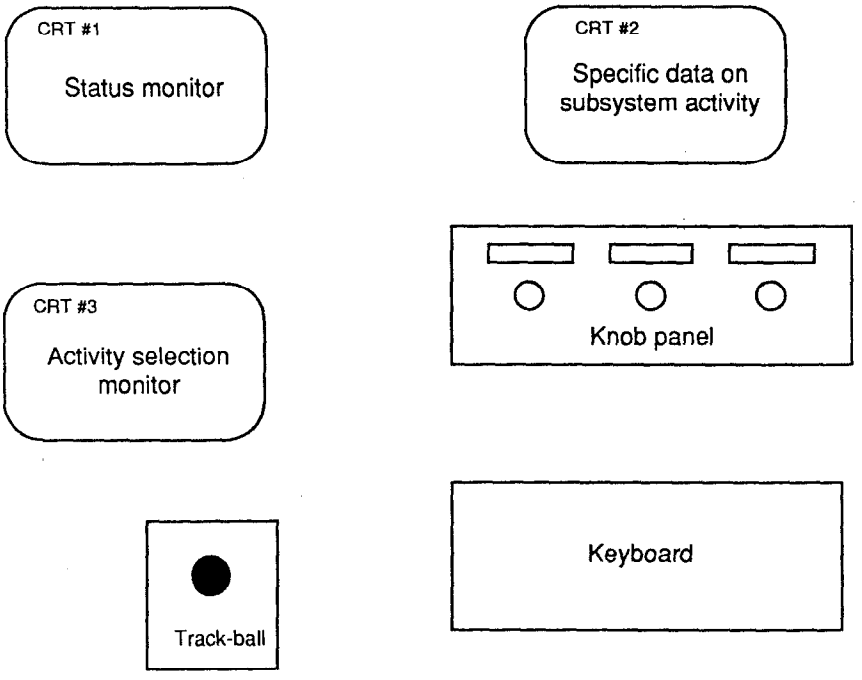

Fig. 5-128. Components of a B Factory control console.

The software will take advantage of the graphics facilities to provide symbolic representations of the machine and its elemental components. This approach guarantees that operators and other users will get a visual image of the present state of the machine. These facilities will be integrated in such a way as to be independent of the underlying hardware.

The operator-control consoles will be implemented in such a way that multiple operators can work separately or in unison on the same or related machine subsystems from identical consoles. This will require two- or three-screen consoles so that operators have a screen for data selection and one or more screens for data or status representation. In addition, summary status displays must be visible around the control room and in remote areas, so that all affected personnel are kept aware of information they need. Some consoles will be located in remote areas to aid commissioning and to provide emergency backup.

5.8.1.2 Database Facility. The database facility includes the data acquisition and control database that describes the characteristics and the operating parameters and limits for all real-time storage ring subsystems. It also includes the server functions that allow noncontrol software to collect and manipulate stored data. The database will be distributed such that local databases maintain and use local data to operate local equipment, whereas critical elements that must be available in multiple databases are broadcast across the entire computer system. This arrangement will minimize data-path bandwidth requirements between operating nodes, while maximizing local data availability, utilization, and manipulation.

These real-time databases will be built up and organized by a readily available relational database that draws on standardized device data structures and device characteristics. This approach will allow automated generation of run-time structures by personnel not familiar with the hardware and will ensure that the proper relationships exist among distributed elements of the database so as to provide updated real-time data to the right software applications on the correct hardware platforms.

5.8.1.3 Model Driver. Accelerator operation and performance will be very closely coupled to a real-time, on-line simulation model of the injector, transport lines, and accelerator optics. This has been done at the SLC, and the same model software can be adapted to the B Factory environment. The model provides expected values when the machine parameters are changed and provides a diagnostic facility when expected and actual values differ.

5.8.1.4 Program Development Facility. The software development environment will be composed of a second large VAX processor, clustered with the primary control VAX and with limited but compatible access to machine networks and systems. The program development system will have access to the operational database and accelerator facilities via the cluster, and it makes available a backup processor to operate the accelerator if the primary computer fails. This secondary operations role requires that the development machine be of similar size to the on-line machine.

The software will be written in such a way as to be database-driven and layered so that elements of the code or hardware configurations can be changed without complex or

extensive rework in the programming. To the extent possible, driver-style interfaces will be used to bridge the system to specific classes of devices or systems so that these elements can be upgraded to keep pace with advances in technology without unreasonable software modifications. Structured analysis and design tools will be used to improve the flexibility, modularity, and reusability of the code, so that generic software can be applied to a wider range of uses. These tools bridge well to modern structured languages, which provide greater software portability across hardware platforms. Software development will be accomplished on workstations with VAX compatibility. This approach makes it possible to control, test, and debug hardware and software from workstations throughout the VAX systems.

5.8.2 Control Distribution

The control system will have its processes distributed spatially and functionally. The SLC injector will continue to use its own control system and will additionally control the injector beam transport lines, while the B Factory control system will run the storage rings and their associated equipment. Consoles for the SLC system will reside in the B Factory control room. Functionally, the control processes will be distributed across the master VAX cluster, the microprocessors in the ring alcoves, and the smart controllers in the power supplies and RF systems. The VAX cluster will deal with the user interface, user analysis and data manipulation, network control, and the run-time database for all physical devices in the system. The alcove microprocessors will be responsible for data acquisition and control forwarding. The smart device controllers will deal with functional control, backup safety monitoring, and calibration of the individual devices. The processors will be linked by standard networks or custom high-speed communication links, depending on their functions. This will allow functionality to be pushed down to the level where the actual control takes place or where data are manipulated.

5.8.2.1 Computers. The centralized computer will be a large VAX-cluster paired processor, with shadowed disks for redundancy and speed. This machine will be a multiple-processor machine with 100 megabytes of main memory. The alcove microprocessors will be 32-bit diskless processors with hardware math support and approximately 4 megabytes of main memory. These units will be RAM based and will receive their systems and database-executable images from the centralized cluster or the network server, depending on the final detailed design. These units could be RISC- or CISC-based processor architectures, depending on the technology available at the time.

The device controllers will be relatively simple and can be implemented with highly integrated controller-oriented chips in either an 8- or 16-bit architecture. The controlling factor in this case will be the availability of software development and maintenance environments.

5.8.2.2 Networks. To the extent possible, general-purpose networks employed at the higher levels of the system will be standard "off-the-shelf" facilities to enhance connectivity and maximize flexibility. These networks, which could be implemented with Ethernet, are consistent with the notion that intelligence should be located where it can be useful, then laced loosely throughout a network.

Special-purpose networks will be required in some data paths, owing to particularly large data bandwidths or requirements for very fast response times. Systemwide networks will be implemented on fiber optics using standard T3 technology, while fast point-to-point links will be established with custom protocols on top of readily available transport hardware. These connections will exist at multiple levels: between large machines, between microcomputers, and between microcomputers and mainframes.

Standard networks utilize standard software, supported industry-wide across hardware platforms, and they are also layered so that the systems in general are extensible. Current technology provides a wide range of server and network-bridge functionality to permit the intelligence centers to operate at the subsystem level, without overloading the network bandwidth.

5.8.2.3 Device Interface. Device interfaces will be implemented around a layered, driver-oriented architecture, so that functional software can relate in a standard way to the driver, thus requiring no interaction or detailed familiarity with the actual physical devices. This approach will allow the use of more generic software and will allow the hardware specifics to change as the technology evolves. The system architecture will involve smart control nodes or clusters around the machine, tied to relatively less smart input-output facilities located adjacent to the equipment being controlled or monitored. Standard data conversion cards, bus structures, and communications facilities exist to support this approach.

5.8.2.4 Timing Systems and Synchronization. Software currently exists in the linac control system to operate the injector and the transport lines to the rings. Synchronizing injector beams with the fill timing of the rings will be straightforward. The timing required for kickers and BPMs already exists. Although there is no need for timing and frequency control to ramp the energy of the rings during operation (because the beams are injected at full energy), provision must be made in the system design to allow slight energy changes to tune to the exact $\Upsilon(4S)$ energy. This capability requires a facility to synchronize the alcove microprocessors and their associated control crates.

5.8.2.5 Access Procedures. Machine configuration changes, made before and after access is permitted to the machine structures and tunnels, will be controlled from the machine control rooms. This access control system will monitor and manage the hardware Personnel Protection Systems, although it will not supplant the hardware for that protection interlock system (see Chapter 8).

Specifically, the computer-controlled ring access control systems will manage the ramp-up, ramp-down, standardization, and calibration tasks associated with turning equipment off or returning it to ready status. These processes will also keep track of personnel in the tunnels during limited access periods to minimize the equipment restoration necessary for turn-on. The processor responsible for this function will be slaved to the database and control activator paths, but will be a separate physical processor, so that the main computer system can be repaired or tested without losing lockup security throughout the facility.

5.8.3 Special Control Zones

5.8.3.1 Injector. There will be two beam transport lines from the injector to the rings, one line for electrons and one for positrons. Both lines will require large numbers of quadrupole and trim magnets for optical changes and steering. All these will be controlled by existing microcomputers in the SLC control system.

5.8.3.2 Interaction Point. The interaction point requires controls to handle the superconducting focusing magnets, as well as some fast-feedback control software to maintain the beam spots at the maximum luminosity. The feedback control loops will run on an interaction area microprocessor and will implement the beam-on-beam scans to measure the beam size, as well as control the beam wiggler magnets to keep the beams in collision at maximum luminosity.

5.8.4 Control System Functionality

5.8.4.1 Problem Reporting. Fault reporting and management will be configured so that the systems identify and report the specific device that failed or indicated an unsafe condition. These faults will be monitored by a separate machine protection system (MPS) that is capable of shutting down the system. Recovery from fault conditions will be automatic.

Diagnostic panels will display equipment or computer system problems through the MPS or computer error log system and will be linked to the run-time database, so that the device or system is correctly identified and located, and the faulty characteristic or parameter described. Such faults can be automatically logged into the existing CATER maintenance-reporting system as well. This system, developed for the SLC, will be responsible for logging and cataloging faults, the urgency of repair, and the responsible support groups. This system will help ensure that support and maintenance work is done on a priority basis and that problems are not lost, only to be rediscovered later.

5.8.4.2 Data Collection and Retention. As part of the B Factory control system, history buffers will sample device status on a periodic basis, so that the configuration and status of the machine can be reviewed in detail later. Configurations can be archived for all or parts of the machine so that the machine can be restored to a known state and optimal orbits replicated.

5.8.4.3 Data Analysis. History plot facilities will be used to review trends or specific events over time. Such facilities are useful in correlating faults, detecting the onset of problems, and identifying optimal operational configurations. Correlation plot facilities will be used to correlate a wide range of data elements with one another to learn more about the interrelationships of machine parameters.

6.
INJECTION SYSTEM

THE basic method proposed to fill the B Factory rings with electrons and positrons is to use the SLC linac, including its damping rings and positron source. Given that the B Factory luminosity lifetime will be of the order of a few hours, our goal is to complete the injection cycle for both electrons and positrons within a few minutes. As will be shown below, the SLC linac (with a few modifications and simplifications) is ideally suited for this function.

By the time the B Factory is operational, it is assumed that the SLC will be nearing the end of its usefulness for high-energy physics research. Even so, it is worth noting that the modifications that will be implemented for the B Factory will not eliminate the independent utility of the SLC. For example, the straight-ahead Final Focus Test Beam area will remain usable for accelerator research. The same will be true of the traditional SLAC fixed-target areas, such as End Station A and the test beam areas. The so-called Nuclear Physics Injector (NPI), located at the beginning of linac Sector 25 and capable of producing 2- to 10-GeV electron beams at the end of the linac for nuclear physics research, will be operable simultaneously with the B Factory injection system, without any interference.

6.1 OVERALL APPROACH AND SPECIFICATIONS

The basic approach adopted for the B Factory injection system is illustrated schematically in Fig. 6-1, and the overall injection specifications and relevant parameters are given in Table 6-1. The fundamental simplification, compared with the SLC, results from the use of two bypass lines, one for nominally 3.1-GeV positrons, the other for nominally 9-GeV electrons. These positron and electron bypass lines start near the end of linac Sectors 3 and 7, respectively, and run to the end of the linac at Sector 30. Once extracted at the correct energies, the beams never reenter the linac, thereby avoiding emittance growth from wakefields in the disk-loaded waveguide and eliminating the need for deceleration (as was used for SPEAR and PEP injection). That portion of the linac downstream of Sector 19 could be used for the acceleration of other beams to higher energies, or for

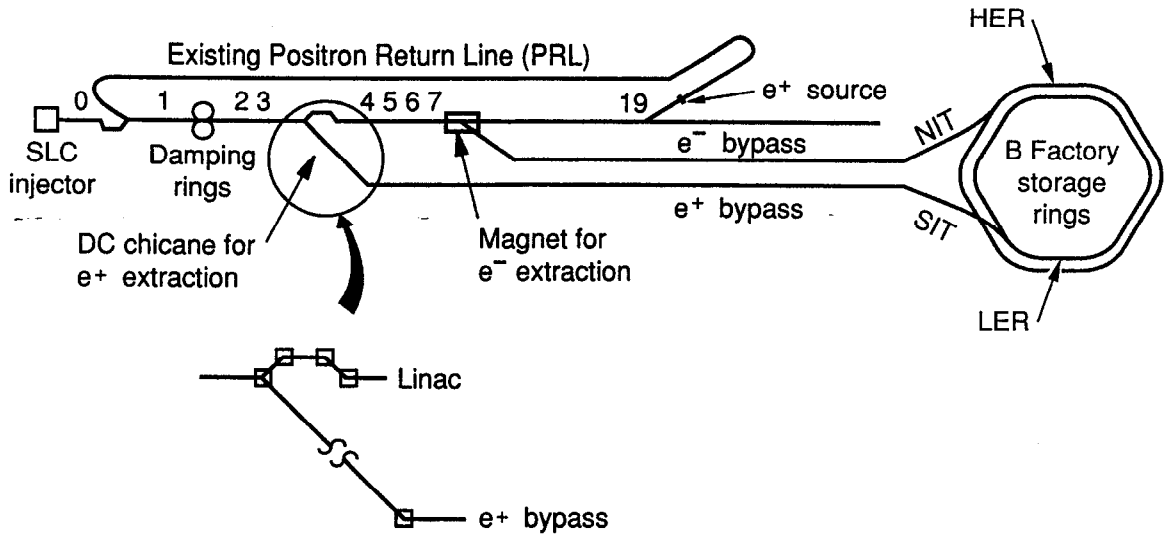

Fig. 6-1. Schematic of the B Factory $e^{\pm}$ injection system, based on use of the SLC linac with bypass lines. The numbers along the linac indicate the location (not to scale) of each sector. Each of the 30 sectors is 100 m long.

separate operation with the NPI, but will be turned off when not needed, to reduce power consumption.

The bypass lines, much like the existing Positron Return Line (PRL) from Sector 19, are located above the existing linac, suspended in the tunnel just below the ceiling. They consist of two parallel and independent FODO arrays. At the end of Sector 30, just before the beam switchyard, each bypass line is directly connected to its corresponding (north or south) injection transport line (NIT or SIT) leading to the B Factory tunnel. The existing NIT and SIT lines will undergo only minor modifications (see below). Injection into the high- and low-energy rings (HER and LER, respectively) will take place in the long straight sections of IR-10 (e^-) and IR-8 (e^+). For both the HER and LER, injection will occur in the horizontal plane, utilizing a combination of DC bumps and pulsed kickers.

The injection scenario proposed here was selected after considering other alternatives, including (i) using only the last one-third of the linac and building a new in-line positron source, (ii) using the NPI injector for electrons only, while using the SLC for positrons, and (iii) keeping a system very similar to the one now used to fill SPEAR and PEP with the SLC, where the low-energy $e^{\pm}$ beams (2.8–10 GeV) are obtained by deceleration downstream of Sector 19. Some of the reasons for ultimately rejecting these alternatives include:

- A new positron source would be very costly and would complicate the transmission of SLC-type beams to the Final Focus Test Beam or End Station A.

Table 6-1. B Factory injection specifications and parameters.

Beam energy	
High-energy ring (e^-) [GeV]	9 [range: 8–10]
Low-energy ring (e^+) [GeV]	3.1 [range: 2.8–4]
Beam current	
High-energy ring[A/10^{10} e^-]	1.48/6777
Low-energy ring [A/10^{10} e^+]	2.14/9799
Particles per bunch	
High-energy ring [10^{10} e^-]	4.1
Low-energy ring [10^{10} e^+]	5.9
Linac repetition rate [pps]	60 or 120
Linac current [10^{10} $e^\pm$ per pulse][a]	0.2–1
Invariant linac emittance [m·rad]	5×10^{-5}
Normal filling time[b]	
Topping-off (80–100%) [min]	3
Filling time (0–100%) [min]	6
Magnet standardization time [min]	15
Ring circumference [m]	2199.318
Revolution period [μs]	7.336
Revolution frequency [kHz]	136.311
Bunch frequency [MHz]	476/2 = 238
Time between bunches [ns]	4.20
Harmonic number	3492
Number of bunches[c]	1746 – 5% = 1658
Horizontal damping time	
High-energy ring [ms]	38
Low-energy ring, with wigglers [ms]	36
Low-energy ring, without wigglers [ms]	150
Nominal horizontal beam emittance [nm·rad][d]	
High-energy ring, horizontal/vertical	48/1.9
Low-energy ring, horizontal/vertical	96/3.8

[a]The SLC routinely delivers 1.5×10^{10} e^+ and 3×10^{10} e^- per bunch on each linac pulse.

[b]Electron and positron bunches are injected on alternate pulses at 60 pps, in which case both rings can be topped-off in 3 minutes.

[c]For filling purposes, the rings will be divided into nine zones of equal length. The 5% gap leaves one zone partially unfilled.

[d]Storage ring emittances are quoted here, and elsewhere in this document, as unnormalized, or geometrical, values.

- NPI-type beams, for electrons only, downstream of Sector 19 would either have bunch currents lower by two orders of magnitude (that is, about 10^8 electrons) or would require upgrading the NPI to SLC standards, a costly operation that would not, in any case, yield SLC-quality emittances without damping rings.
- Multibunch electron injection, that is, with a train of bunches 4.2 ns apart, would only pay off if the linac were not operated with SLED, so that a long pulse train of at least 200 bunches (about 840 ns) could be accelerated and stored. This would require a costly move of the NPI to about Sector 20 to obtain the required 9–10 GeV, and would mean tying up that entire part of the linac solely for this purpose. Furthermore, this approach would not permit single-bunch electron filling and would make the electron injection scheme very different from, and less flexible than, positron filling—an undesirable feature per se. Finally, this filling method is undesirable for the storage ring feedback systems, which benefit from a scheme in which the injected beam comes in small increments, as discussed in Section 5.6.
- Using the SLC in the "SPEAR-PEP" filling mode would have all the disadvantages of back-phasing the latter part of the linac and simultaneously having to handle beams of 3.1 and 9 GeV of opposite charges.

A slightly less costly implementation for the proposed bypass scheme might be to use a single, common line for both positrons and electrons beyond Sector 7. Such a scheme could be made to work with a weaker focusing system for the electrons but with twice as many correctors and beam position monitor (BPM) electronic processing systems. Moreover, it would require a second chicane at the Sector 9 junction point, larger-aperture quadrupoles and BPMs, and a method of separating the unequal-energy beams at the end of the linac into the NIT and SIT lines. These complications would likely lead to operational difficulties arising from steering and instrumentation problems. The resulting compromises would almost inevitably lead to inefficiencies and an overall decrease in the robustness of the injection system.

After considering the various scenarios, we adopted the more flexible and reliable scheme described here, with independent bypass lines. As outlined in Section 6.5, the optimum injection pattern involves "topping-off" the rings approximately once every hour, so the operational benefits of having a robust injection scheme are extremely important.

As shown in Table 6-1, the bypass lines are designed to accommodate an energy range of 2.8–4 GeV for positrons and 8–10 GeV for electrons. When filled to the nominal operating point (corresponding to the design luminosity of 3×10^{33} cm^{-2} s^{-1}), the LER will have a current of 2.14 A, or roughly 6×10^{10} positrons per bunch, and the HER will have a current of 1.48 A, or about 4×10^{10} electrons per bunch. The normal filling process will consist of topping-off the rings when the stored currents drop to 80% of these values. Thus, the topping-off operation will consist of delivering roughly 10^{10} particles to each of the 1658 bunches in each ring. For each bunch, this will be accomplished in five (nonconsecutive) linac pulses, at a rate of 60 pps. Currently, the SLC routinely delivers 3×10^{10} electrons and 1.5×10^{10} positrons per pulse to the rings. It will be extremely easy to deliver less than one-fifth of this charge per pulse to the rings.

At 60 pps (interleaved) for both e^- and e^+, the filling operation should take (1658/60) × 5 = 140 seconds, that is, less than 3 minutes.

When filling from zero (empty rings), the linac will be run with roughly 10^{10} $e^{\pm}$/pulse, and all of the 1658 bunches will be filled to about 80% of their final charge. This operation will also take about four or five linac pulses, or less than 3 minutes, to fill both storage rings; an additional 3 minutes will then be needed to top-off, giving a total filling time of 6 minutes.

Another great simplification will result from making the ring RF frequency 476 MHz (that is, exactly one-sixth of the 2856-MHz linac frequency). The drive system along the 3-km linac already operates at 476 MHz, and extending it to the B Factory (or vice-versa) will be very easy. With this choice, all the key RF frequencies (the damping rings at 714 MHz, the linac at 2856 MHz, and the two collider rings at 476 MHz) will be harmonically related. For proper spacing around the rings, every second bucket (4.20 ns apart) will be filled, giving a bunch repetition frequency of 238 MHz. With a harmonic number of 3492 (= $2^2 \times 3^2 \times 97$) and a 5% gap for ion control, there will be 1658 filled buckets. As explained later, for filling purposes each ring will be divided into nine equal "zones," of which one will be left half empty to avoid ion trapping in the HER. By filling the bunches in sequential zones, the time that elapses between each individual bucket fill will be 27.6 seconds.

In the following sections, we describe the elements of the proposed injection system.

6.2 SLC MODIFICATIONS

As illustrated in Fig. 6-1, positrons will be extracted from the linac near the end of Sector 3 and electrons near the end of Sector 7. These choices provide considerable latitude in obtaining the desired energies, as the linac can provide roughly 1.8 GeV per sector with SLED. At each extraction point, a segment equivalent to one linac girder (about 12 m) will be cleared for new equipment. The lengths of the positron and electron bypass lines are 2.7 and 2.3 km, respectively.

6.2.1 Extraction Method

To understand the pulse sequence and method of extraction from the linac, we must first review how the SLC currently functions (see Fig. 6.2a). For the SLC, two electron bunches and one positron bunch are accelerated with each linac macropulse. Two of the bunches are used for the electron-positron collisions in the SLC arcs, while the extra ("scavenger") electron bunch is used to create the positron bunch for the next pulse. To accomplish this, at 60 or 120 pps, Sectors 2 through 30 are pulsed essentially simultaneously (with just enough delay to accommodate the 10-μs particle transit time) and Sectors 0 and 1, upstream of the damping rings, are pulsed roughly 12 μs later to receive the positrons generated at Sector 19, which return via the PRL. In Sectors 2 through 19, the positron bunch comes first, followed approximately 60 ns later by the first electron bunch and another 60 ns later by the second electron bunch. Both of these electron bunches are extracted (with some difficulty) on the same pulse from the north damping ring. As mentioned, the second bunch is normally redirected by a pulsed

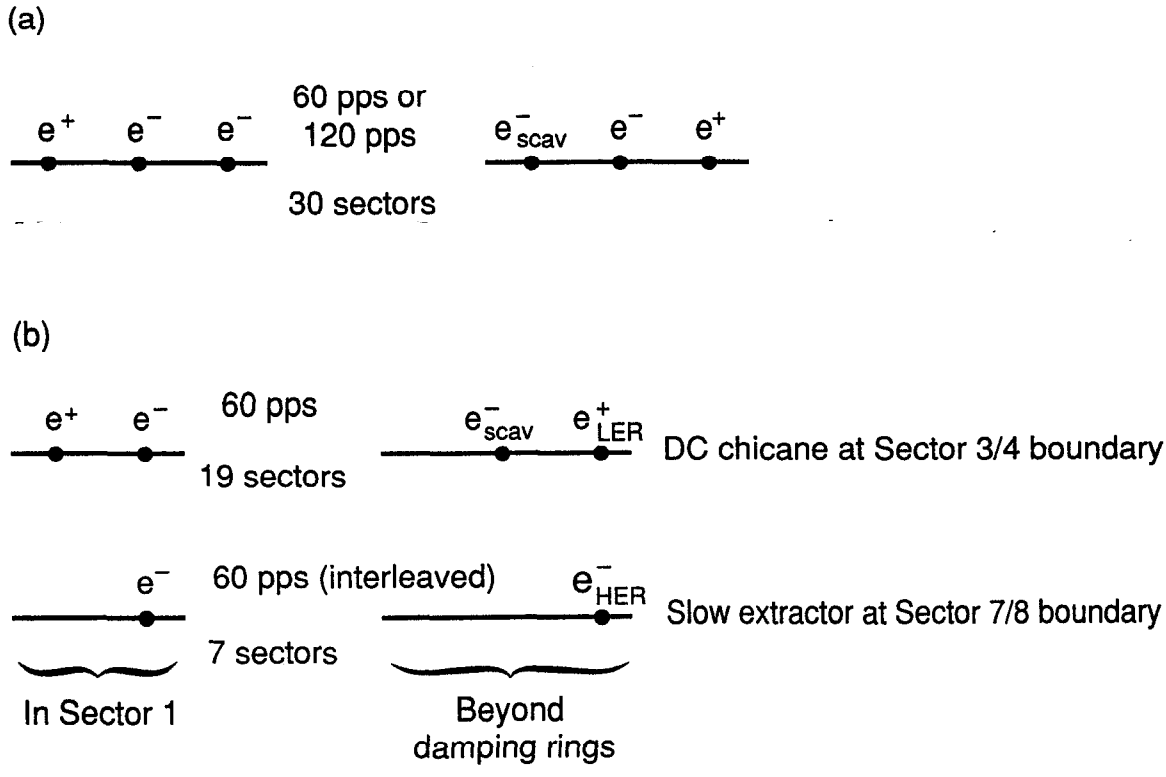

Fig. 6-2. Linac pulse and bunch sequence for (a) typical SLC operation and (b) injection into the B Factory.

magnet and Lambertson septum in Sector 19 to produce the positrons in the positron alcove, while the first electron bunch goes on to the SLC north arc. In Sectors 0 and 1, the order of the bunches is inverted (for beam-loading reasons) and the newly generated electron bunches from the injector gun are placed ahead of the bunch returning from the positron source. The spacing between the three bunches is dictated by the almost diametrically opposite positions that they occupy in the damping rings, and by the maximum appropriate distances at which they can ride on the SLED wave to acquire the proper energies in the linac.

There are a number of different ways in which the SLC pulse sequence could be modified to fill the B Factory, but probably the simplest is shown in Fig. 6-2b. Here, at the end of Sector 3, a DC chicane (see Fig. 6-1) set for an energy of about 3.1 GeV extracts the positrons and reinjects the electrons into the linac. On one 60-pps time slot, the positron bunch comes first and the second bunch is the scavenger electron bunch, which makes the positrons. (We define a 60-pps time slot as a set of 60 pulses synchronized with one 60-cycle phase. When the accelerator runs at 120 pps, it uses two such slots, equally spaced in time.) Only one electron bunch is in the north damping ring at a time, and this considerably eases the difficulty of extraction compared with present SLC operation. To let the scavenger electron bunch reach Sector 19, the pulsed magnet at the end of Sector 7 is turned off during this time slot. When the positron bunch returns via the PRL, only one electron bunch is generated at the gun and stored in the north

damping ring, while the positron bunch is stored in the south damping ring. The electron bunch is ejected from the north damping ring and accelerated to the end of Sector 7, 8.3 ms (1/120 of a second) later. This time, the extractor magnet is turned on and the electron bunch is launched into the electron bypass line. After 12 μs, the injector gun generates a new electron bunch that is stored in the north damping ring to become the next scavenger bunch, 8.3 ms later. Subsequently, the whole pattern is repeated.

Note that in this mode of injection there is no need for any new fast-pulsed magnet: The chicane is DC and the magnet at the end of Sector 7 is on and off during successive pulses. Sectors 8 through 19 run at 60 pps and Sectors 1 through 7 run at 120 pps. Total power consumption for these linac pulses is less than 10 MW AC.

6.2.2 Bypass Lines

Let us now consider the bypass lines. These are simple FODO arrays, suspended from the ceiling. We envision a pair of 4-in.-diameter beam pipes located roughly 25.5 in. above the linac. The positron bypass line reaches its final elevation in Sector 5 (approximately 32 in. to the south of the linac axis); the electron bypass line arrives at the same elevation in Sector 9 (approximately 18 in. to the south of the linac axis). To achieve this, the first chicane magnet (see Fig. 6-3) at the end of Sector 3 will be installed at a tilt of 51° with respect to the vertical. This will permit the positron beam to reach the bypass line after deflection in a single plane. A second magnet of the pair (see Fig. 6-1) straightens out the beam in the line. Meanwhile, three similar magnets bend the electron beam back and reinsert it into the linac. At the end of Sector 7, two pulsed magnets extract alternate electron bunches at 35° with respect to the vertical (see Fig. 6-3). (These magnets will be very similar to the 40 PM1 and 40 PM2 magnets now used for PEP.) The pulsed magnets are followed by a DC dipole to increase the upward kick and a slightly stronger DC reverse-bend magnet to direct the electron beam into its bypass line.

The bypass lines will be fabricated from 4-in. seamless aluminum tube with stainless-steel transitions at the ends for flanges. The 4-in.-diameter tube provides sufficient pumping conductance, but every 50 m it is necked down to about a 1-in. diameter to allow for small-bore quadrupoles. Where the two lines are parallel (from Sector 9 through 30), they are cross-connected for common pumping. For each line, every 100-m length (one FODO cell) has two quadrupoles, two BPMs (each with a readout in a single plane), two corresponding correctors for steering, and one 120-L/s pump. Isolation valves and roughing connections are provided every 200 m. Matching quadrupoles at both ends of the bypass lines need individual power supplies, but in the long FODO array, the quadrupoles are powered in series, in two strings each, to reduce costs. Profile monitors are provided to check emittance and beam shape along the way. A list of bypass line components is shown in Table 6-2. Relevant beta and dispersion functions for the positron beam, as it is extracted from the linac and injected into the bypass line, are shown in Fig. 6-4. The corresponding functions for the electron beam are similar.

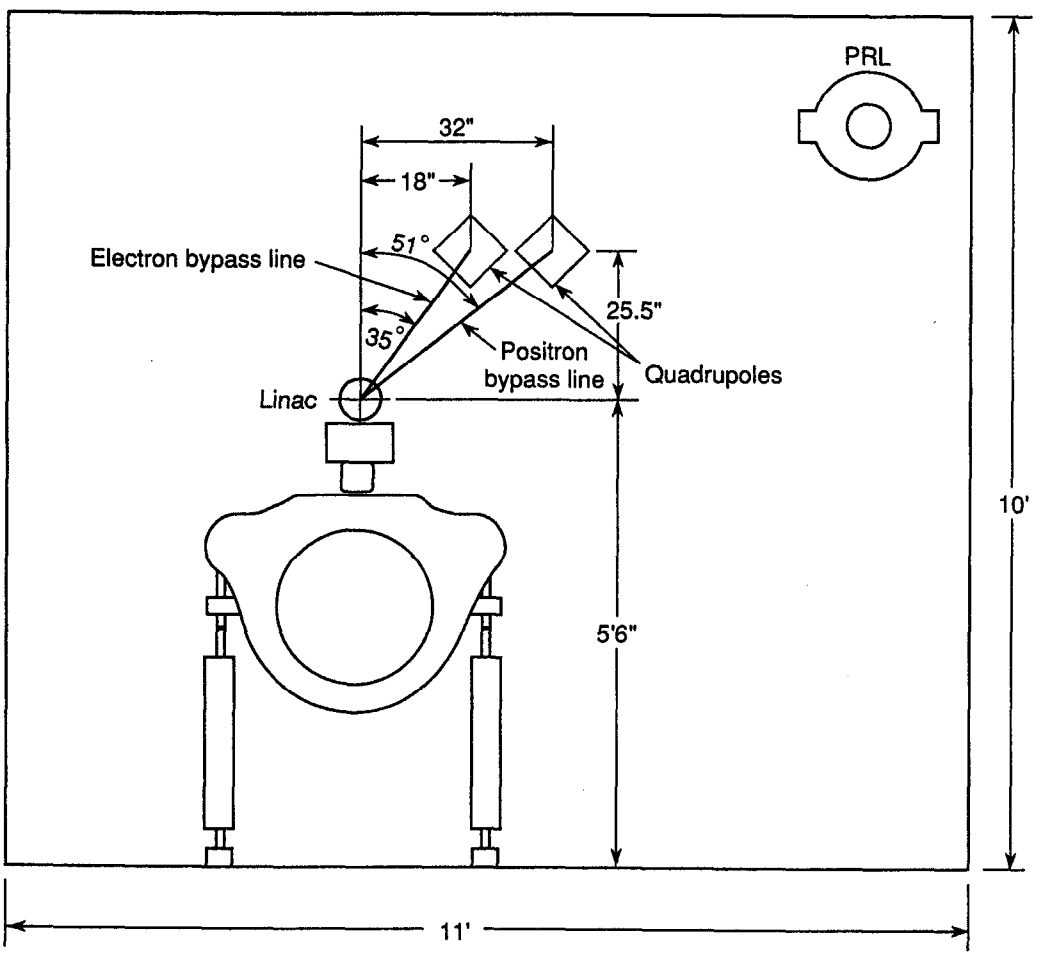

Fig. 6-3. Cross section of linac housing showing the location of the electron and positron FODO array quadrupoles. Note the tilts of the extraction planes.

Table 6-2. Linac bypass line components and specifications.

	Positron line	Electron line
Length [km]	~2.6	~2.2
Energy [GeV]	2.8–4	8–10
No. of quadrupoles		
Matching	24	24
FODO array	52	44
Steering correctors	64	56
Beam position monitors	64 (32 readouts)	56 (28 readouts)
Profile monitors	2	2
Pumps (120 L/s)	29	23
Vacuum roughing connections	29	23
Fast valves	1	1
Isolation valves	14	13

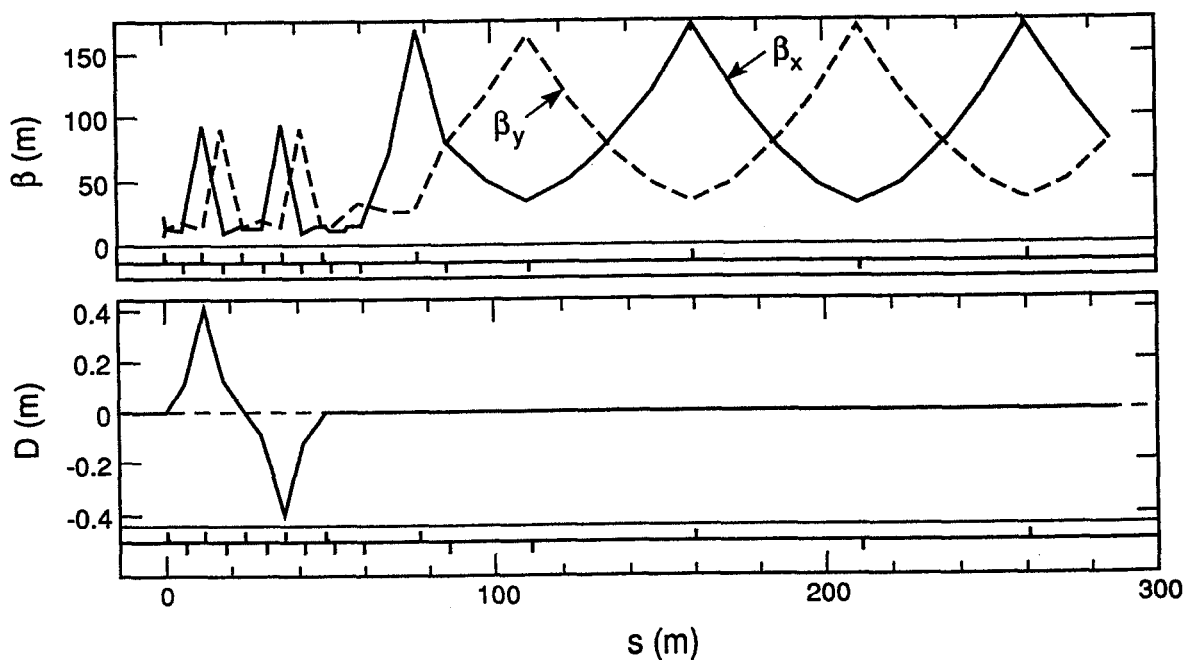

Fig. 6-4. Optical functions β_x, β_y, and D in the first magnet of the chicane, the diagonal extraction line, the matching section, and the first 200 m of the bypass line.

6.3 UPGRADE OF THE NIT AND SIT LINES

Except for a few modifications and improvements, the existing NIT (e^-) and SIT (e^+) lines, shown in Fig. 6-5, will be used in their entirety. At the end of Sector 30, the in-line equipment used for PEP will be removed and the bypass lines connected to the NIT and SIT lines upstream of the existing B3 magnets. Three new DC dipoles in each line are necessary to obtain the proper bends upstream of the B3 magnets, and these will be slightly rotated to align the beam trajectory properly.

We now briefly review the NIT and SIT optics, the magnets and power supplies, the instrumentation, and the vacuum systems.

6.3.1 Optics

Figure 6-5 indicates the arrangement of bending magnets, focusing magnets, and instrumentation elements for the identical NIT and SIT lines. Each consists of 11 bending magnets (of which B1 and B2 will be replaced) and 24 quadrupoles, making up three 360° achromats (the first two in the horizontal plane, the third in the vertical plane). The beam transport system is designed to accept an energy spread of ±0.8% and has a momentum resolution of better than ±0.1%. The design apertures are ±25 mm for the horizontal good-field region in the quadrupoles and ±10 mm vertically. The periodic FODO array is designed for a phase shift of 90° per cell.

When the lines were properly set up for PEP, beam transmission and monitoring presented no major difficulties. One improvement that will be implemented for the B Factory is to install additional BPMs (see below) at the end of each bypass line and to use feedback to correct the beam position and angle at that point. If the beam then moves in the Q4 dispersive region, it will be because of energy drift and jitter, which will be corrected separately. Currently, because the lines are achromatic at the injection septum, energy jitter in the linac does not move the beam (and thus cannot be discerned) at that point. Injection into the HER and LER, much like PEP, will likely be quite sensitive to linac energy variations, and it will clearly be beneficial to observe beam energy drift or jitter and to correct it.

Since injection into the HER and LER will take place in the middle of IR-10 and IR-8, respectively, the ends of the NIT and SIT lines will be extended about 40 m from their present termination points, and four additional quadrupoles (similar to the existing ones), with corrector windings and built-in position monitors, are added. The elevations of these parts of the NIT and SIT lines will be somewhat different from those of the present layouts, because the elevations of both the HER and LER will differ from that of the present PEP ring.

6.3.2 Magnets and Power Supplies

Details of the magnets can be found in the Injection Section of the *PEP Design Handbook* [1977]. The present injection line magnets can be used without modification,

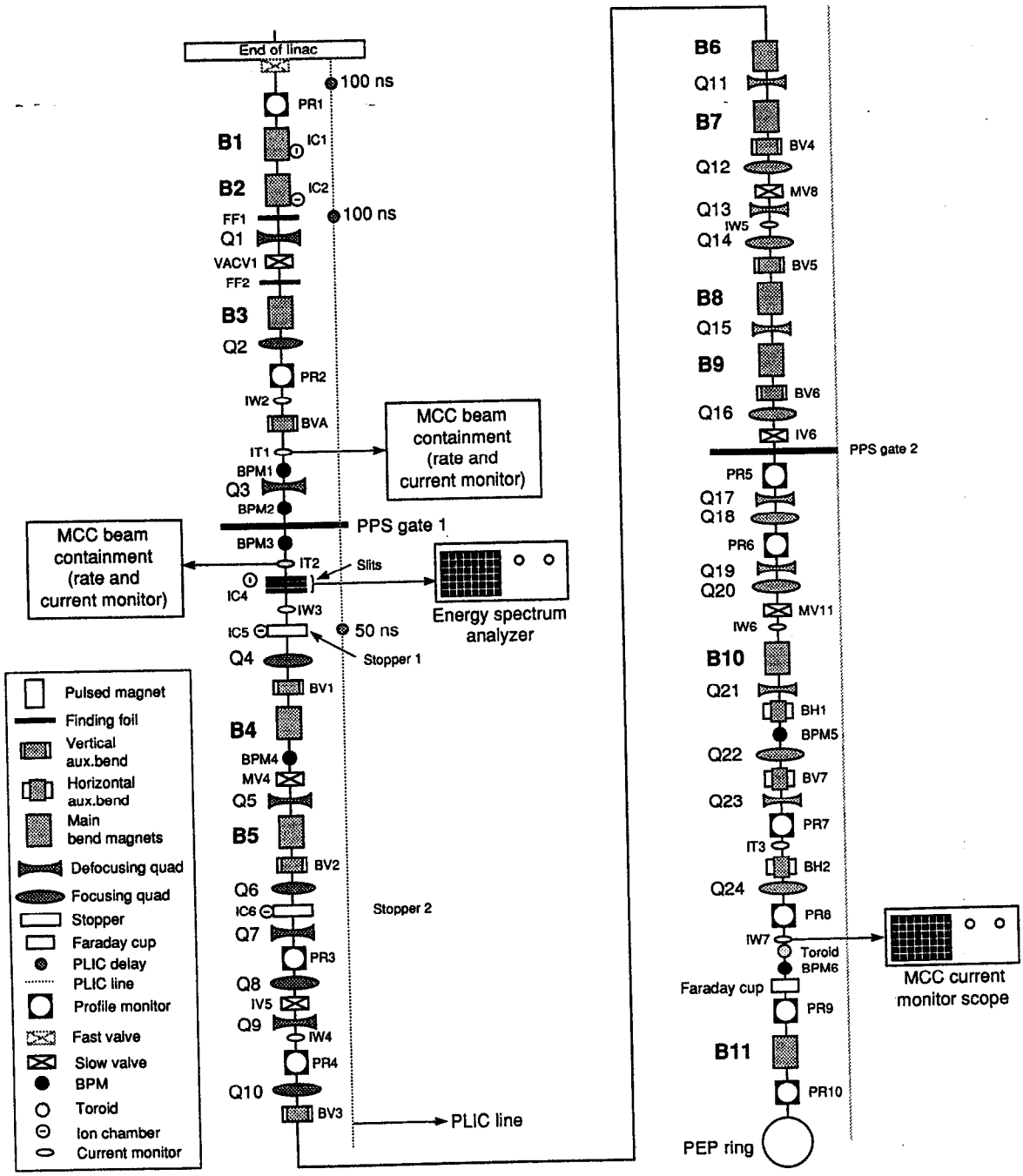

Fig. 6-5. Schematic layout of the identical NIT and SIT lines. For the B Factory, magnets B1 and B2 will be replaced.

but they must be slightly repositioned. The present power supplies will be upgraded, and their control, presently performed by a PDP-11 system, will be switched to a modern unified control system.

6.3.3 Instrumentation

Most of the instruments shown in Fig. 6-5 are satisfactory and will remain in place. Originally, beam position and shape were measured at 10 locations along each injection line, using scintillation screens. Over the past few years, six additional SLC-type stripline BPMs, also indicated in Fig. 6-5, have been installed in both the NIT and SIT lines. These BPMs are considerably larger than the standard SLC BPMs, but they use the same readout electronics. The first four BPMs are located in the region of maximum dispersion, and the last two are located close to the injection septum to allow both (x, x') and (y, y') to be determined for the beams just before injection into the rings. To implement the improvements in monitoring capability referred to above, and thus to achieve better overall control of the orbits, an additional 10 BPMs will be installed in each line, located in or near the quadrupoles; these provide beam position information approximately every 90° in betatron phase. Beam current is now measured by toroids installed in the NIT and SIT lines, as shown in Fig. 6-5. The operation of these devices is satisfactory, and they will be retained.

6.3.4 Vacuum Systems and Beam Pipes

The vacuum systems and beam pipes for the NIT and SIT lines are described in the *PEP Design Handbook* [1977]. The present design produces a pressure of about 100 nTorr, which has proved satisfactory in all respects.

6.4 INJECTION INTO THE HER AND LER

In contrast to the single PEP ring, for which the injection lines come down vertically into the plane of the ring and are tangent to the inside, the HER and LER injection lines will be brought down on the outside of the two rings—into the plane of the HER at IR-10 and into the plane of the LER at IR-8. The method of injection we have adopted is very similar to the one used in PEP. It assumes $\beta_x = 80$ m and $\beta_y = 20$ m in the 40-m-long injection regions, as shown in Fig. 6-6 and described in Section 4.1.

Horizontal injection occurs as shown in Fig. 6-7. The closed orbit of the stored beam is distorted by means of four DC bump magnets (not shown) and three kickers. Details of the horizontal phase space (x, x') for the stored and injected beam are shown in Fig. 6-8 at three consecutive points in time following the turn-on of the DC bump magnets:

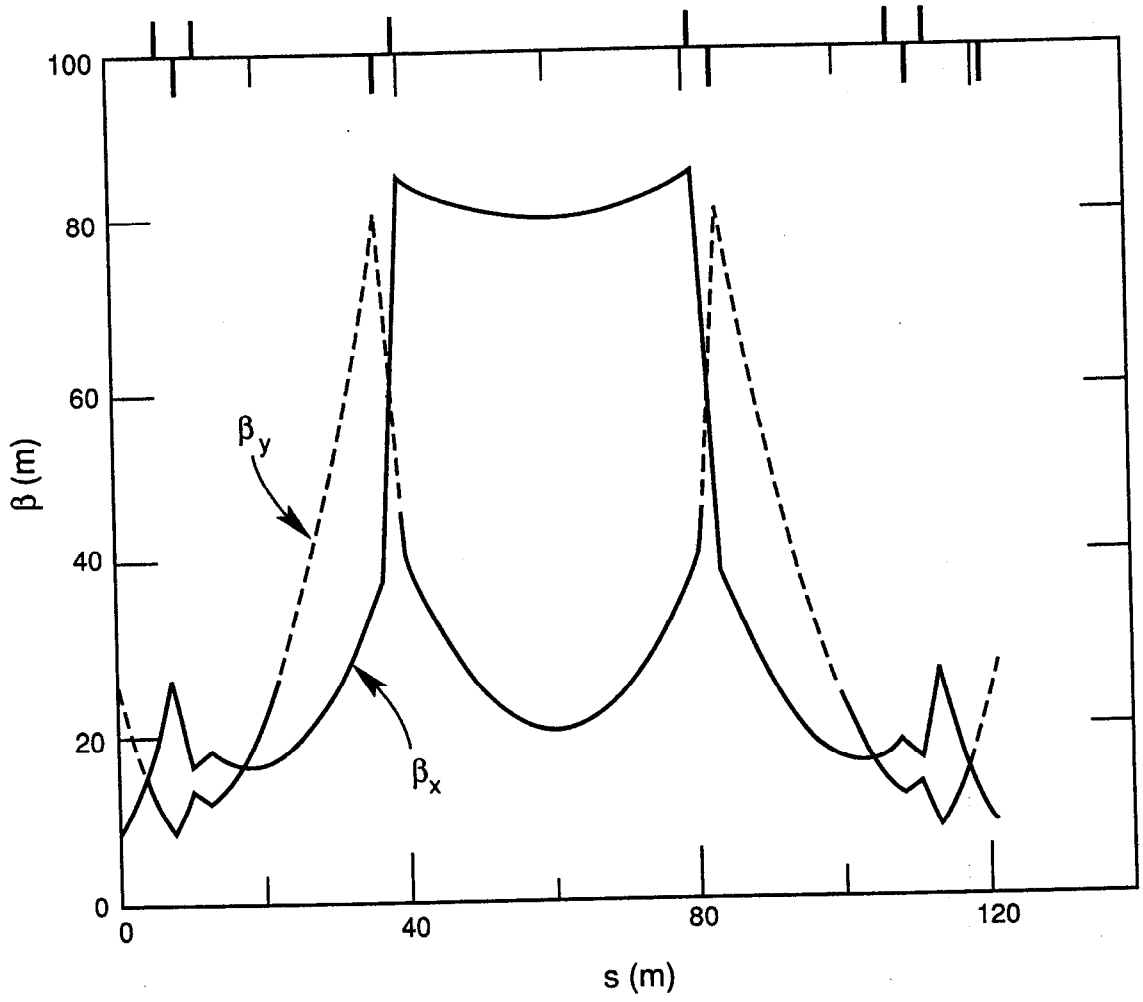

Fig. 6-6. Twiss parameters β_x and β_y in the injection straights of the HER or LER.

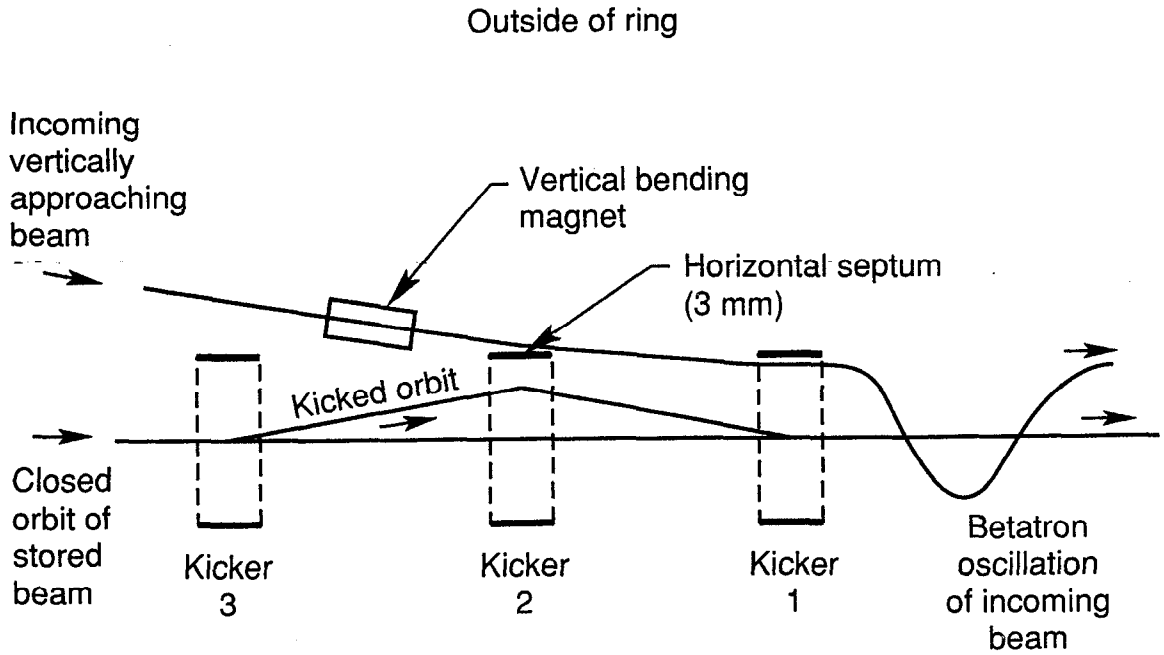

Fig. 6-7. Schematic of the horizontal injection scheme (DC bump magnets not indicated), showing closed and kicked stored orbits, and incoming injected beam (HER or LER). Note that kicker 2 kicks the stored and injected beams in opposite directions.

(i) Stored beam is moved to DC bumped position, $10\sigma_x$ away from the inner edge of the 3-mm septum.

(ii) Stored beam is kicked within $6\sigma_x$ of the septum inner edge; incoming beam from the linac is tangent to the stored-beam orbit and within $2\sigma_i$ of the outer septum edge.

(iii) Four turns later, the stored beam is back to its DC bumped orbit; the incoming beam is inside the ring within $2\sigma_x$ of the inner septum edge, ready to damp and merge with the stored beam.

In Fig. 6-8, it is assumed that the injected beam has $\beta_x = 30$ m. As shown in Fig. 6-6, in the vertical plane, the beams go through a waist. Typical characteristics of the kicker magnets and their power supplies are summarized in Table 6-3; these parameters will be optimized during the detailed design stage of the project.

For injection purposes, each ring is divided into nine "zones" of equal length. A zone has a length of about 244 m (or 815 ns) and contains 194 bunches. One of these zones in each ring will remain about half empty to leave a gap for ion control. We describe here the process for filling the LER at a 60-Hz rate; the HER is filled in a similar way. The transverse damping time for the HER is 37 ms. If the damping contribution of the wigglers in the LER is ignored—a worst-case situation in terms of injection—then the LER has a damping time of 150 ms.

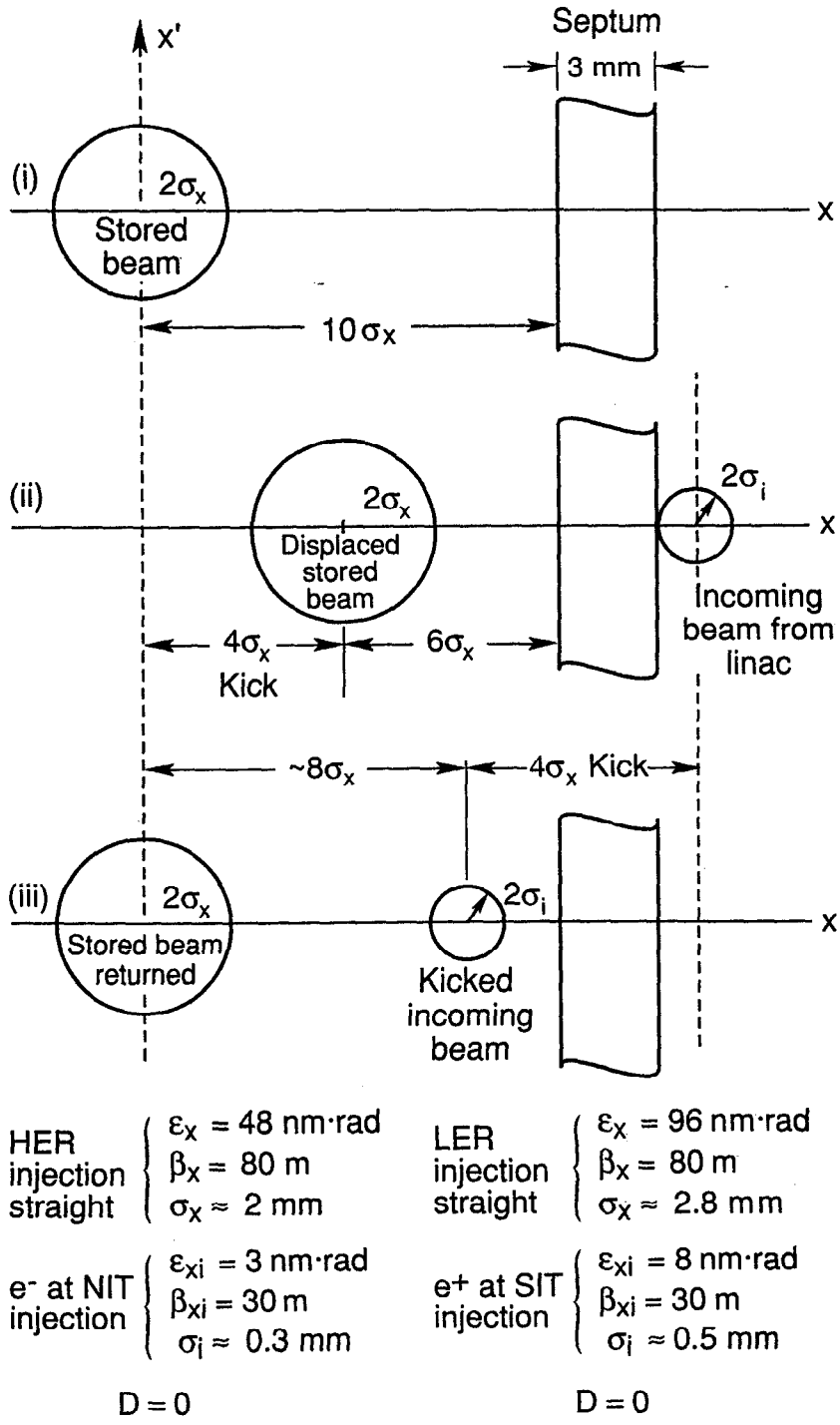

Fig. 6-8. Horizontal transverse phase space (x, x') of stored and incoming beams during three successive steps of the injection process (HER and LER). The position of the stored beam is shown after it has been moved to the right by roughly 0.5 cm by the DC bump magnets. The diameters of the stored and incoming beams are not drawn to scale.

Table 6-3. Examples of characteristics of K1, K2, and K3 kicker magnets and pulsers.

Aperture dimensions (cm)	Total inductance[a] (μH)	Length (m)	Damping (Ω)	Current, I_{max} (kA)	Voltage (kV)
Magnet:					
LER K1 or K3					
6.4 × 6.4	0.93	1	7.5	0.57	5.8
LER K2 (septum)					
6.4 × 6.4	1.56	2	12.5	0.57	9.7
HER K1 or K3					
4.8 × 4.8	0.93	2	7.5	1.1	11
HER K2 (septum)					
8 × 8	1.56	4	12.5	1.1	18.2

[a]Kicker is housed in a pipe of radius r equal to aperture width. Connections inductance, assumed to be 0.3 μH, is included. The connections inductance does not enter into the magnetic field calculations.

As shown in Fig. 6-9, the beginning of each zone is determined by the time onset of the kicker current pulses. All three kicker pulsers are identical, consisting of critically damped RLC circuits that rise and fall to practically zero within less than 1500 ns. The first bucket to be filled in zone n is located roughly 200 ns after the beginning of the kicker pulse so as to ride on the flat top where sensitivity to time jitter is minimized. Since the rise time of the pulse is much shorter than the fall time, bunches recently stored in zone $n - 1$ are unaffected. Bunches in zone $n + 1$ (at least 815 ns later) are kicked slightly, but since they have been in the ring for the longest time, their orbits are almost fully damped, and, to the extent that the kickers are matched, these bumps are closed. Thus, single buckets in zones 1 through 9 are filled in succession, after which, 9 times 1/60th of a second, or 150 ms, later (that is, one damping time in the LER in the absence of wigglers), the next adjacent buckets (4.2 ns later) in each zone are filled, and so on. With this method, damping in the LER, even without wigglers, is adequate.

The entire filling sequence of the 1658 bunches will be computer controlled and automated. Computer control of the process, in conjunction with the proper triggers (synchronized through the 476-MHz clock and countdown electronics) will be simpler and more straightforward than that in PEP, where the RF frequency is not harmonically related to that of the linac.

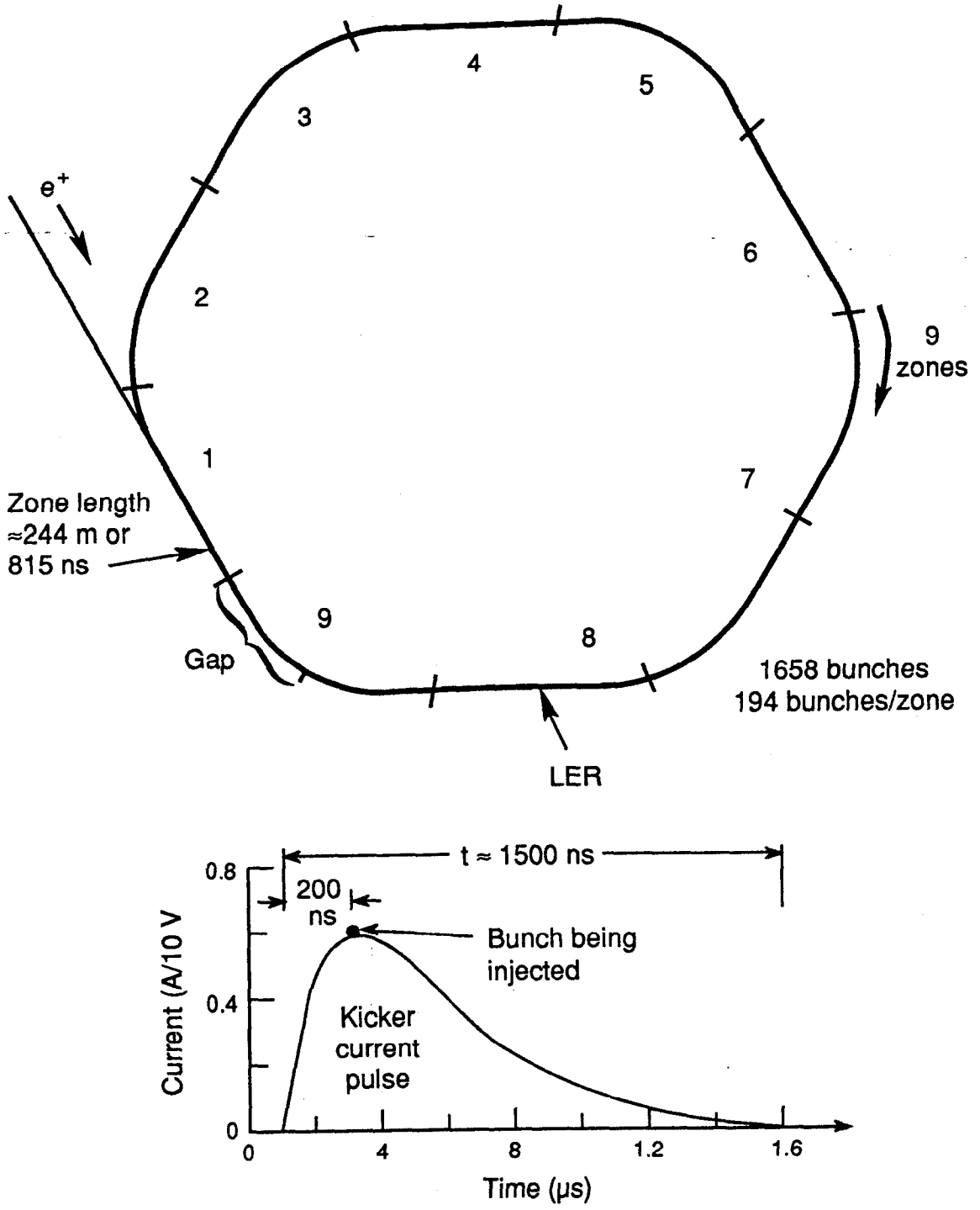

Fig. 6-9. Azimuthal zone filling sequence for the LER, showing nine zones. The kicker current pulse shown (equal for all kickers) was computed by assuming a charged, critically damped RLC circuit [$R = 2\,(L/C)^{1/2}$] in which the current reaches its maximum at $t = 2\,L/R$ after a thyratron is fired and allows the circuit to be discharged.

6.5 OPTIMUM TIME BETWEEN FILLS

As part of the design for the injection system, it is useful to estimate the optimal time between injection cycles (fills). By "optimal" we mean the filling pattern that maximizes the average luminosity. Clearly, this optimal value depends on the time course of the luminosity following injection, which will be determined to some extent by the details of storage ring operation. Still, it is useful here to get a sense of the likely interval between fills. Our assumptions, stated below, are intended to err on the side of conservatism, thus yielding a worst-case estimate (smallest value) for this interval. In particular, we have taken a simple model in which the bunch sizes do not vary with time. The appropriate luminosity formula is then

$$\mathcal{L}(t) = \frac{N_{b1}(t)N_{b2}(t)n_{bi}f_i}{2\pi\sqrt{(\sigma_{x1}^{*2} + \sigma_{x2}^{*2})(\sigma_{y1}^{*2} + \sigma_{y2}^{*2})}} \tag{6-1}$$

All time-dependent terms are indicated explicitly in Eq. 6-1. The σ_{xi}^* and σ_{yi}^* are the transverse rms spot sizes at the interaction point (IP). We assume here that

- Bunches are distributed such that every bunch meets an opposing bunch at the IP. Thus, $n_{b1}f_1 = n_{b2}f_2$ is the bunch collision frequency, where f_i is the revolution frequency and n_{bi} is the number of bunches for beam i.
- All bunches in a given beam have the same number of particles (N_{bi} for beam i).
- Any modifications to the above formula from beam-beam considerations, finite bunch lengths, and nonzero crossing angles are independent of time.

To the extent that the individual beams decay according to exponential decay laws, the luminosity will also decay exponentially, and the desired optimization is straightforward. However, the beams are not expected to decay in a purely exponential way. For example, in beam-gas collision processes, the loss rate is proportional to the gas pressure, which in turn depends on the beam current. For the present calculations, we make the pessimistic assumption that the pressure does not decrease as the current decreases. Then beam-gas losses yield an exponential time dependence. In addition, beam-beam scattering losses, notably $e^+e^- \rightarrow e^+e^-\gamma$ do not give an exponential luminosity dependence. However, it can be shown [Porter, 1990] that if we make the exponential approximation, with a time constant given by the exact $1/e$ decay time, then the error is at most a few percent for times of interest to us. Thus, we start with a luminosity that depends on time according to

$$\mathcal{L}(t) = \mathcal{L}_0 e^{-t/\tau} \tag{6-2}$$

The decay time τ is dominated in the present design by the bremsstrahlung and Coulomb beam-gas scattering. Including these and additional losses due to beam-beam bremsstrahlung and elastic scattering, and those due to Touschek scattering, gives $\tau = 1.9$ hr, with the assumptions discussed above.

The scenario we envision is that a data-taking period T for the experiment is long compared with the injection time and the stored-beam time (that is, there are many such fills in a data run). In this case, it is sufficient to replace the actual distribution of injection times with a single average injection time, which we call t_I. We further assume that we take data for a fixed time interval t_c following injection, prior to beginning the next injection, and that each fill begins with the same initial luminosity ($\mathcal{L}_0$). Finally, we assume that no useful data are accumulated during injection. Given this scenario, we wish to find the optimal value for t_c.

The total integrated luminosity accumulated during our data run is given by

$$\int_0^T \mathcal{L}\, dt = n \int_0^{t_c} \mathcal{L}_0 e^{-t/\tau}\, dt \tag{6-3}$$

where $n = T/(t_c + t_I)$ is the number of injection-coast cycles in the run. The ratio of the actual integrated luminosity to that obtained if the machine were capable of running the entire time at its peak luminosity is then

$$\frac{1}{\mathcal{L}_0 T} \int_0^T \mathcal{L}\, dt = \frac{\tau}{t_c + t_I}\left(1 - e^{-t_c/\tau}\right) \tag{6-4}$$

This quantity (and hence the actual integrated luminosity) is maximized when t_c is chosen to satisfy the condition

$$\frac{t_c + t_I}{\tau} = e^{t_c/\tau} - 1 \tag{6-5}$$

Thus, the maximum average luminosity possible is

$$\langle \mathcal{L} \rangle_{\max} = \mathcal{L}_0 e^{-t_c/\tau} \tag{6-6}$$

with t_c given by Eq. 6-5.

For simplicity, we assume that the injection time required is independent of the coast time t_c. For our parameters, this is a good approximation. Thus, we assume a fixed injection time of six minutes: approximately three minutes of overhead to change both accelerator and detector states between injection and stored-beam conditions, plus about three minutes for the actual top-off.

Solving Eq. 6-5 then gives an optimal time between fills of about 35 minutes. This yields an average luminosity of 74% of the peak luminosity. We note that the injection conditions are nearly optimum over a rather broad range; changing the stored-beam time from its optimal value of 40 minutes to 60 minutes reduces the average luminosity by only a few percent. It is somewhat more important to keep the injection time small; increasing the average injection time to 10 minutes reduces the average luminosity to 68% of its peak value.

6.6 SUMMARY

With minor modifications, the SLC linac will serve as a well-optimized and powerful injector for the B Factory. The ability to fill the storage rings rapidly will be of great benefit not only for the operational stage, but also for the earlier commissioning stage in which the vacuum chamber walls must be scrubbed by synchrotron radiation. As discussed in Section 5.6, there are also advantages to the single-bunch filling scheme adopted here. This approach lessens the power demands on the feedback system, which might otherwise be dominated by considerations of injection jitter.

7.

CONVENTIONAL FACILITIES

SINCE the B Factory will occupy the existing PEP tunnel and make use of the existing SLC linac, no conventional construction is required. However, modifications will be necessary to mechanical and electrical facilities, as described below. This chapter also describes necessary removals, including the steps to be followed in disassembling and refurbishing the magnets. Finally, in Section 7.2.3, the installation procedure for the new facility is given in broad outline.

7.1 SITE AND UTILITIES

7.1.1 PEP Buildings and Underground Structures

The PEP conventional facilities consist of all beam housings (bored and cut-and-cover tunnels), research halls, support buildings, roads, earthwork, fencing, landscaping, AC power, mechanical utilities, and sewers and drainage facilities (see Fig. 7-1). The only changes to these facilities that will be needed to accommodate the B Factory are modifications of the cooling water system and the electrical distribution system.

An Environmental Impact Statement (EIS) for PEP was issued by the Energy Research and Development Administration in 1976. There will be no changes to the PEP conventional facilities that will affect the conclusions of the PEP EIS.

The PEP tunnel, above-ground structures, and utility structures were designed to withstand a major earthquake. Accordingly, they are expected to suffer only minor or moderate damage in an earthquake that will cause widespread devastation in the surrounding region [Savage, 1990, and references therein; Earth Sciences Associates, 1982]. The earthquake on October 17, 1989, which was not very severe locally, caused no damage to the PEP tunnel, buildings, or utilities. There was, however, some permanent displacement of the PEP tunnel, and the PEP ring magnets moved enough to require realignment [Fischer, 1989].

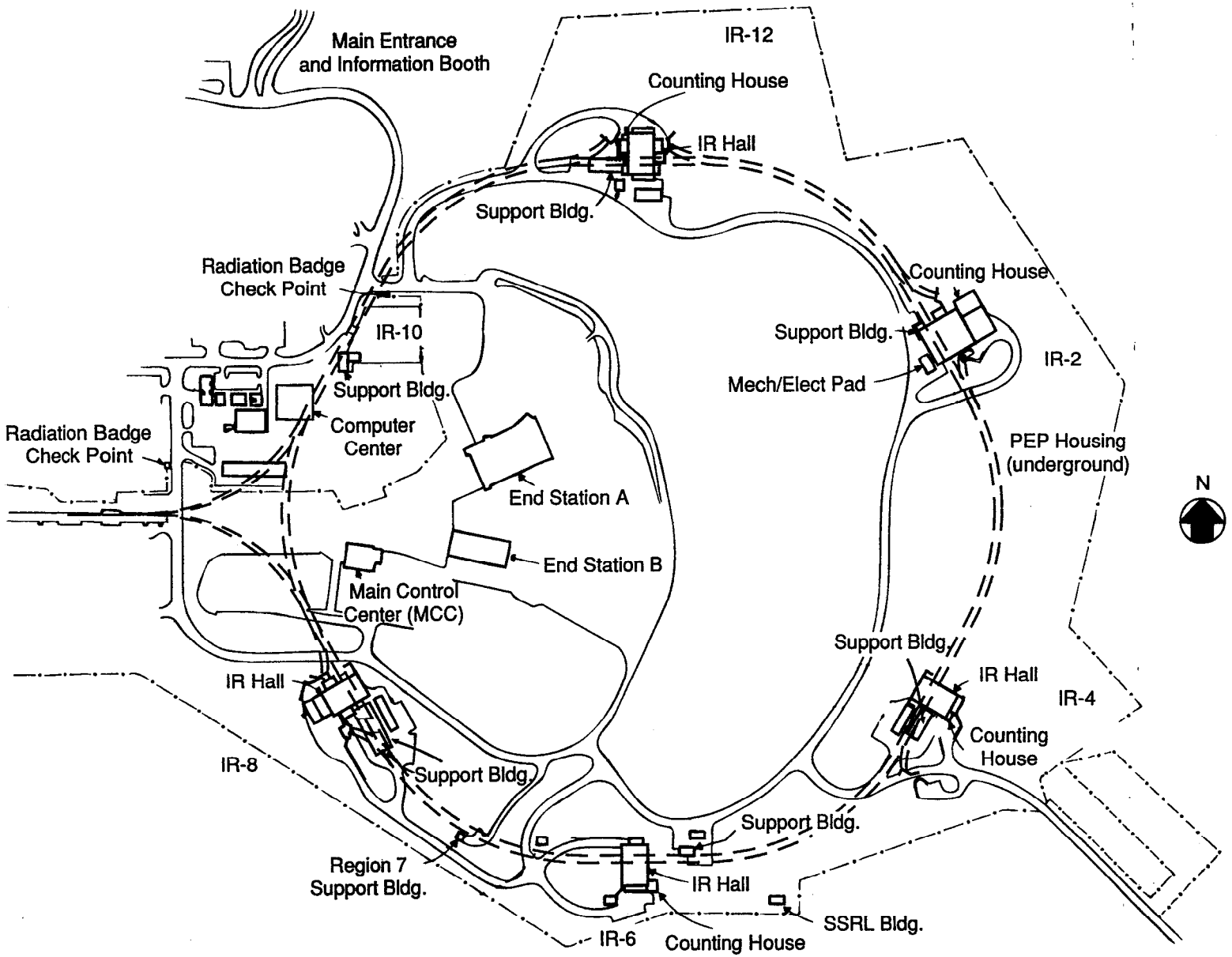

Fig. 7-1. Site map of the PEP facility.

7.1.1.1 Beam Housings. Beam housings include the PEP main ring tunnel, ring access tunnels, injection beam tunnels and their junctions with the accelerator housing and the storage ring, and all penetrations into the tunnels. Where deep underground, the underground structures were built by tunneling methods; elsewhere cut-and-cover methods were used. Beam housings are concrete lined, painted white, and continuously ventilated. Telephone service is provided. The tunnels are protected from fire by detection and sprinkler systems.

Water seepage in the PEP tunnel in the vicinity of IR-10 has been a nagging problem for many years. The seepage water is corrosive and attacks iron, aluminum, and some plastics. It also supports the growth of algae. The water has a high mineral content, which produces deposits that can block drainage pipes and clog drainage channels and gutters. Rather than stopping water seepage, a program of water management has been used in the vicinity of IR-10. Covers were installed over equipment, water was diverted, and grooves were cut into the concrete floor to channel the water to the drainage gutter. Domestic water has been introduced to maintain the flow, dilute the groundwater to prevent precipitation of minerals, flush out solids, and discourage the growth of algae. These measures have been fairly successful: *Water seepage has never caused an interruption of PEP operations.*

This same method of water management will be used for the B Factory. Prior to installation of the machine components, the affected area will be thoroughly cleaned. Protective covers will be installed over all B Factory equipment in the leaky sections of the tunnel, and provisions will be made for guiding leakage into the drainage gutters. Regular maintenance will be provided to keep drains and gutters clear and pumps running.

7.1.1.2 Support Buildings. Support buildings are provided for instrumentation and controls (I&C) equipment at IR-2 and IR-6; for RF, I&C, and magnet power supplies at IR-4 and IR-12; and for RF, I&C, magnet power supplies, and overall operational control of the storage ring at IR-8. Additional special support buildings are located at region 7 and IR-10.

7.1.2 Mechanical Facilities

7.1.2.1 PEP Site Cooling Water. The machine components in the storage rings and the detector will be cooled by closed-loop low-conductivity water (LCW) systems. These are, in turn, cooled by a cooling tower water (CTW) system. Existing PEP systems will be used wherever possible.

A four-cell cooling tower, rated at 21 MW, is located near the Main Control Center. The CTW is distributed around the PEP ring to equipment pads at PEP regions 2, 4, 6, 8, and 12. At IR-4, IR-8, and IR-12, closed-loop cooling water systems circulate LCW to cool PEP equipment. Each system has a heat exchanger that is cooled by CTW. The PEP water systems are (i) the klystron tube and ring magnet cooling systems, (ii) the RF cavity and vacuum chamber cooling systems, and (iii) the experimental equipment cooling systems. Regions 2 and 6 each have an experimental equipment cooling system. Currently, CTW is circulated through the system by four pumps located at the south side

of the existing cooling tower. The pumps are rated at 3800 gpm, so four pumps are required to be in operation. One additional pump will be installed to provide an installed backup.

The present cooling tower capacity is inadequate for the B Factory, which will require 32 MW of cooling; an additional 5 MW will be required for SPEAR and the research yard. We assume that the beam switchyard, SLD, and the SLC collider hall will require only house power by the time the B Factory is commissioned. Accordingly, the following modifications of the existing cooling tower cells will be made to provide the required 37-MW capacity: The existing fill will be replaced with new high-performance PVC fill; the drift eliminators will be replaced with new PVC drift eliminators; and the distribution system laterals and nozzles will be replaced with bigger laterals and large-orifice nozzles. These changes will not affect the size or external appearance of the towers. The CTW piping to the PEP ring is adequate to handle the higher flow.

The total cooling load for the B Factory is higher than the PEP load, and the distribution of loads between the LCW systems, above and below ground, is different from that at PEP. The PEP heat exchangers will be replaced with new, larger, plate-type heat exchangers. The LCW system pumps will be replaced with pumps of larger capacity. In addition, piping will be rearranged to better match the heat exchangers to the loads. The loads will be segregated so that copper and aluminum items are not in the same loops.

The LCW systems will be connected to B Factory loads as described in the following paragraphs. (The names used for the cooling systems below correspond to their current functions.)

IR-12. The RF-vacuum cooling system will supply cooling water to six RF cavities and one-third of the vacuum chambers. The experimental equipment cooling system will supply cooling water to the three IR-12 klystrons and to one of the LER wiggler synchrotron radiation dumps. The klystron-magnet cooling system will supply cooling water to the power supplies, IR-12 RF circulators and tees, and one-third of the ring magnets.

IR-2. The B Factory detector will be installed at IR-2. The cooling water for the 3-MW detector magnet will be provided by the IR-2 experimental equipment cooling system.

IR-4. The RF-vacuum cooling system will supply cooling water to six RF cavities and one-third of the vacuum chambers. The experimental equipment water system will supply cooling water to four of the IR-4 klystrons, circulators, and tees and to six RF cavities. The klystron-magnet cooling system will supply cooling water to the magnet power supplies, two of the IR-4 klystrons and circulators, and one-third of the ring magnets.

IR-6. The experimental equipment water system will supply cooling water to one of the LER synchrotron radiation dumps.

IR-8. The RF-vacuum cooling system will supply cooling water to six RF cavities and one-third of the vacuum chambers. The experimental equipment water system will supply cooling water to four of the IR-8 klystrons and six RF cavities. The klystron-magnet water system will supply cooling water to the magnet power supplies, two of the IR-8 klystrons, circulators, and tees, and one-third of the ring magnets.

7.1.2.2 Cooling Water for Injection System Components. The magnets for the injection system for the B Factory will be supplied with cooling water from existing headers in the accelerator housing and the NIT and SIT tunnels. Magnet power supplies will be located above ground and will be supplied with cooling water from existing headers.

7.1.3 Electrical Facilities

SLAC receives power from two sources: A 230-kV line with a 300-MW capacity and a standby 60-kV line with an 18-MW capacity. The two sources are asynchronous and cannot be operated in parallel. The master substation is located at Sector 30 on the south side of the linac. No expansion of the high-voltage feeders or the master substation is required for the B Factory.

The maximum electrical power demand for the B Factory ring and experimental apparatus will be 32 MW. The anticipated load is broken down by region in Table 7-1.

Electrical power to the B Factory ring and the detector in IR-2 will be distributed at 12.47 kV through the PEP ductbank to the six regional substations at regions 2, 4, 6, 8, 10, and 12.

The distribution of the RF klystrons and cavities around the ring was chosen to match the availability of power. There will be three 1.1-MW klystrons and six 500-kW cavities at IR-12, and six klystrons and twelve cavities at both IR-4 and IR-8. It will be necessary to install additional cables to IR-2, IR-4, and IR-8 to match the B Factory loads in these regions. The cables will be installed in the existing PEP ductbank.

Table 7-1. Anticipated electrical loads for the B Factory.

	Anticipated loads	
Region	in kW	in kVA
2	4,580	5,720
4	10,260	14,900
6	560	700
8	9,890	13,700
10	760	700
12	6,000	7,500
Total	32,050	43,220

High-voltage disconnect switches will be installed at 22 locations on the electrical equipment pads at regions 4, 8, 10, and 12 to make it possible to work on electrical equipment without shutting down the entire electrical distribution system.

The power supplies for the B Factory injection system will be located above ground; power will be supplied by existing circuits.

7.1.4 Interaction Region

PEP has five interaction halls suitable for the assembly and operation of a large particle detector. Current plans are to install a detector in IR-2 for the B Factory.

The IR-2 experimental hall is 20 m wide in the beam direction and 32 m long. It is equipped with a 50-ton overhead crane. The beam height is 4 m above the floor. The building can be divided into two spaces by a shielding-block wall, which makes it possible to work on a detector when it is off the beamline and beams are circulating. There is a two-story counting house on the north side of the experimental hall with 370 m^2 of floor space. Five megawatts of AC power will be available at IR-2. The cooling water system will be expanded to handle this load by the addition of a heat exchanger.

7.2 REMOVALS AND INSTALLATIONS

7.2.1 Space Requirements

Construction of the B Factory requires that the PEP tunnel be cleared of all existing magnets and related components. Table 7-2 summarizes the components to be removed.

Table 7-2. Summary of components to be removed from the PEP tunnel.

Component	Number	Weight (tons)
Bending magnets	192	1,416
Low-field bends	24	18
Quadrupoles	216	405
Insertion quads	24	207
Miscellaneous quads	48	60
Sextupoles	192	33
Concrete rafts	216	925
Miscellaneous supports	400	32
Total		3,096

The storage and refurbishing space required for these and other components is shown in Table 7-3. These requirements have been minimized by assuming that unwanted components (for example, the concrete rafts) will be discarded. Recent tests, conducted throughout PEP, showed no residual radioactivity above background in the rafts. They can thus be disposed of in a conventional manner. With the 32,100 ft^2 of crane-covered space already identified at SLAC (Table 7-4), and with additional space to be made available at other collaborating laboratories, no additional buildings will be required at SLAC during construction of the B Factory.

7.2.2 Disassembly and Removals

7.2.2.1 Main Tunnel. PEP disassembly will commence with the bending magnets in the water-affected area in regions 9 and 11 (see Fig. 7-1). The removal rate of these components will be two magnets or three rafts per day. At this rate, the PEP tunnel can be cleared in approximately nine months. Fixtures used for disassembly and removal will be designed to ensure that previously obtained alignment information for the bending magnet cores will be preserved.

Once removed from the tunnel, the main coils, trim coils, and other ancillary equipment will be removed from the cores. The coils will be inspected for possible radiation damage and will receive an approved water-sealing coating. The cores will be inspected for damage and will be repainted. New trim coils will be wound and installed, and the magnet then reassembled. To assure the magnetic quality of these refurbished magnets, each one will be mechanically checked for twist, roll, and gap. Previous measurements at SLAC using this technique have shown that magnetic measurements are necessary only on a sample basis, provided that mechanical measurements are completed on each magnet. This procedure will be followed for the refurbished magnets.

The quadrupole-sextupole raft structure will be removed after the main bending magnets. With the bending magnets removed, the unwanted aluminum vacuum chamber will be exposed, which will allow cutting adjacent to the quadrupole-sextupole pairs. This will decrease the total time for raft removal, since the quadrupoles and sextupoles will not have to be opened in the tunnel. Careful attention will be given to those components that can be reused, namely, beam position monitors, bellows, ion pumps, and flanges. After the quadrupole-sextupole pairs are removed from the tunnel, they will be transported to a refurbishing area where they will be opened and the vacuum components removed. Tests will be made to determine the extent of radiation damage to the coils. If undamaged, they will be removed from the cores and resealed. The cores will then be repainted prior to reassembly.

Since the quadrupole magnets underwent magnetic measurements prior to PEP installation, it may not be necessary to remeasure each magnet again. Previous data have shown that the magnetic characteristics of the magnet can be duplicated, provided good mechanical measurements are taken and specific reassembly techniques are used. With the previous PEP magnetic information at hand, sample tests can be performed to ensure that the magnetic properties are preserved. The refurbished magnets can then be mounted on a new support and rough-aligned using gauges and fixtures. When the vacuum chambers and beam position monitors become available, the cores will be opened and the

Table 7-3. Space required for preinstallation, PEP disassembly, and B Factory component assembly.

Component	Space requirement (ft^2)
PEP disassembly	
Bending magnets	10,000
Quadrupole/sextupole pairs	2,500
Rafts	10,000
Miscellaneous magnets	1,500
Miscellaneous supports	2,000
Vacuum components	2,000
Miscellaneous	1,000
HER assembly	
Bending magnet assembly	1,000
Quadrupole assembly	600
Quadrupole fabrication	600
Sextupole fabrication	600
Sextupole assembly	600
Support assembly	600
Mechanical measurement	1,000
Mechanical alignment	1,000
Magnetic measurement	3,000
Coil storage	1,000
Hose factory	500
Miscellaneous storage	500
LER assembly	
Bending magnet assembly	1,000
Quadrupole assembly	500
Sextupole assembly	500
Support assembly	500
Mechanical measurement	500
Mechanical alignment	750
Magnetic measurement	1,000
Coil storage	500
Miscellaneous storage	250
Total	45,500

Table 7-4. Crane-covered SLAC space available for B Factory construction activities.

Area	Space available (ft^2)	Current use
Light assembly	11,500	SLD
Heavy fabrication (center bay)	7,500	Storage
IR-6	4,500	SLD
IR-8	4,500	SLD
IR-12	4,100	SSRL
Total	32,100	

chamber package installed. At this time, precision mechanical alignment will be accomplished. This alignment process will be completed in a temperature-controlled area, using precision optical alignment docks to ensure that the beam position monitors and magnet components are aligned to within a few thousands of an inch.

Generally, much of the existing PEP cable plant will be used for the HER and LER. For example, all of the vacuum system cables will remain in place and will be connected to new equipment in locations nearby. In some instances, splicing and other means may be needed to make up the required lengths. Unneeded cabling will be removed and, in some cases, stored for later reuse.

To ensure adequate documentation and control during disassembly and subsequent reassembly, travelers will be attached to each component for tracking. Databases will be set up to ensure that other information regarding these components is readily available. Data taken during PEP construction regarding mechanical and magnetic measurements can be retrieved in such a way as to allow comparison of these properties.

With the tunnel housing empty, the floor will be cleared of all attachments used for PEP. New support points for the B Factory rings will be accurately placed by an alignment team. Surveys are currently under way to determine what other equipment, such as utilities, must be modified and installed once the alignment process is complete in a given section of the tunnel.

7.2.2.2 Interaction Regions. In addition to the beamline components, existing experiments at PEP will require removal. Means will be sought for these experiments to be used by others prior to B Factory construction, but if no satisfactory alternatives are suggested, these experiments will be dismantled or moved to other areas to allow B Factory operation.

PEP IR-2—Time Projection Chamber (TPC). The TPC Facility will be removed from PEP to allow installation of the new B Factory experiment.

PEP IR-4—MAC. Since the MAC detector is capable of moving off-line within a short period, it will be moved from the interaction area to the assembly area. This will

permit this detector to be evaluated by others for possible use elsewhere and places it in an area that is not fully utilized.

PEP IR-6—HRS. The detector iron will be relocated from the IR to the rear IR hall assembly area. This places the detector in an area where it will not interfere with activities in the main assembly area, and which has been identified as a possible work and storage area for the B Factory.

PEP IR-8—DELCO. This detector has been removed from PEP, but support structures used for this detector are within the IR, as are some detector parts. These items will be removed and pose no significant space demands. This IR hall has also been identified as a possible storage and working area for the B Factory.

PEP IR-12. The Mark 2 detector has been removed from this region, which is currently being used by SSRL as an assembly area. This hall has been identified as a storage and working area for the B Factory.

7.2.3 Installation

7.2.3.1 High-Energy Ring. Installation of the HER components (Table 7-5) will begin after alignment teams have located support points. Anchor bolts will be installed for the bending magnet supports, which will be the first components to be reinstalled for the B Factory. After the supports are grouted and aligned, the bending magnets will be installed using new installation fixtures. Caution will be taken to ensure that all magnets are handled in an approved manner. The quadrupole-sextupole pairs on their prealigned supports will be installed in a similar way. After this, the vacuum chamber will be placed in the bending magnets and the fixed flanges made up. The final connection will be the HER flexible bellows unit. During the entire installation process, quality control

Table 7-5. Inventory of HER components.

Component	Quantity	Total weight (tons)
Bending magnets	212	1,433
Quadrupoles	272	514
Sextupoles	144	26
Bending magnet supports	192	36
Quadrupole/sextupole supports	192	8
Quadrupole supports	96	6
Total		2,023

measures will be undertaken to ensure that each component is installed according to written procedures. Documentation regarding the installation, fabrication, and refurbishing process of the B Factory components will also be filed according to written procedures.

7.2.3.2 Low-Energy Ring. The LER components (Table 7-6) will become available after the HER is installed, owing to the fact that they must all be fabricated. Accordingly, since these magnets are installed above the HER, they will be installed on the "C" support structure as a prealigned unit. Quality control and documentation measurements will be taken, as described for the HER.

7.2.3.3 Cable Plant Installation

Raceways. Cables will run in 4-in.-deep, ladder-type steel cable trays, conduits, and wireways from points of origin to terminations. Instrumentation and DC cables will extend in the air from the cable trays to the devices served. Long runs will be supported. Barriers in the cable trays or separate cable trays will be used to carry conductors for different functions (for example, DC, instrumentation, AC power, etc.). AC cables extended from cable trays to equipment will be run in rigid conduit, flexible conduit, or other approved raceways.

Cables between the klystron gallery and the accelerator tunnel will be run in conduits in the existing 30-in. vertical penetrations between the two areas. Cable grips will support the vertical load of cables at the point of entry into the conduits.

All raceways will be bonded for electrical continuity.

Additional cable trays will be installed in the accelerator tunnel and the klystron gallery to support cables.

Existing cable trays in the PEP housing will be utilized for the new cable systems. Additional trays will be installed in the existing interaction halls to carry cables for components in the halls. New cable trays will be installed in the RF areas of the support buildings to support the cable plant.

Large DC Cables. Existing DC circuits in the PEP ring are capable of supplying both the HER and the LER large magnet circuits. There are twenty-one 1-in.-OD, PVC-

Table 7-6. Inventory of LER components.

Component	Quantity	Total weight (tons)
Bending magnets	208	227
Quadrupoles	298	289
Sextupoles	144	26
Dipole/quadrupole/ sextupole supports	192	77
Quadrupole supports	96	17
Total		636

jacketed, water-cooled cable circuits, extending completely around the ring, with taps to power supplies and magnets served, utilizing air-cooled conductors to bridge the gap. In addition, 6 air-cooled 350-MCM aluminum cables run through the same route. Existing circuits will be modified to reach the new magnet locations. Modifications will consist of jumpers in locations no longer served and additional taps into existing cables for new magnet locations. Water cooling will no longer be required, owing to the lower magnet currents.

Many of the existing power supplies will be reassigned or removed. Changes to the existing large DC cables will be made as appropriate.

Power supplies for the injection system magnets will be located in the klystron gallery. Cables will run from power supplies in the klystron gallery, in cable trays and through penetrations, to the accelerator housing. They will exit the penetrations to a cable tray and will be routed to the magnets served.

Trim and Steering Circuits. Existing trim and steering cables will be disconnected from the PEP magnets and removed to the terminal cabinets that formerly served them. New trim and steering circuits will be fed from a power supply utilizing one of the former large power supply circuits for its main power distribution. Separate DC-to-DC converters will serve local magnet trim circuits. As with the large DC cables, trim and steering cables for the injection lines will originate at power supplies in the klystron gallery.

Instrumentation and Control Cables. A wide variety of cable types will be utilized for the I&C systems. Where practical, cables will be preassembled with connectors, as complete units. In many cases, cable connectors will be installed in the field. Multiconductor I&C cable will be type TC (tray cable), with overall shield. Safe High-Voltage (SHV) connectors will be utilized where required. High-voltage circuits will be run separately from other circuits.

New I&C cables in the injection system will be routed through cable trays to vertical penetrations and then to cable trays in the accelerator tunnel, and hence to the instruments served.

AC Circuits. The existing AC distribution system for ring components, removed to allow the dismantling of the PEP ring, will be reinstalled in appropriate locations. New AC systems will be provided for all I&C racks, power supplies, and other components not presently served. Rigid steel conduits or cable trays will be used for 480-V circuits; 208Y/120-V circuits will be run in EMT or other suitable raceways. Wireways will be used for 480-V and 208Y/120-V circuits where required.

Grounding. All elements of the new rings, the IR, and the injection beamlines will be grounded to the existing SLAC ground system. Connections will be made by clamp-type connectors, for easy removal. The grounding connectors will be carefully torqued.

8.

SAFETY AND QUALITY ASSURANCE

FROM a safety standpoint, the B Factory does not present any significant new problems. All of the anticipated hazards are ones that SLAC has faced during previous construction or experimental activities and for which programs are in place to protect the environment and the health and safety of workers and others.

Installation of the B Factory in the existing PEP tunnel at SLAC will enable us to take advantage of a number of existing, proven safety features and systems. The fact that these features are already present and operational in the tunnel will provide an extra measure of safety during the decommissioning of PEP and the installation and commissioning of the B Factory.

The SLAC safety organization will ensure that all safety aspects of the design, installation, testing, and operational phases of the project are reviewed and approved by the cognizant SLAC safety committees, including the Safety Overview Committee, the Hazardous Experimental Equipment Committee, the Radiation Safety Committee, the Electrical Safety Committee, the Non-Ionizing Radiation Safety Committee, and the Earthquake Safety Committee [SLAC Environment and Safety Office, 1987].

8.1 FIRE SAFETY

The existing fire safety system in the PEP tunnel and experimental areas will remain operational throughout the installation, commissioning, and operation of the B Factory. All areas are classified as Ordinary Hazard, Group I. The tunnel sections, interaction region halls, and support building are protected by automatic wet sprinkler systems and smoke detectors. The sprinkler systems are designed for a coverage of 0.15 gpm/ft^2. The ring is divided into twelve zones, each with its separate water supply. Six of these zones supply water to the centers of the curved sections of the tunnel. The remaining six supply water to the interaction regions (IRs). The counting houses and control room are protected by a smoke detector that actuates a pre-action, air-supervised sprinkler. The substation is protected by a heat detector that actuates a deluge system. The smoke detectors are of a high-voltage type that is no longer manufactured. These will be replaced with low-voltage components to facilitate system maintenance.

With the exception of regions 8 through 12, each curved section of the PEP tunnel has three fans: two intake and one exhaust. Owing to the presence of above-ground structures above regions 8 through 12, the ventilation configuration there is somewhat different, with a total of five fans: two intake and three exhaust, including one double-volume exhaust fan. The fans automatically stop operating when the fire alarm sounds. The Fire Department then has the option of restarting any of the fans to provide fresh air or to exhaust smoke. The Fire Department's controls for this purpose are located on above-ground pedestals.

SLAC contracts with the Palo Alto Fire Department to provide an on-site fire station and emergency response services. The Palo Alto Fire Department also provides ongoing fire safety inspections of SLAC facilities, as well as personnel training.

8.2 RADIATION SAFETY

The design and operation of all facilities at SLAC are governed by the ALARA (as low as reasonably achievable) policy. Thus, SLAC has always maintained radiation dose limits below the maximum allowed by regulation.

8.2.1 Radiation Shielding

Shielding for the B Factory will conform to the Design and Control section of DOE Order 5480.11, Section 9(J) [*SLAC Radiation Safety Procedures*, 1990]. The design criterion will be 1 rem/yr at the shield surface for normal beam losses. This assumes a 2000-hr working year and an occupancy factor of 1. In addition, SLAC internal design criteria will require that (i) the boundary dose be limited to 5 mrem/yr for 6000-hr beam operation and (ii) a maximum radiation level of 25 rem/hr be allowed at the outer surface of the shield from an accidental beam loss.

The PEP tunnel was originally designed for 200-GeV protons. Since the shielding requirements for protons are far more stringent than those for electrons, present shielding is more than adequate for 18-GeV electrons and will also be adequate for the B Factory, assuming maximum values for energies and currents.

The IRs in PEP were originally designed for about 20 kW of injected power at 18 GeV, though injection was always limited to 1 kW. Radiation has never been a problem at these low power levels. The B Factory design calls for typical injection power levels of 3.2 nC/pulse × 60 pps × 9 GeV = 1.7 kW, well below the original design criterion for the IRs. (Even at the highest conceivable injection power of 8 nC/pulse × 120 pps × 10 GeV = 9.6 kW, there is a factor of two safety margin compared with the original PEP shielding design.) Thus, we expect little or no radiation in these areas during normal B Factory operation.

The loss of the circulating beams in the case of the thinnest shielding (that is, a curtain wall in an IR) would result in an integrated dose-equivalent of less than 75 mrem. Since the total energy of the two circulating beams, at their maximum allowable currents of 3 A, is only 253 kJ, the potential for activating air, ground, or beamline components is very low. Operational experience with PEP and SPEAR indicates that air, ground, and beamline component activation are not major radiological problems.

8.2.2 Personnel Protection System

The Personnel Protection System (PPS) currently in place in the PEP tunnel is designed to protect personnel from radiation, electrical, and RF hazards. This is accomplished through a system of electronically interlocked gates, lights, alarms, and operator displays and controls [Constant et al., 1977; Smith and Constant, 1981]. (See below for further discussion of electrical and RF safety considerations.) With installation of the B Factory in the tunnel, the PPS will undergo necessary upgrades and enhancements to address the new facility and operating conditions, but will remain largely the same in terms of its overall design and function. The five existing access states, as shown in Table 8-1, will be retained, as will the lighting controls and audio signals that alert personnel to a change in access state.

Because the B Factory high- and low-energy rings (HER and LER) will be assembled within the existing PEP housing structure and because their injection lines will occupy the existing north and south injection transfer (NIT and SIT) lines, the present PPS perimeter control and interlock facility can be utilized with some modification and upgrades. The perimeter access points into the housing tunnels from all the IR halls and the personnel and equipment tunnel access gates can be fully utilized as part of an upgraded distributed PPS system. All displays and remote control functions available in the PEP control room will be retained. In addition to interfacing with the existing hardware panels, the upgraded system will provide software-driven CRT displays and touch-panels from a dedicated distributed PPS controller system. Personnel badge reading and monitoring capability will be utilized for access control.

Table 8-1. Access states of the current PEP Personnel Protection System [SLAC Radiation Rule Book, 1990].

NO ACCESS	Beam on or potential for beam to be on.
RESTRICTED ACCESS	Similar to CONTROLLED ACCESS, but electrical hazards and x-rays from the RF system may be present. Because of additional hazards, access is allowed only as necessary to knowledgeable persons.
CONTROLLED ACCESS	Beam off. Electrical and RF hazards off. Zone has been searched. Persons are identified, are logged in and out, and must carry a key from the keybank.
IN SEARCH	Beam off. Electrical and RF hazards off. Doors electrically locked until search completed.
PERMITTED ACCESS	Assurance that beam and RF hazards cannot come on. All door releases are enabled (doors are "open").

The PPS stopper logic will be modified to accommodate the new HER, LER, NIT, and SIT configurations. The emergency-off button configuration will remain the same. In general, the new ring configurations will not impose any major new PPS logic requirements. Tone loop systems will be reconfigured to be compatible with the upgraded distributed controller logic.

Existing doors and gates will be upgraded to improve reliability. The current system provides seven complete access modules located at or near the five IR halls. Each entry module includes keybanks, video cameras, and direct voice communications via intercom and telephone. In addition, five equipment/personnel entry points are located around the periphery of the PEP ring, together with 13 additional key-operated personnel access/egress points. All of these points can be "crashed" for emergency exit.

There are 15 zone barrier gates in the PEP tunnel that require "access state" compatibility to allow passage in either direction. These zones will be retained for the B Factory, and logic requirements will not change. RF areas will continue to be located at the IR halls 4, 6, and 8. The four NIT/SIT barrier gates between the beam switchyard and the PEP tunnels will also remain.

The current PPS safety system interface (SSI) provides for electrical and RF hazard safety interlocks distributed throughout the PEP ring and at IR halls 4, 6, and 8. The input interface to this system will be expanded to accommodate additional RF and magnet power supply requirements, and the control logic will be upgraded to a distributed control interface that will be compatible with the PPS technology.

8.2.3 Beam Containment System

The redesigned NIT/SIT lines will be monitored by toroid current monitors located at their entry portals and will be instrumented in much the same way as are the existing beamlines [Constant et al., 1977]. Each beamline (NIT and SIT) will have two toroids that feed wideband balanced-input preamps located near the beamlines. These preamps will drive fan-out distribution amplifiers in the main control room area. These, in turn, will distribute the beam-induced current signals to average-current monitors, repetition-rate monitors, and pulse-to-pulse peak-current monitors. Each current-monitoring device will generate test signals between beam pulses that will be redistributed to the beamline toroids and fed back to the processing electronics to provide a closed-loop test capability.

The existing Beam Containment System (BCS) is primarily analog in nature and requires many careful setup adjustments to achieve the operational protection limits required by these beamlines. The present BCS will therefore be upgraded, utilizing digital processing techniques to capture beam-pulse information and generate the necessary interlocks. The upgrade will include the use of state-of-the-art wideband preamps, flash ADCs, serial data links, digital discrimination logic, and intelligent processors. The B Factory BCS will utilize this design upgrade in the implementation of its required interlocks, thereby providing rapid setup, flexibility, and improved reliability.

8.2.4 Radiation Safety Training

In accordance with SLAC's implementation plan for DOE Order 5480.11 (Radiation Protection for Occupational Workers), all regular SLAC employees and any persons who work at the laboratory longer than one month must receive training in radiation fundamentals. In addition, those workers whose assignments make it likely that they will receive a total occupational radiation dose greater than 100 mrem in one year receive extensive radiation safety training and are required to pass an examination. The latter class of workers is recertified by examination every two years.

8.3 NONIONIZING RADIATION SAFETY

The radio-frequency (RF) energy system for the B Factory will incorporate all the safety measures that are currently in place at PEP [Allen and Karvonen, 1978]. These include the use of pressurized waveguides and strict procedures for mechanical assembly and inspection.

Each waveguide network will be pressurized with regulated 0.25-psig instrument air. Since the volumetric supply rate is limited, a leak in the waveguide will cause a drop in pressure, actuation of a pressure switch, and shutdown of the rings. After the leak is repaired, a field measurement will be made to check for RF leakage. Normal ring operation may resume when the pressure in the waveguide is restored and the RF field survey is completed.

Pressurization guards mainly against operation with a missing piece of waveguide or an improperly assembled flanged joint. Although the most likely cause of RF leakage under operating conditions is that a waveguide joint has been left open, it is possible that the system could be gas-leak-tight and not RF-leak-tight. This could occur, for example, if the flange bolts are not tightened enough to fully compress the rubber gas seal. Thus, proper torquing of the flange bolts is necessary to prevent possible RF leakage at the flange joint.

During assembly and installation of the waveguide components, all flange bolts will be torqued and all field-assembled waveguide joints will be tested by pressurization and checked for bubbles. Joints must be free of visible bubbles. After installation, an inspector will measure the torque on a minimum of six bolts chosen at random on each flange. If the torques exceed specified levels, the inspector will then initial and date the flange joint, thus indicating that the joint is acceptable. If the joint is not acceptable, all the bolts on the flange must be retorqued and remeasured.

After the requirements for gas leak checking and bolt torquing are satisfied, a check for RF leakage around each accessible flanged joint will be made. If the test is satisfactory, an adhesive label with the inspector's initials and the date will be applied across each joint. An intact and signed label on each waveguide joint is always a prerequisite to operational transmission of RF through a waveguide network. The coaxial connectors at the final drive amplifier and at the input to the klystron will also be surveyed for possible leakage.

When a klystron is disconnected from the waveguide between the klystron and the circulator, a cover will be bolted over the open end of the waveguide on the cavity side. The cover will be inspected and labeled and the waveguide pressurized before any beam can be stored in the ring. Also, a pressure switch interlock in the waveguide close to the klystron will prevent high voltage from being applied to a klystron when it is disconnected from the waveguide feeding its cavities.

B Factory operations staff will conduct RF radiation hazard surveys at least every 90 days to ensure that the RF leakage level is less than 1 mW/cm^2.

8.4 ELECTRICAL SAFETY

It is SLAC policy that every necessary precaution is taken in the performance of work to protect all persons on the site from the risk of electrical shock and to minimize the probability of damage to property due to electrical accidents. This policy is implemented by assigning responsibility and adhering to basic safety principles, as stated in the *SLAC Electrical Safety Policy* [1990] and the *SLAC Electrical Safety Standards* [1990], and by complying with regulations and procedures appropriate to each operation. A 4-hour electrical safety training course is provided by the Laboratory for those workers who are likely to be exposed to high-voltage hazards.

Several B Factory subsystems will employ high voltages. For example, voltages in the detector subsystems used to achieve gas amplification could reach 7 kV DC. The controls and work procedures necessary to ensure safe work on these systems are well-understood. The interlocking of these systems will implement SLAC's established procedures for lockout and tagout and for working on energized equipment only under very limited and controlled conditions to ensure safe operation.

Special procedures are in place to permit authorized personnel to occupy areas adjacent to energized hazardous magnets. These procedures are called RASK, for "Restricted Access Safety Key." Under these procedures, a special RASK authorization form must be filled out to obtain a key that enables the hazardous supply under test. Testing is done in accordance with written procedures. The emergency-off buttons remain active and will crash off the power supply when pushed. The RASK system will remain operational during construction of the B Factory. Thus, we will have the advantage of having this safety system in place during installation and testing of the magnets.

During the life of the PEP tunnel, there has been some damage to junction boxes and conduit due to water seepage near IR-10. Owing to the difficulty in obtaining a tight water seal in the shotcrete-lined tunnel, water flow has been managed through a series of efforts, including covering vulnerable equipment and installing drainage gutters to channel the flow of water [Weidner, 1990; see also Section 7.1.1]. No electrical accidents have occurred as a result of the water seepage. To address this continuing problem over the life of the B Factory, additional improvements to the drainage system are planned, as described in Chapter 7. Further, the entire electrical distribution system now in place will be inspected, and any elements of the system that are damaged or vulnerable to damage will be replaced and maintained in a manner that will ensure safe

operation. All new electrical installations will be in accordance with current applicable codes and requirements.

8.5 CONSTRUCTION

The SLAC Environment Safety and Health (ES&H) Division has primary responsibility for overseeing safety compliance by construction contractors. This responsibility, which is carried out in concert with SLAC plant engineers, contract administrators, and line supervisors, includes

- Apprising contractors of SLAC and DOE safety criteria prior to construction
- Conducting periodic inspections of contractor construction areas to evaluate the quality of the contractor's safety compliance program
- Receiving contractor accident reports and compiling information for reporting to DOE

8.6 EMERGENCY PREPAREDNESS

Like all experimental equipment at SLAC, the B Factory will be designed, constructed, and operated in a manner that minimizes the risk of injury to property or personnel as a result of a natural disaster or other emergency situation. In the event of any abnormal condition, the interlock system will automatically shut the machine down until the situation is diagnosed and corrected. The formal emergency planning system described in the *SLAC Emergency Planning Booklet* [1988] will help to ensure a logical, organized, and efficient response to any emergency. It sets forth specific steps to deal with various emergency conditions, identifies the appropriate personnel to act as resources, and provides a chain of command for responding to unplanned events.

The emergency situation most likely to arise at SLAC is an earthquake. As indicated in Section 7.1.1, the PEP tunnel and related structures are designed to withstand the effects of a major earthquake. In addition, all mechanical components of the B Factory will be secured to protect persons working nearby. This will be assured by a review of the design and installation of the experimental equipment by the SLAC Earthquake Committee, as mandated by the *SLAC Safety Program* [SLAC Environment and Safety Office, 1987]. Further, as with all activities at SLAC, operation of the B Factory will be covered by the *SLAC Earthquake Emergency Plan* [1987], which outlines the procedures to be followed in the event of an earthquake severe enough to cause possible structural damage or personal injury.

8.7 ENVIRONMENTAL PROTECTION

8.7.1 Disposal of PEP Components

Decommissioning PEP and making room in the tunnel for installation of the B Factory will require the removal of 925 tons of concrete rafts and hundreds of tons of other materials. The concrete rafts have been surveyed and found to be free of radioactivity other than background activity from radon (^{214}Bi, ^{214}Pb) and ^{40}K. The concrete may therefore be disposed of as nonhazardous waste. All other items will be surveyed before they are removed from the tunnel and will be handled in a manner appropriate to the level of residual radioactivity present. Those materials that may be reused in the B Factory will be held in a secure area until they are reinstalled. All scrap will be disposed of in accordance with approved procedures.

8.7.2 Ongoing Environmental Protection Activities

In accordance with 29 CFR 1910.1200 (the OSHA hazard communication standard), SLAC has developed a *SLAC Hazard Communication Program* [1986]. Under this program, SLAC conducts regular inventories of hazardous materials, makes Material Safety Data Sheets (MSDSs) available to all employees, ensures appropriate labeling of hazardous materials, trains employees to identify and control hazards in the workplace, and informs users, contractors, and temporary employees of the hazards that may be encountered at SLAC.

Construction and operation of the B Factory is not expected to cause any additional impact on the groundwater at SLAC. Preservation of groundwater quality is ensured through implementation of the groundwater monitoring program [Earth Sciences Associates, 1991], which SLAC has instituted in compliance with DOE Order 5400.1.

8.8 DETECTOR SAFETY ISSUES

A separate CDR and safety evaluation will be prepared and submitted for the B Factory detector. This discussion is intended merely to summarize the safety and environmental hazards posed by the detector and to describe the means proposed to mitigate them.

The detector for the B Factory will be similar, from a safety point of view, to particle physics detectors at many other storage rings. It is therefore possible to evaluate with some confidence potentially hazardous conditions that must be protected against. The detector systems may employ gases with a small but significant flammable component. This is also a standard situation. Safety procedures in this case involve (i) the proper venting of gases in such a way as to prevent the accumulation of explosive concentrations, (ii) the placement and proper maintenance of flammable-gas detectors on the detector itself and in the regions of gas storage and mixing, (iii) the proper siting and installation of pressure vessels, (iv) the interlocking of high voltages so as to prevent

sparks that could ignite the mixture, and (v) the training of operators regarding proper safety procedures.

The final potential safety hazard is the cryogenic system associated with the superconducting solenoidal magnet. This system must handle liquid helium to cool the magnet. Safety considerations here mainly involve prevention of spills of cryogens (liquid helium and liquid nitrogen), which could cause injury by freezing or by creating an oxygen-deprived atmosphere upon evaporation. This will be done by engineering the system such that large liquid spills can be prevented, even in the event of a major line rupture; by the installation of low-oxygen detectors; by the proper engineering of pressure vessels and attendant systems; and by extensive training of the system operators and maintenance personnel. If a superconducting Q4 magnet is chosen for the B Factory, these measures will be applied to it as well. Further, the volume of cryogens will be much smaller for the Q4 magnet.

8.9 QUALITY ASSURANCE

The B Factory management is strongly committed to the implementation of a quality assurance (QA) program for the design, construction, and operation of the B Factory. A dedicated QA manager, reporting directly to the B Factory project leader, is planned. Working together with QA staff at SLAC and the various B Factory subsystem managers, the B Factory QA manager will develop and implement a QA plan that will ensure that the B Factory is built to applicable SLAC, LBL, government, and industry standards and codes. The QA plan will include, at the minimum, consideration of

- Purchased material controls
- Design controls
- Drawings, procedures, standards, and databases
- Document control
- Controls for fabrication, assembly, installation, and operation
- Inspection and testing
- Internal and external audits
- Quality reports

We plan to institute a flexible database management program (we foresee using ORACLE along the lines followed by the LEP project at CERN), which will allow us to keep track of every component of the machine for the full duration of the project. In this way, for every machine component, all items of an historical and/or characterization nature, be they documentation, vendor, maintenance history, etc., will be encoded and cross-linked. This system will also provide a unique, modifiable means of maintaining the machine parameters that will allow the engineering staff easy and accurate access to any parameter they need, and will avoid the promulgation of out-of-date parameters.

In addition to the salary for a QA manager, the budget presented in Chapter 9 includes considerable funds for engineering staff who will perform QA tasks for each

individual subsystem. Funds have been included for inspection at both on-site and off-site (that is, vendor) facilities.

Project management is committed to an ongoing process of subsystem review. These reviews will be staffed by a combination of in-house and outside experts, whose job will be to provide technical input for all phases of the project. Part of their function will be to ensure that proper standards of quality are maintained at all times. This process of expert review has already been used on the project; four in-depth reviews were held to solicit a candid technical evaluation of the critical items of the design presented in this report. The review teams were asked to draw attention to any design features that would lead to unreliable or poor-quality machine operation. The reports from these four review teams, along with supporting documentation, are available in a companion document.

9.

COST AND SCHEDULE

THE Asymmetric B Factory project involves an upgrade of the SLAC accelerator complex. This upgrade includes construction of the high- and low-energy rings in the existing PEP tunnel and construction of bypass lines for the electrons and positrons in the existing linac enclosure. Many PEP components will be reused, and additional savings will accrue from the reuse of hardware from SLAC installations other than PEP. Although no conventional construction is required, minor modifications to the electrical and cooling-water systems are included in the project scope. The cost estimate presented here includes only the construction activities and does not include either the costs of preconstruction R&D or the preoperations costs associated with project commissioning.

9.1 COST ESTIMATE

The B Factory cost estimate was generated, and will be subsequently monitored, through a work breakdown structure (WBS), described in Section 9.3. The total construction cost, in FY 1991 dollars, is $167.2 million. This estimate is presented in Table 9-1; the associated schedule (see Section 9.2) assumes an optimum funding profile.

Contingency is an explicit line item that was determined after a detailed analysis of each of the major subsystems. The contingency varies from system to system, depending upon the complexity of the system and the details of our understanding. In those cases where PEP components are being duplicated, we have felt justified in assigning a lower-than-average contingency. The percentage of contingency varies between 20% (for a well-defined and well-understood magnet system) and 60% (for the less well-defined interaction region components). The overall contingency for the project is 26%. Table 9-1 includes the individual contingency assigned to each subsystem.

An associated schedule for preconstruction R&D (not shown here) has been used to ensure a realistic construction schedule. That is, the schedule presented in Section 9.2 takes proper account of the time required for R&D activities prior to detailed design and hardware fabrication.

Table 9-1. Estimated cost, in FY91 dollars, of the Asymmetric B Factory.

WBS code	System	Cost (FY1991 K$)	Contingency (%)	Contingency (FY1991 K$)
1	**Asymmetric B Factory**	**129,844**	**26**	**33,559**
1.1	**High-Energy Ring**	**58,525**	**25**	**14,748**
1.1.1	High-Energy Ring Magnets	3,127	20	625
1.1.2	Magnet Power Supplies	2,381	20	476
1.1.3	RF System	20,350	25	5,088
1.1.4	Vacuum System	21,547	25	5,387
1.1.5	Feedback System	2,586	40	1,034
1.1.6	Instrumentation and Electronics	1,944	25	486
1.1.7	Installation	5,415	26	1,417
1.1.8	Alignment	1,175	20	235
1.2	**Low-Energy Ring**	**41,425**	**24**	**10,069**
1.2.1	Low-Energy Ring Magnets	10,564	20	2,113
1.2.2	Magnet Power Supplies	1,953	20	391
1.2.3	RF System	10,180	25	2,545
1.2.4	Vacuum System	12,767	25	3,192
1.2.5	Feedback System	2,200	40	880
1.2.6	Instrumentation and Electronics	1,859	25	465
1.2.7	Installation	1,520	27	407
1.2.8	Alignment	382	20	76
1.3	**Interaction Region**	**4,376**	**39**	**1,706**
1.3.1	Interaction Region Magnets	1,583	60	950
1.3.2	Power Supplies	605	20	121
1.3.4	IR Vacuum System	836	25	209
1.3.6	Instrumentation and Electronics	316	45	142
1.3.7	Installation	1,036	27	284
1.4	**Injection System**	**8,242**	**25**	**2,045**
1.4.1	Injection System Magnets	1,951	25	488
1.4.2	Magnet Power Supplies	1,234	20	247
1.4.4	Vacuum System	1,322	25	331
1.4.6	Instrumentation and Electronics	615	25	154
1.4.7	Installation	2641	28	729
1.4.8	Alignment	479	20	96

Table 9-1 continued

1.5	**Control System**	**8,890**	**33**	**2,961**
1.5.1	System Engineering	4,737	32	1,508
1.5.2	Hardware	4,153	35	1,453
1.6	**Conventional Facilities**	**5,480**	**26**	**1,449**
1.6.1	Electrical Utilities	3,549	20	710
1.6.2	Mechanical Utilities	1,763	40	705
1.6.3	Site Work	168	20	34
1.7	**Safety and Protection**	**606**	**20**	**121**
1.8	**Management**	**2,300**	**20**	**460**
1.8.1	Administration	1,500	20	300
1.8.2	Quality Control & Quality Assurance	200	20	40
1.8.3	Planning and Scheduling	200	20	40
1.8.4	Budget	200	20	40
1.8.5	Office Staff	200	20	40
	Indirects	**3,820**		**0**
	Incremental Indirects	2,820		0
	University Indirects	1,000		0
	PROJECT TOTAL: 167,223			

Using this construction schedule, we have developed the funding profile shown in Table 9-2. This profile is presented both in constant FY 1991 dollars and in then-year dollars (based on DOE guidelines). The escalation has been done to the midpoint of the project (June 1994) using DOE construction escalation figures of 4.5% (FY 1991), 5.1% (FY 1992), 5.6% (FY 1993), 5.7% (FY 1994). Labor rates used in determining the project costs are summarized in Table 9-3. In some cases—for example, magnet and vacuum systems fabrication—it was assumed that dedicated contract labor shops would be set up. Otherwise, the rates were based on current laboratory shop rates—mostly the shop rates at SLAC.

9.2 CONSTRUCTION SCHEDULE

The overall construction schedule is shown in Figs. 9-1a and 9-1b. This schedule, based on an optimum funding profile, shows that the B Factory can be completed in a 3-1/2 year construction period. If construction begins in FY 1993, the project would be completed during FY 1996.

Table 9-2. Profile for construction funds in FY 1991 and then-year dollars.

	FY 1993	FY 1994	FY 1995	FY 1996	Total
FY 1991 (K$)	40.0	63.0	47.0	17.2	167.2
Then-year (K$)	44.6	74.0	58.0	22.0	198.6

Table 9-3. SLAC shop rates used to establish the cost estimate.

Shop Description	Rate ($/hr)
Mechanical Engineer	53.20
Mechanical Design	37.10
Mechanical Fabrication	56.95
Mechanical Technician	38.75
Mechanical Alignment	51.15
Plating Shop	73.05
Electrical Engineer	47.02
Electrical Design	41.70
Electrical Fabrication Technician	32.00
Plant Engineer	47.85
Plant Engineering Drafting	43.40
Software Engineer	43.33
Software Coordinator	38.52
Davis-Bacon Labor	55.00

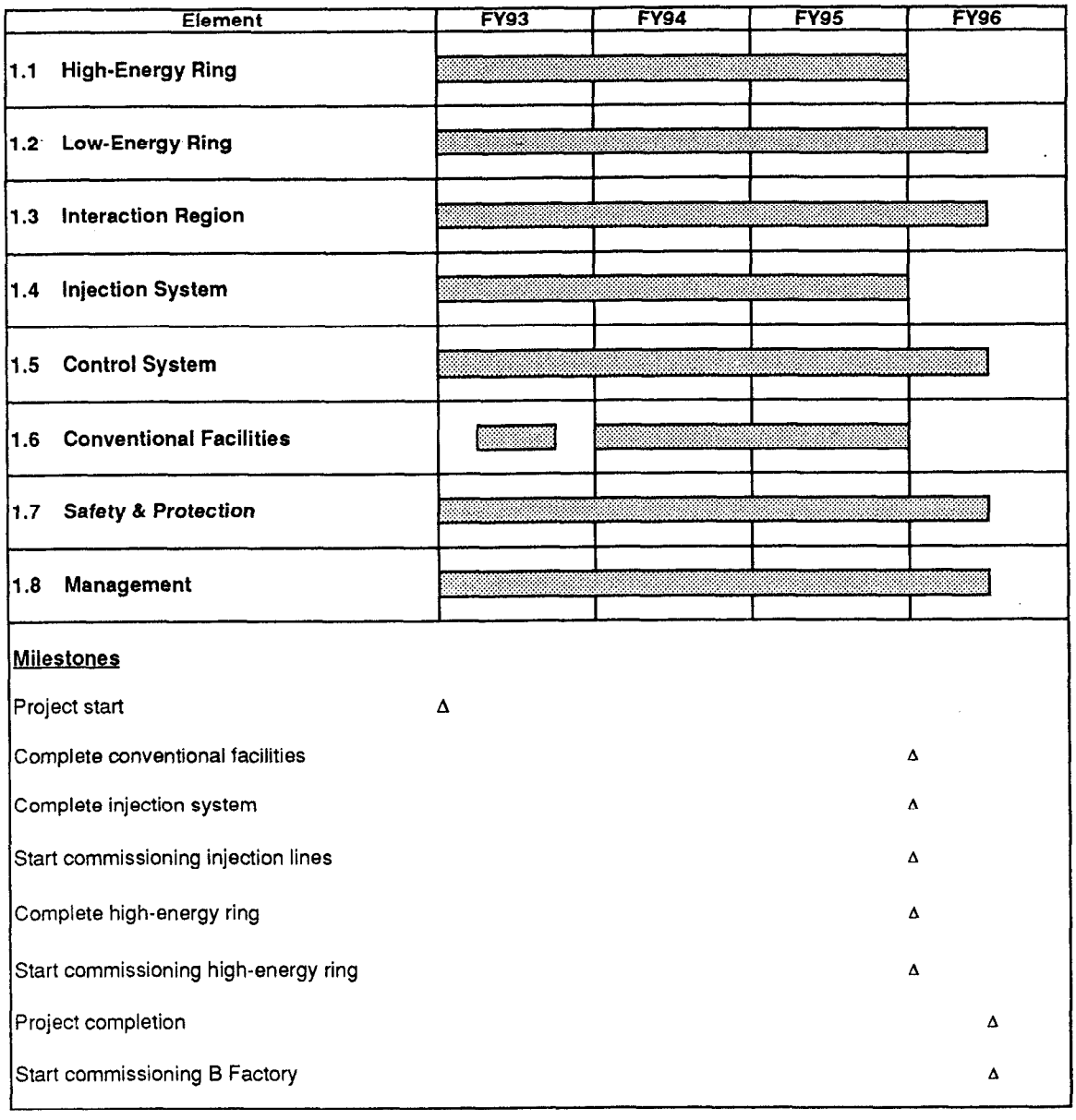

Fig. 9-1a. Overall schedule and project milestones for construction of the Asymmetric B Factory.

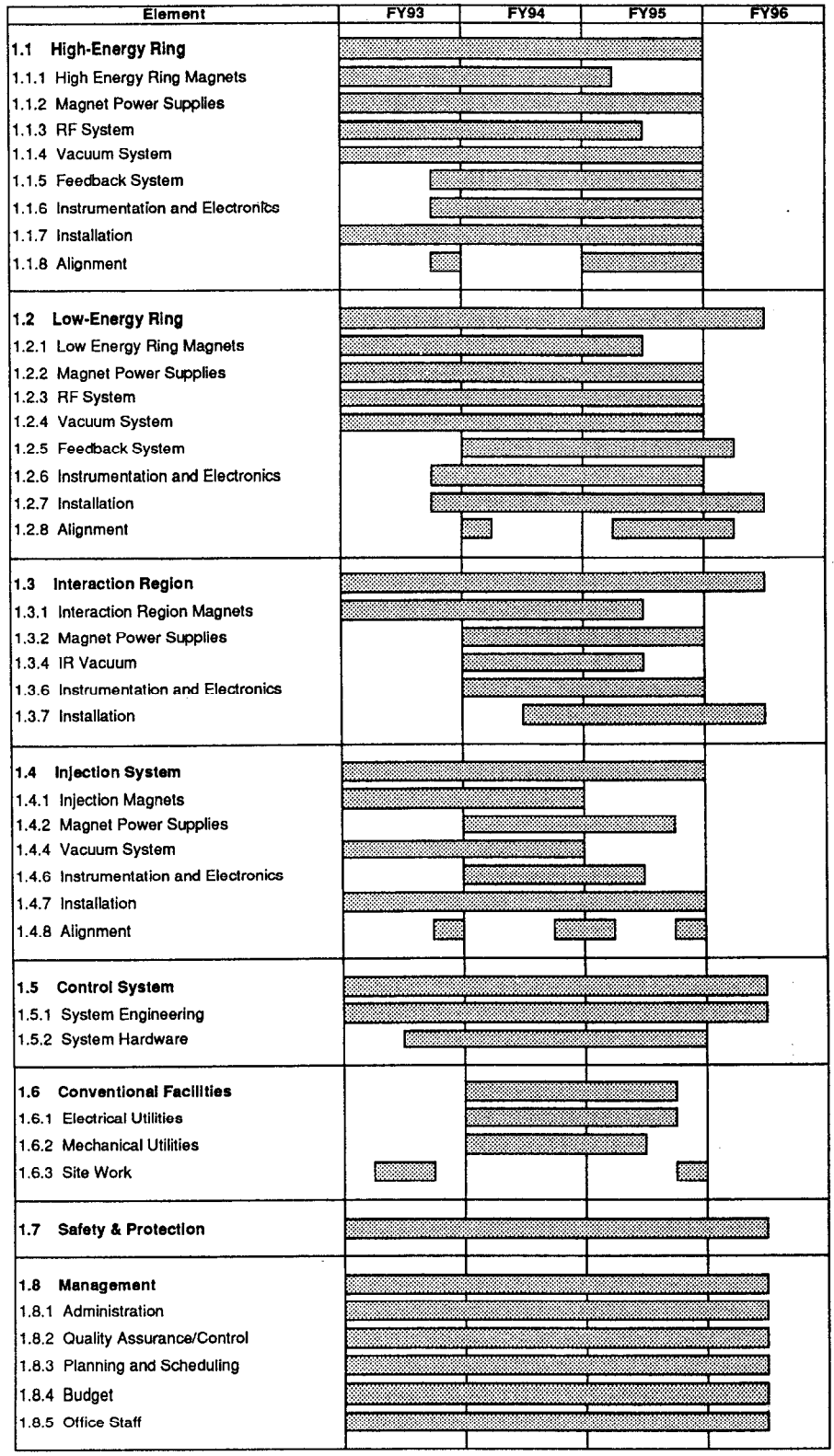

Fig. 9-1b. Project schedule (to WBS level 3) of the Asymmetric B Factory.

9.3 WORK BREAKDOWN STRUCTURE

The work breakdown structure was designed to be consistent with project management's need to track detailed costs of all B Factory subsystems. It conforms to the structure used by the SLAC Accounting Office for reporting costs and commitments to B Factory management. The levels are defined as follows:

- Level 1 = x *Asymmetric B Factory*
- Level 2 = x.x *Major systems*
- Level 3 = x.x.x *Subsystems*
- Level 4 = x.x.x.x *Subsystem detail*

Definitions for levels two and three of the WBS for the Asymmetric B Factory are given below.

1.1 High-Energy Ring. The B Factory utilizes a reconfigured and refurbished PEP storage ring, operating at 9 GeV, as the high-energy storage ring.

1.1.1 High-Energy Ring Magnets. The existing PEP magnets will be refurbished and reconfigured in the PEP tunnel. Additional quadrupoles will be added to maintain the beam focusing in the long straight sections.

1.1.2 High-Energy Ring Magnet Power Supplies. The existing PEP large power supplies will be refurbished; additional supplies will be acquired as needed for the new magnets. Monitoring systems will be constructed.

1.1.3 High-Energy Ring RF System. New high-power, low-impedance copper cavities, driven by commercially available 1-MW klystrons, will be designed and fabricated or purchased. This system, which is needed for the new operating conditions of the high-energy ring, will be at a higher frequency (476 MHz) than the original PEP RF system (353 MHz).

1.1.4 High-Energy Ring Vacuum System. The high circulating currents of the B Factory result in high synchrotron radiation power on the vacuum chamber wall. The existing PEP vacuum chamber will be replaced with a new copper chamber to provide the appropriate low pressure and thermal management. Costs of installation of the chamber are included here.

1.1.5 High-Energy Ring Feedback System. To control coupled-bunch instabilities in the high-energy ring, one longitudinal and two transverse feedback systems will be employed. These will be wideband, bunch-by-bunch systems, designed and built primarily in-house but using commercially obtained power amplifiers.

1.1.6 High-Energy Ring Instrumentation and Electronics. Beam position monitors, profile monitors, and various other beam diagnostic devices will be designed and fabricated.

1.1.7 High-Energy Ring Installation. The existing PEP storage ring will be disassembled, refurbished, and reassembled into its new configuration for the B Factory high-energy ring. Both RF and electrical installation are included here.

1.1.8 High-Energy Ring Alignment. The reinstallation of the PEP ring in its new configuration will require a realignment of all components.

1.2 Low-Energy Ring. The low-energy ring of the B Factory is a completely new ring having a circumference of 2200 m, to be located atop the high-energy ring in the PEP tunnel. Its nominal operating energy is 3.1 GeV.

1.2.1 Low-Energy Ring Magnets. The magnet system for the low-energy ring is modeled after that of the high-energy ring, with the lengths of some of the components reduced because of the lower energy. Designs and fabrication techniques closely follow those used successfully in the construction of the PEP magnets.

1.2.2 Low-Energy Ring Magnet Power Supplies. The bulk of the power supplies required for the low-energy ring are existing, refurbished PEP and other SLAC supplies.

1.2.3 Low-Energy Ring RF System. New high-power, low-impedance 476-MHz RF cavities, each driven by a commercially available 1-MW klystron, will be fabricated for the low-energy ring. No additional penetrations or surface buildings will be required.

1.2.4 Low-Energy Ring Vacuum System. The vacuum system for the low-energy ring utilizes a copper beam tube in those regions where the photon flux is high (the area just downstream of the bends) and a stainless-steel beam tube elsewhere.

1.2.5 Low-Energy Ring Feedback System. The feedback demands of the low-energy ring are comparable to those of the high-energy ring. These bunch-by-bunch feedback systems will be capable of damping both transverse and longitudinal instabilities.

1.2.6 Low-Energy Ring Instrumentation and Electronics. Beam position monitors, current monitors, profile monitors and other beam-monitoring devices and their associated electronics are included here.

1.2.7 Low-Energy Ring Installation. The low-energy ring magnetic components will be installed on preassembled and prealigned girders. The supports for these girders are an extension of the high-energy ring supports. Both RF and electrical installation are included here.

1.2.8 Low-Energy Ring Alignment. Conventional optical alignment tooling, already available at SLAC, will be modified to align the low-energy ring.

1.3 Interaction Region. The B Factory will have one interaction point, located at IR-2.

1.3.1 Interaction Region Magnets. Since the B Factory consists of two separate rings, special magnets are necessary to bring the beams into collision and then to return them to their respective rings. Included are the septum quadrupoles, as well as the permanent-magnet bending and focusing elements and their trim windings.

1.3.2 Interaction Region Power Supplies. Power supplies, as well as current-monitoring equipment are required for the septum quadrupoles, as well as for some conventional quadrupoles located in this area. Power for the permanent magnet trim windings is also included here.

1.3.4 Interaction Region Vacuum System. This includes all vacuum chamber elements in the interaction region, including the special thin-walled beryllium beam pipe for the detector, radial ion pumps, masks, etc.

1.3.6 Interaction Region Instrumentation and Electronics. Special care must be taken to monitor the beam position and measure the luminosity in the interaction region both to maximize the luminosity and to avoid background problems.

1.3.7 Interaction Region Installation. This entry includes the costs associated with the electrical and mechanical installation of the B Factory final focusing elements, including alignment costs. The IR components will be prealigned in a support barrel to ensure proper relative alignment through the detector.

1.4 Injection System. The injector for the B Factory is the SLAC linac. Separate bypass beamlines for positrons and electrons will be provided in the linac housing. These beams will be delivered to the NIT and SIT tunnels that now supply beams to PEP, and then transported in new transfer lines to the high- and low-energy ring injection straight sections.

1.4.1 Injection System Magnets. New magnets are required for the transport lines from linac sector 3 to the SIT line (for positrons) and from linac sector 7 to the NIT line (for electrons). Both the NIT and SIT lines will be upgraded at their entrance and exit ends.

1.4.2 Injection System Magnet Power Supplies. The existing NIT and SIT line bending magnet and quadrupole power supplies will be refurbished. New trim dipole power supplies will be added, and the power supply control and monitoring equipment will be upgraded. The positron and electron bypass lines will use existing bending magnet power supplies and new quadrupole supplies. Magnet control and monitoring equipment will be all new.

1.4.4 Injection System Vacuum System. Roughing fingers and necessary valving and piping for the bypass lines and the NIT and SIT lines are included here, as are ion pumps and their controllers.

1.4.6 Injection System Instrumentation and Electronics. New beam position monitors, profile monitors, and wire scanners will be installed in both the bypass lines and the NIT and SIT lines.

1.4.7 Injection System Installation. Two new beam transfer lines must be installed, bypassing the linac, to transport electrons to the NIT line and the positrons to the SIT line. The NIT and SIT lines will be extended by approximately 50 m and partially rebuilt.

1.4.8 Injection System Alignment. The two new bypass lines must be aligned and matched to the extraction from the linac and the injection into either the NIT or the SIT line. The NIT and SIT lines require realignment, as do their injection lines into the high- and low-energy rings.

1.5 Control System. The control system for the B Factory is modeled after the existing control system at the SLC.

1.5.1 Control System Engineering. This entry represents the engineering effort necessary to develop control software and hardware to operate the B Factory.

1.5.2 Control System Hardware This item represents the cost of the main control computer and various control consoles, networks, and electronics that link the subsystems to the control computer.

1.6 Conventional Facilities. The B Factory utilizes the existing PEP facility. No new conventional construction is required. The PEP electrical distribution system will be modified to accommodate the new load distribution of the B Factory. Similarly, the water system will be upgraded to replace some parts and slightly reconfigured to reflect the new B Factory loads.

1.6.1 Electrical Utilities. This entry reflects the cost of reconfiguring the PEP electrical distribution system to match B Factory requirements. It also includes the cost of upgrading the pumping capacity of the PEP cooling tower.

1.6.2 Mechanical Utilities. This entry represents the costs associated with upgrading the PEP cooling tower pumping system, the replacement of all the PEP LCW heat exchangers, and the modifications to the linac LCW system to accommodate the injector bypass lines.

1.6.3 Site Work. This involves improving the water management within the PEP tunnel. A small portion of the tunnel will be cleaned and water-diverting hardware will be installed.

1.7 Safety and Protection. Included here are costs associated with upgrading the fire-protection system and the rework of the personnel protection system. The salary of a full-time safety inspector will also be covered.

1.8 **Management.** This entry reflects the costs associated with the overall management of the project, i. e., effort that is not otherwise included in any of the various subsystem costs. (Salaries for lead engineers are associated with the costs of their respective subsystems.) Included are such things as project administration (1.8.1 and 1.8.5), quality control and quality assurance activities (1.8.2), planning and scheduling (1.8.3), and budget-related activities (1.8.4). In addition to the effort called out here, additional effort in some of these areas will be provided through the incremental indirect costs.

10.

SUMMARY

IN this report we have described a design for a high-luminosity Asymmetric B Factory to be built in the PEP tunnel on the SLAC site. This proposal, a collaborative effort of SLAC, LBL, and LLNL, is the culmination of more than two years of effort aimed at the design and construction of an asymmetric e^+e^- collider capable of achieving a luminosity of $\mathcal{L} = 3 \times 10^{33}$ cm^{-2} s^{-1}.

The configuration adopted utilizes two storage rings, an electron ring operating at 9 GeV and a positron ring at 3.1 GeV, each with a circumference of 2200 m. The high-energy ring is an upgrade of the PEP storage ring at SLAC; all PEP magnets and most power supplies will be reused. The upgrade consists primarily of replacing the PEP vacuum chamber and RF system with newly designed versions optimized for the high-current environment of the B Factory. The low-energy ring will be newly constructed and will be situated atop the high-energy ring in the PEP tunnel. Utilities already installed in the PEP tunnel are largely sufficient to operate the two B Factory storage rings.

Siting the Asymmetric B Factory at SLAC offers a number of important advantages. The existing 2200-m-circumference PEP tunnel provides sufficient space to construct the two-ring collider, and it permits a flexible design with conservative parameters. The bending radius accommodated by the arc sections, 165 m, allows the use of low-field bending magnets, thereby keeping the synchrotron radiation power density to reasonable levels (only 5 kW/m at the design current for the high-energy ring). The availability of six long (110 m) straight sections increases the flexibility of the design and easily accommodates the requirements for beam separation, tune control, injection, and the detector. (There is room for a second detector if extra funds become available.) Because the PEP tunnel was originally sized to house two rings, space is also fully adequate for the addition of the B Factory low-energy ring. Indeed, no conventional construction will be necessary for the B Factory at SLAC, saving both cost and time in making the B Factory operational. The tunnel is adequately shielded against the additional radiation that results from high-luminosity operation, and the IR hall is sufficient to accommodate the envisioned detector and its ancillary equipment.

A unique advantage of the SLAC site is the availability of the most powerful positron injection system in the world—the SLC linac. This feature is crucial for the operation of the collider as a "factory," because maintaining a high average luminosity depends strongly

on achieving rapid injection. The linac injection system is also the ideal choice in terms of the requirements of the storage ring feedback systems, because it provides a small amount of charge per injection shot, thus ensuring that the feedback systems are not overloaded by injection transients.

The design approach followed here has focused on achieving the performance goals of the B Factory in a reliable manner. This has meant designing the hardware from the outset with sufficient operating margin, as well as providing good diagnostics as part of the design. Where possible, we have adopted parameters consistent with established collider practice. For example, the required beam currents of 1.48 A and 2.14 A in the high- and low-energy rings, respectively, are split into 1658 bunches. Therefore, the single-bunch parameters (length, current, emittance, beam-beam tune shift) are all conventional and do not require any extrapolation from the operating experience of present machines.

Our choice of many low-intensity bunches, as opposed to fewer high-intensity bunches, avoids difficulties associated with single-bunch instabilities, though it does not change the need for a state-of-the-art feedback system to manage coupled-bunch instabilities. In our approach, the design challenges for the Asymmetric B Factory are restricted to a few selected areas. These areas, listed below, are all amenable to attack by standard engineering approaches and, though demanding, can be handled by applying and extending existing techniques in a reasonably well-understood manner.

Based on our studies, we have concentrated the design effort on those aspects where the most difficult technical challenges exist. These include

- Vacuum system
- RF system
- Multibunch feedback system
- Beam separation and detector masking system

For each of these areas, careful and systematic design work has been undertaken to identify the problems (associated mainly with the required high beam currents) and then to solve them. To ensure that our solutions are effective and appropriate, international experts in each of the above areas were brought to SLAC or LBL to review and validate our design concepts. In each case, the outcome of this process was favorable, thereby verifying the basic soundness of our design.

For the vacuum system, we have adopted a copper vacuum chamber patterned after the HERA design. Copper exhibits good thermal properties and a low rate of photon-induced gas desorption, thus ensuring a low pressure in the face of approximately 2 A of beam current in each ring. Detailed estimates of photon desorption and two- and three-dimensional thermal calculations of the chamber have demonstrated that the approach is an effective one.

The RF system is based on a standard room-temperature cavity design that includes waveguides to damp the unwanted higher-order modes of the structure. This approach has been shown (by means of three-dimensional electromagnetic calculations) to reduce the Q values of higher-order modes to very low values that are favorable for the stabilization of coupled-bunch motions. Furthermore, experiments have been performed on a simple pillbox cavity that confirm the results of the calculations and demonstrate the capability of reaching, or even exceeding, the required amount of damping.

The multibunch feedback system is based on a bunch-by-bunch approach. Extensive simulations have shown that the system will perform effectively under either injection or colliding-beam conditions. The feedback system makes use of commercially available wideband power amplifiers and requires a power level of 2 kW for the longitudinal case and even less for the transverse case. An advantage of our approach is that the feedback system will deal with any form of bunch motion, whatever the cause. Thus, even coherent disturbances arising from the beam-beam interaction can be controlled.

We have carefully designed a beam separation scheme to minimize detector backgrounds, and we have invested substantial effort in detailed simulations of the effects on detector background of both synchrotron radiation photons and lost electrons. This aspect is a challenge for the B Factory because we must achieve the same level of background typically found in today's colliders, but at a beam current an order of magnitude higher. Our masking design gives roughly a factor of 100 safety margin with respect to synchrotron radiation background limitations and about a factor of 15 margin with respect to lost particles. We have also shown the system to be stable against reasonable changes in our design assumptions by examining misalignments of magnets and masks.

The construction of the Asymmetric B Factory at SLAC is an ambitious and exciting project, both as an extension of the accelerator builder's art and as a contributor to our understanding of one of the most fundamental questions in our Universe—the origin of *CP* violation. The SLAC site, with its large-circumference tunnel and the world's most powerful positron injector, is an ideal base from which to launch such a project. Moreover, the combination of the three participating laboratories, SLAC, LBL, and LLNL, offers a pool of accelerator physics, high-energy physics, and engineering expertise unmatched anywhere—a team fully capable of dealing with the challenges that the high-luminosity Asymmetric B Factory presents. There is, in addition, a large community of physicists worldwide who eagerly await the exceptional physics opportunities afforded by the B Factory.

The time is at hand to begin the construction of this frontier facility for high-energy physics research. Based on a 3-1/2 year construction schedule, the Asymmetric B Factory could begin operation at the end of FY 1996. Thereafter, we envision a vigorous research effort that will last for at least 15 years and will address with unique efficiency some of the crucial problems in high-energy physics today.

ACKNOWLEDGMENTS

ALTHOUGH it is not possible to thank individually all of the many people who contributed to the B Factory Conceptual Design Report, a few names stand out. This report could not have been completed without the superb organizational and editing skills of Douglas Vaughan, who served as its technical editor; the dedication he has shown is evident in the report. The staff of the LBL Information Resources Department, including Loretta Lizama, who kept the myriad figures in order and provided editorial assistance; Jean Wolslegel and Connie Silva, who were responsible for the superb—and tireless—technical typing efforts; and technical illustrators Marilee Bailey, Linda Geniesse, Ralph Dennis, John Flambard, and Bill Bero, who took excellent care with the many drawings, were the unsung heros of this work. All of these people literally worked day and night to get the job done. The efforts of Andrea Chan at SLAC, who served as the conduit for the huge number of computer files that were part of this multi-laboratory collaborative effort, were also crucial to the completion of this document. It is a pleasure to thank all of them—and even more of a pleasure to have had the opportunity to work with such dedicated professionals.

REFERENCES

Albrecht, M., et al., 1987. *Phys. Lett.* **192B,** 245.

Alexandrov, A., A. Hutton, and P. Logatchev, *Synchrotron Radiation Power Calculations and Bending Radius Choice for the LER*, SLAC Internal Report ABC-13.

Allen, M., and L. Karvonen, 1978. *Precautions against RF Radiation Leakage in PEP*, SLAC-PTM-177.

Altarelli, G., and F. Buccella, 1964. *Nuovo Cimento* **34**, 6385.

Ballion, R., et al., 1989. In Proceedings of the 2nd International Conference on Brazing, High-Temperature Brazing, and Diffusion Welding, Essen.

Barletta, W. A., and A. Garren, 1990. *Radiation from Wigglers in the Low Energy Ring of an Asymmetric B-Factory*, ABC Note 30 and LLNL Internal Report.

Bassetti, M., and G. A. Erskine, 1980. *Closed Expression for the Electric Field of a Two-Dimensional Gaussian Charge,* CERN-ISR-TH/80-06; see also lectures by E. Keil and G. H. Rees in *Theoretical Aspects of the Behaviour of Beams in Accelerators and Storage Rings*, CERN 77-13.

Billing, M., 1990. Private communication.

Bowden, G., 1985. SLAC CN 314.

Bowden, G., and G. Putallaz, 1985. *A Positioning System for the Final Quadrupole Triplet*, Final Focus memo.

Brown, K. L., et al., 1977. *TRANSPORT,* SLAC-91.

Carey, D. C., et al., 1982. *DECAY TURTLE,* SLAC-246.

Chao, A. W., and J. Gareyte, 1976. *Scaling Law for Bunch Lengthening in SPEAR-II*, SLAC Note SPEAR-197, PEP-224.

Chin, Y. H. , 1990. "Symmetrization of the Beam-Beam Interaction," in *Beam Dynamics Issues of High Luminosity Asymmetric Collider Rings,* A. M. Sessler, ed., *AIP Conf. Proc.* **214**, 424; also Y. H. Chin, LBL-27665, 1989.

Chin, Y. H., 1988. *Program MOSES, Mode-Coupling Single-Bunch Instability in Electron Storage Rings, Version 2.0,* CERN/LEP-TH/88-05.

Christenson, J., et al., 1964. *Phys. Rev. Lett.* **13,** 138.

Conciauro, G., and P. Arcioni, 1990. "A New HOM-free Accelerating Resonator," in Proceedings of the 2nd European Particle Accelerator Conference, Nice.

Constant, T. N., et al., 1977. *Operational Experience with SLAC's Beam Containment Electronics,* SLAC-1901.

Corlett, J. N., 1989. "Higher-Order Modes in the SRS 500 MHz Accelerating Cavities," in Proceedings of the 1989 IEEE Particle Accelerator Conference, Chicago, pp. 211–213.

Corlett, J. N., and S. F. Hill, 1989. *Measurement of the Damping of Higher-Order Modes in the Cavity by Waveguide Filters,* SRS/APN/89/96.

Earth Sciences Associates, 1982. *Appendix C Seismic Considerations for Design of the SLC Tunnels.*

Earth Sciences Associates, 1991. *Stanford Linear Accelerator Center Ground Water Monitoring Network Environmental Assessment,* ESA project 3472.

Feasibility Study for an Asymmetric B Factory Based on PEP, 1989. LBL PUB-5244, SLAC-352, CALT-68-1589.

Fischer, G. E., 1989. *SLAC Site Geology, Ground Motion and Some Effects of the October 17, 1989, Earthquake,* SLAC-358.

Foerster, C. L., H. Halama, and C. Lanni, 1970. "Photon-Stimulated Desorption Yields from Stainless-Steel and Copper Plated Beam Tubes with Various Pretreatments," *J. Vac. Sci. Technol. A* **8**(3), 2856.

Funakoshi, F., et al., 1990. "Asymmetric B-Factory Project at KEK," in *Beam Dynamics Issues of High-Luminosity Asymmetric Collider Rings,* A.M. Sessler, ed., *AIP Conf. Proc.* **214,** 575.

Furman, M. A., 1991a. *The Hourglass Reduction Factor for Asymmetric Colliders,* ABC-21/ESG-161.

Furman, M. A., 1991b. *Luminosity Formulas for Asymmetric Colliders with Beam Symmetries,* ABC-25/ESG-0163.

Gaede, G., et al., 1980. DESY M-80/08.

Garren, A. A., et al., 1989. "An Asymmetric B-Meson Facility at PEP," in Proceedings of the 1989 IEEE Accelerator Conference, p. 1847.

Gröbner, O., et al., 1983. "Studies of Photon Induced Gas Desorption Using Synchrotron Radiation," *Vacuum* **33**, 397.

Halama, H. J., and Y. Guo, 1990. "Non-Evaporable Getter Investigation at the National Synchrotron Light Source," submitted to Proceedings of Second Topical Conference on Vacuum Design of Synchrotron Light Sources, Argonne National Laboratory, November 1990.

Halbach, K., 1981. *Nucl. Instrum. Methods* **187,** 107.

Hartill, D., 1990. "CESR B," invited talk at the International Workshop on Accelerators for Asymmetric B-Factories, KEK, October 4–6, 1990.

Hartwig, H., and J. S. Kouptsidis, 1974. "A New Approach for Computing Diode Sputter-Ion Pump Characteristics," *J. Vac. Sci. Technol.* **11,** 1154. These design rules give satisfactory agreement with the measured performance of SLAC radial ion pumps.

Heifets, S., 1990a. *HOM Losses at the IR of the B Factory*, SLAC Note ABC-14/AP-81.

Heifets, S., 1990b. *Preliminary Estimate of B Factory Impedance*, SLAC Note ABC-21.

Heins, D., et al., 1989. *Wideband Multibunch Feedback Systems for PETRA*, DESY 89-157.

Henke, H., and I. Wilson, 1981. *Thermal Analysis and Loss in Shunt Impedance of the LEP Accelerating Cell,* LEP Note 309.

Herb, S. W., 1989. *IEEE Trans. Nucl. Sci.* **NS34,** 1434.

Herrmann, W., and W. Szyszko, 1989. *IEEE Trans. Magnetics* **25,** 3278.

Hirata, K., 1990. "The Beam-Beam Interaction: Coherent Effects," in Beam Dynamics Issues of High-Luminosity Asymmetric Collider Rings, A.M. Sessler, ed., *AIP Conf. Proc.* **214,** 175.

Hitlin, D., 1989. SLAC-353, LBL PUB-5245, CALT-68-1588.

Hitlin, D., 1991. SLAC-373, LBL PUB-30097, CALT-68-1697.

Investigation of an Asymmetric B Factory in the PEP Tunnel, 1990. LBL PUB-5263, SLAC-359, CALT-68-1622.

Investigation of an Asymmetric B Factory in the PEP Tunnel, 1990. LBL PUB-5263, SLAC-359, CALT-68-1622.

Jackson, G., 1990. *AIP Conf. Proc.* **214.**

Jacob, A. F., G. R. Lambertson, and W. Barry, 1990. "Higher-Order Mode Damping in an ALS Cavity," in Proceedings of the 2nd European Particle Accelerator Conference, Nice, pp. 928–930.

Jenkins, T. M., W. R. Nelson, and N. Jpe, 1990. *Synchrotron Radiation Leakage from the B-Factory Beam Pipe*, ABC Note 17.

Kheifets, S. A., J. M. Paterson, and G.-A. Voss, 1989. SLAC-PUB-5011.

Kim, K.-J., 1986. "Angular Distribution of Undulator Power," *Nucl. Instrum. Methods* **A246**.

Krishnagopal, S., and R. H. Siemann, 1990. "A Comparison of Flat Beams with Round," in *Beam Dynamics Issues of High-Luminosity Asymmetric Collider Rings*, A.M. Sessler, ed., *AIP Conf. Proc.* **214,** 278.

Krishnagopal, S., and R. Siemann, 1990. "Bunch-length Effects in the Beam-Beam Interaction," *Phys. Rev.* **D41,** 2312.

Kroll, N., and D. Yu, 1990. *Computer Determination of the External Q and Resonant Frequency of Waveguide Loaded Cavities*, SLAC-PUB-5171.

Laslett, L. J., S. Caspi, and H. Helm, 1987. *Particle Accelerators* **22,** 1 .

Lightbody, J. W., Jr., and J. S. O'Connel, 1988. "Modeling Single-Arm Electron Scattering and Nucleon Production from Nuclei by GeV Electrons," *Computers in Physics,* May/June, p. 57.

Mathewson, A. G., et al., 1990. "Comparison of Synchrotron Radiation Induced Gas Desorption from Al, Stainless Steel and Cu Chambers," submitted to Proceedings of Second Topical Conference on Vacuum Design of Synchrotron Light Sources, Argonne National Laboratory, November 1990.

Nakada, T., ed., 1990. *Feasibility Study for a CERN B Factory in the CERN ISR Tunnel*, CERN 90-02.

Nelson, W. R., G. J. Warren, and R. C. Ford, 1975. *Radiation Dose to Coil Windings and Production of Nitric Acid and Ozone from PEP Synchrotron Radiation*, PEP Note PEP-109.

Nelson, W. R., H. Hirayama, and D. W. O. Rogers, 1985. *The EGS4 Code System,* SLAC-265.

Nir, Y., et al., 1990a. *Nucl. Phys.* **B345,** 301.

Nir, Y., et al., 1990b. *Phys. Rev.* **D42,** 1473.

Nir, Y., et al., 1990c. *Phys. Rev.* **D42,** 1477.

Oddone, P. J., 1987. In Proceedings of the UCLA Workshop: Linear Collider $B\bar{B}$ Factory Conceptual Design, p. 243.

Oide, K., and K. Yokoya, 1989. SLAC-PUB-4832.

1-2 GeV Synchrotron Radiation Source: Conceptual Design Report, 1986. LBL PUB-5172 Rev.

Padamsee, H., et al., 1990. "Superconducting Cavities for a B-Factory—Interim Progress Report," in *Beam Dynamics Issues of High-Luminosity Asymmetric Collider Rings,* A.M. Sessler, ed., *AIP Conf. Proc.* **214,** 508.

Palmer, R., 1988. SLAC-PUB-4707.

PEP Design Handbook, 1977. Stanford Linear Accelerator Center and Lawrence Berkeley Laboratory, H. Wiedemann, Ed.

Phinney, N., 1985. *Report on the SLC Control System,* SLAC report 3668.

Phinney, N., and H. Shoaee, 1987. *The SLC Controls System—Status and Development,* SLAC report 4215.

Piwinski, A., 1977. *IEEE Trans. Nucl. Sci.* **NS-24,** 1408.

Piwinski, A., 1990. DESY HERA report 90-04.

Piwinski, A., 1991. To be published.

Piwinski, A., and A. Wrulich, 1976. DESY report 76/07.

Porter, F., 1990. CALT-68-1611; to be published in *Nucl. Instrum. Methods A.*

Rice, D., 1989. Presentation at Third Advanced ICFA Beam Dynamics Workshop on Beam-Beam Effects in Circular Accelerators, Akademgorodok, Novosibirsk, USSR.

Rice, D., 1990. *In Beam Dynamics Issues of High Luminosity Asymmetric Collider Rings,* A. M. Sessler, ed., *AIP Conf. Proc.* **214,** 219.

Rivkin, L., 1987. "Collective Effects in PEP," in Proceedings of the Workshop on PEP as a Synchrotron Radiation Source, October 20–21, 1987, p. 139.

Rivkin, L., 1990. "B-Meson Factory in the CERN-ISR Tunnel," *Beam Dynamics Issues of High-Luminosity Asymmetric Collider Rings,* Berkeley, CA, A.M. Sessler, ed., *AIP Conf. Proc.* **214,** 536.

Rogers, D. W. O., 1984. "Fluence to Dose Equivalent Conversion Factors Calculated with EGS3 for Electrons from 100 keV to 20 GeV and Photons from 11 keV to 20 GeV," *Health Phys.* **46**, 891.

Sagan, D., R. Siemann, and S. Krishnagopal, 1990, Cornell report CLNS 90/1001.

Sands, M., 1970. *Physics of Electron Storage Rings—An Introduction*, SLAC report SLAC-121.

Savage, W. P., 1990. *Potential Earthquake Effect on B-Factory at PEP*, SLAC report.

Seeman, J. T., 1985. "Nonlinear Dynamics Aspects of Particle Accelerators," in Proceedings of the Joint US-CERN School on Particle Accelerators, Sardinia, Italy, J. M. Jowett, M. Month, and S. Turner, eds., *Springer-Verlag Lecture Notes in Physics* **247**, p. 121.

SLAC Earthquake Emergency Plan, 1987.

SLAC Electrical Safety Policy, 1990.

SLAC Electrical Safety Standards, 1990.

SLAC Emergency Planning Booklet, 1988.

SLAC Environment and Safety Office, 1987. *SLAC Safety Program.*

SLAC Hazard Communication Program, 1986.

SLAC Radiation Rule Book, 1990.

SLAC Radiation Safety Procedures, 1990.

Smith, H., and T. Constant, 1981. *Radiation and Electrical Safety Systems for PEP*, SLAC-2675.

Spencer, J. E., 1985. SLAC-PUB 3647.

Taylor, B. 1990. Private communication.

Tennyson, J. L., 1990. "The Beam-Beam Limit in Asymmetric Colliders: Optimization of the B-Factory Parameter Base," in *Beam Dynamics Issues of High Luminosity Asymmetric Collider Rings*, A. M. Sessler, ed., *AIP Conf. Proc.* **214**, 130.

Tennyson, J. L., 1991a. *Long-Range Forces in APIARY-6*, ABC Note 28.

Tennyson, J. L., 1991b. *Choosing the APIARY-6 Tunes: Luminosity Considerations*, ABC Note 29.

Ueda, S., et al., 1990. "Photodesorption from Stainless-Steel, Aluminum Alloy, and Oxygen-Free Copper Test Chambers," submitted to Proceedings of Second Topical Conference on Vacuum Design of Synchrotron Light Sources, Argonne National Laboratory, November 1990.

Van Bibber, K., 1989. *Nucl. Instrum. Methods* **B40/41,** 436.

Weidner, H., 1990. *Seepage into PEP Tunnel,* SLAC-ABC-10.

Zholents, A. A., 1990. "Novosibirsk B-Factory," in *Beam Dynamics Issues of High-Luminosity Asymmetric Collider Rings*, A. M. Sessler, ed., *AIP Conf. Proc.* **214,** 592.

Zisman, M. S., 1990a. In *Beam Dynamics Issues of High-Luminosity Asymmetric Collider Rings*, A. M. Sessler, ed., *AIP Conf. Proc.* **214,** 81.

Zisman, M. S., 1990b. *Influence of Collective Effects on the Performance of High Luminosity Colliders*, ABC Note 8.

Zisman, M. S., et al., 1988. *Study of Collective Effects for the PEP Low-Emittance Optics*, LBL Report LBL-25582, SSRL ACD Note-59.

Zisman, M. S., S. Chattopadhyay, and J. Bisognano, 1986. *ZAP User's Manual*, LBL Report LBL-21270.

APPENDIX A: PARAMETERS

THIS appendix contains a summary of the B Factory accelerator parameters. It is intended to give a self-consistent snapshot of the machine design. As such, values are often given to more precision than would ultimately be relevant (or even measurable) in an operating accelerator. We start with a few specific comments on the tables to follow.

General Machine Parameters. As is conventional, we quote the luminosity at zero bunch length, constrained by design to 3.00×10^{33} cm^{-2} s^{-1}. If we take into account the geometric effect of a finite bunch length, the luminosity is reduced by about 5% to 2.83×10^{33} cm^{-2} s^{-1}.

The $1/e$ luminosity decay time is estimated under the conservative assumption that the spot sizes remain constant, that is, that the luminosity goes like the product of the two beam currents. It includes beam loss estimated from $e^+e^- \rightarrow e^+e^-$, $e^+e^- \rightarrow e^+e^-\gamma$, beam-gas bremsstrahlung, beam-gas Coulomb, and Touschek intrabeam scattering. These estimates are made for a 10σ limiting transverse aperture (for an uncoupled beam horizontally and fully coupled beam vertically).

Lattice Cell Parameters. There are four "standard straights" in the HER and two in the LER. These include the two phase control straights in each ring. In addition, there is an "injection straight" and an "IR straight" in each ring, and two "wiggler straights" in the LER.

APPENDIX A

TABLES

TABLE A–1

General Machine Parameters

Parameter	Symbol	High energy ring	Low energy ring	Units
Center-of-mass energy	$E_{\text{c.m.}}$	10.580		GeV
Beam energy	E	9.000	3.109	GeV
Peak luminosity	L	3.00×10^{33}		$\text{cm}^{-2}\text{s}^{-1}$
$1/e$ luminosity decay time	τ_L	1.92		hr
Number of populated bunches	n_b	1658	1658	
Number of empty bunches	$n_b(\text{gap})$	88	88	
Bunch spacing	s_b	1.2596		m
Machine circumference	L	2199.318	2199.318	m
Horizontal tune	ν_x	25.280	32.280	
Vertical tune	ν_y	24.180	35.180	
Momentum compaction	α_p	.00244	.00149	
Natural energy spread	σ_E	5.50	2.97	MeV
Natural fractional energy spread	δ_E	6.1×10^{-4}	9.5×10^{-4}	
Natural bunch length	σ_ℓ	1.00	1.00	cm
Circulating current	I	1.479	2.140	A
Number of particles/bunch	N_b	4.084×10^{10}	5.911×10^{10}	
Horizontal damping time	τ_x	37.2	36.5	ms
Horizontal emittance	ϵ_x	48.24	96.48	nm–rad
Vertical emittance	ϵ_y	1.93	3.86	nm–rad
Natural chromaticity, Horizontal	ξ_x	−35.662	−51.800	
Natural chromaticity, Vertical	ξ_x	−46.652	−55.114	
Horizontal damping partition number	J_x	0.9914	1.0050	
Vertical damping partition number	J_y	1.0000	1.0000	
Longitudinal damping partition number	J_E	2.0086	1.9950	
Energy variation of J_x	$dJ_x/d\ln E$	−275.36	−7.88	
Energy Variation of J_y	$dJ_y/d\ln E$	0	-0.78	
Energy Variation of J_E	$dJ_E/d\ln E$	275.36	8.66	
Estimated Touschek lifetime	τ_{IB}	188	65	hr

TABLE A–2

Interaction Region Parameters

Parameter	Symbol	High energy ring	Low energy ring	Units
Horizontal beta function at IP	β_x^*	75.00	37.50	cm
Vertical beta function at IP	β_y^*	3.00	1.50	cm
Horizontal dispersion at IP	D_x^*	0.000	0.000	m
Vertical dispersion at IP	D_y^*	0.000	0.000	m
Horizontal spot size at IP	σ_x^*	190	190	μm
Vertical spot size at IP	σ_y^*	7.6	7.6	μm
Beam cross half-angle	θ_x	0.0		mrad
Beam-beam linear tune shift	$\Delta\nu_x$	0.030	0.030	
Beam-beam linear tune shift	$\Delta\nu_y$	0.030	0.030	
$e^+e^- \rightarrow e^+e^-\gamma$ beam lifetime	τ_{Br}	21.9	35.5	hr
$e^+e^- \rightarrow e^+e^-\gamma$ luminosity lifetime	τ_{Br}	17.2		hr
Beam pipe inner radius at IP	r^*	2.50		cm
IP to first magnet distance	d_f	0.200		m
Detector solenoid field	B_{sol}	1.00		T
Detector solenoid length	L_{sol}	4.00		m

TABLE A–3

RF System Parameters

Parameter	Symbol	High energy ring	Low energy ring	Units
Circulating current	I	1.479	2.140	A
Natural bunch length	σ_ℓ	1.00	1.00	cm
RF frequency	f_{RF}	476.0	476.0	MHz
Harmonic number	h	3492	3492	
Synchrotron tune	ν_s	0.0522	0.0498	
Synchrotron frequency	f_s	7.1	6.8	kHz
Energy loss per turn	U_{0i}	3.58	1.24	MeV
Synchrotron radiation power	P_{SR}	5.29	2.66	MW
HOM power	P_{HOM}	0.53	0.94	MW
Cavity wall loss total	P_{Wall}	2.45	1.26	MW
Total RF power	P_{RF}	8.27	4.86	MW
Klystron power total	$P_{tot\,\mathrm{Klys.}}$	10.00	5.00	MW
RF voltage	V_{RF}	18.48	9.45	MV
Synchronous phase angle	ϕ_s	167.7	169.8	deg
Fractional energy RF aperture	$f_E(\mathrm{RF})$	0.0105	0.0173	
Fractional energy aperture	f_E	0.0061	0.0095	
Number of klystrons	N_{klys}	10	5	
Power/klystron	P_{klys}	1.00	1.00	MW
Number of cavities	N_{Cavity}	20	10	
Shunt impedance	R_s	3.5	3.5	MΩ
Gap voltage	V_g	0.93	0.94	MV
Accelerating gradient	E	4.20	4.27	MV/m
Wall loss/cavity	P_{Wall}	0.122	0.126	MV
Coupling factor, no beam	β	3.7	3.6	
Unloaded Q	Q	30000	30000	

TABLE A–4

Instrumentation and Feedback

Parameter	Symbol	High energy ring	Low energy ring	Units
Number of BPMs	N_{BPM}	144	144	
Number of BPMs/cell		1	1	
Bunch spacing	t_b	4.202		ns
RF frequency	f_{RF}	476.0	476.0	MHz
Longitudinal feedback system				
Beam pickup central frequency		2856	2856	MHz
Phase detector dynamic range		±15.0	±15.0	deg
Phase detector resolution		0.50	0.50	deg
Bunch-to-bunch signal isolation		> 26	> 26	dB
Kicker structure operating frequency	f_{kick}	1.071	1.071	GHz
Number of kicker units	N_{kick}	4	3	
Kicker length	L_{kick}	0.32	0.32	m
Kicker bandpass		241	241	MHz
Kicker shunt impedance	Z_{kick}	1600	1600	Ω
Power for 1 kV		313	313	W
Maximum voltage/turn		4	3	kV
Transverse feedback system				
Number of kicker units	N_{kick}	2	1	
Kicker length	L_{kick}	0.32	0.32	m
Kicker shunt impedance	Z_{kick}	2950	2950	Ω
Power per kicker		332	678	W

TABLE A–5

Vacuum Parameters

Parameter	Symbol	High energy ring	Low energy ring	Units
Vacuum (design):				
Arcs		5×10^{-9}	7.5×10^{-9}	Torr
Straights		3×10^{-9}		Torr
Upstream of IP		1×10^{-9}		Torr
Local maximum at IP		1×10^{-8}		Torr
Value assumed for lifetime		5×10^{-9}	6×10^{-9}	Torr
Horizontal chamber aperture	a_x	9.0	9.0	cm
Vertical chamber aperture	a_y	5.0	5.0	cm
Dipole critical energy	ϵ_{crit}	9.8	2.2	keV
Beam-gas bremss. beam lifetime	τ_{BGbrem}	8.0	7.4	hr
Beam-gas Coulomb beam lifetime	τ_{BGcoul}	27.4	6.9	hr
Nominal desorption for Cu	η_{Cu}	2×10^{-6}		$\frac{\text{molecules}}{\text{photon}}$
Pumping speed in arc cell		1912 125	680 44	L/s L/s/m
Pumping speed in straight cell		460 30	440 29	L/s L/s/m
Pumping speed in RF cavity		500	500	L/s

TABLE A–6

Lattice Cell Parameters

Parameter	Symbol	High energy ring	Low energy ring	Units
Standard arc cells				
Number of cells	N_{cell}	72	72	
Cell Layout		QF-B-QD-B		
Cell length	L_{cell}	15.125	15.125	m
Phase advance	ϕ_c	60.0	80.0	deg
Dipole magnetic length	L_B	5.400	1.000	m
Dipole field at E_{des}	B_B	0.1819	0.3394	T
Bend radius	ρ	165.012	30.558	m
Dispersion suppressor cells				
Number of cells	N_{cell}	24	24	
Cell Layout		QF-B-QD-B		
Cell length	L_{cell}	16.013	16.013	m
Phase advance	ϕ_c	~ 90	~ 90	deg
Dipole magnetic length	L_B	5.400	1.000	m
Dipole field at E_{des}	B_B	0.1819	0.3394	T
Bend radius	ρ	165.012	30.558	m
Standard straight cells				
Number of cells	N_{cell}	32	16	
Cell Layout		QF-O-QD-O		
Cell length	L_{cell}	15.125	15.125	m
Phase advance	ϕ_c	~ 60	~ 90	deg

TABLE A–7

Main Dipole Parameters

Parameter	Symbol	High energy ring	Low energy ring	Units
Magnet designation		2.8C212	2.8C40	
Number of magnets	N_B	192	192	
Dipole field at E_{des}	B_B	0.1819	0.3394	T
Integrated field at E_{des}	$\int B d\ell$	0.9824	0.3394	T-m
Pole width	w_B	8.425	7.500	in
Gap height	h_B	2.787	2.787	in
Core length	$L_{\text{core}\,B}$	209.84	36.58	in
Dipole magnetic length	L_B	212.60	39.37	in
Width of useful field (0.1%)		4.725	4.000	in
Lamination height	$h_{\ell B}$	15.433	16.000	in
Lamination width	$w_{\ell B}$	18.189	17.800	in
Packing factor (minimum)		96	96	%
Core weight	$m_{\text{core}\,B}$	14168	2000	lb
Ampere-turns per pole at E_{des}		5279	9600	A-turns
Turns/pole		8	15	
Pancakes/pole		1	1	
Conductor width		2.402	2.000	in
Conductor height		0.7087	0.3125	in
Cooling hole diameter		0.25	0.1875	in
Conductor cross section area		1.59	0.60	in^2
Current at E_{des}	I_B	659.9	640.0	A
Resistance	R_B	5.50	7.20	mΩ
Power at E_{des}	P_B	2.40	2.95	kW
Voltage drop at E_{des}	V_B	3.63	4.61	V
Coil weight	$m_{\text{coil}\,B}$	585	200	lb
Number of water circuits		2	2	
Water flow rate		1.2	1.2	gpm
Water pressure drop		50	100	psi
Temperature rise		7.6	9.4	°C

TABLE A–8

Miscellaneous HER Dipole Parameters

Parameter	Value	Units
Magnet designation	2.8C40	
Number-of magnets	4	
Field at E_{des}	0.0356	T
Integrated field at E_{des}	0.0356	T-m
Magnet designation	5.25C80	
Number of magnets	8	
Field at E_{des}	0.0166	T
Integrated field at E_{des}	0.0332	T-m
Pole width	5.9	in
Gap height	5.276	in
Core length	73.622	in
Magnetic length	78.740	in
Magnet designation	5.25C80	
Number of magnets	8	
Field at E_{des}	0.0214	T
Integrated field at E_{des}	0.0428	T-m

TABLE A–9

Miscellaneous LER Dipole Parameters

Parameter	Value	Units
3 degree wiggler dogleg		
Magnet designation	2.8C80	
Number of magnets	4	
Field at E_{des}	0.2716	T
Integrated field at E_{des}	0.5432	T-m
1.3 degree vertical bend		
Magnet designation	2.8C20	
Number of magnets	4	
Field at E_{des}	0.4707	T
Integrated field at E_{des}	0.2354	T-m
0.75 degree vertical bend		
Magnet designation	2.8C20	
Number of magnets	4	
Field at E_{des}	0.2716	T
Integrated field at E_{des}	0.1358	T-m
2.5 degree IR bend		
Magnet designation	2.8C40	
Number of magnets	2	
Field at E_{des}	0.4526	T
Integrated field at E_{des}	0.4526	T-m
1.078 degree IR bend		
Magnet designation	2.8C40	
Number of magnets	1	
Field at E_{des}	0.1952	T
Integrated field at E_{des}	0.1952	T-m
0.176 degree IR bend		
Magnet designation	2.8C40	
Number of magnets	1	
Field at E_{des}	0.0319	T
Integrated field at E_{des}	0.0319	T-m

TABLE A–10

Main High Energy Ring Cell Quadrupole Parameters

Parameter	Value						Units
Magnet designation	4Q21	4Q29	4Q21	4Q29	4Q39	4Q39L	
Principal function	QD arcs	QF arcs	QD Sup.		QF Sup.	Straights	
Number of magnets	66	72	24	12	24	60	
Gradient at E_{des}	7.29	5.58	7.99	5.59	5.39	4.05	T/m
Pole tip field at E_{des}	0.3640	0.2790	0.3990	0.2790	0.2700	0.2030	T
Gradient length product	4.070	4.089	4.461	4.096	5.385	4.050	T
Inscribed radius	1.968	1.968	1.968	1.968	1.968	1.968	in
Minimum gap	1.457	1.457	1.457	1.457	1.457	1.457	in
Core length	21.00	27.86	21.00	27.86	38.35	38.39	in
Magnetic length	21.98	28.85	21.98	28.85	39.33	39.37	in
Lamination height	13.98	13.98	13.98	13.98	13.98	10.50	in
Lamination width	13.35	13.35	13.35	13.35	13.35	10.50	in
Packing factor (minimum)	98	98	98	98	98	98	%
Core weight	2882	3824	2882	3824	5263	3455	lb
Amp-turns per pole at E_{des}	7243	5546	7937	5553	5357	4027	A-turns
Turns/pole	56	56	56	56	56	37	
Pancakes/pole	1	1	1	1	1	1	
Conductor width	0.500	0.500	0.500	0.500	0.500	0.500	in
Conductor height	0.500	0.500	0.500	0.500	0.500	0.500	in
Cooling hole diameter	0.250	0.250	0.250	0.250	0.250	0.250	in
Conductor cross section area	0.197	0.197	0.197	0.197	0.197	0.197	in^2
Current at E_{des}	129.3	99.0	141.7	99.2	95.7	108.8	A
Resistance	72.7	91.8	72.7	91.8	121.45	80.24	mΩ
Power at E_{des}	1.22	0.90	1.46	0.90	1.11	0.95	kW
Voltage drop at E_{des}	9.40	9.09	10.30	9.10	11.62	8.73	V
Coil weight	233	308	233	308	396	396	lb
Number of water circuits	1	1	1	1	1	1	
Water flow rate	0.65	0.55	0.65	0.55	0.50	0.50	gpm
Water pressure drop	150	150	150	150	150	150	psi
Temperature rise	7.1	6.2	8.5	6.2	8.4	7.2	°C

TABLE A–11

Miscellaneous HER Quadrupole Parameters

Parameter	Value	Units
QFI1 injection straight (4Q39)		
Number of magnets	2	
Gradient at E_{des}	3.43	T/m
Pole tip field at E_{des}	0.172	T
QDI2 injection straight (4Q39)		
Number of magnets	2	
Gradient at E_{des}	3.96	T/m
Pole tip field at E_{des}	0.198	T
QFI3 injection straight (6Q60)		
Number of magnets	2	
Gradient at E_{des}	0.86	T/m
Pole tip field at E_{des}	0.069	T
QDI4 injection straight (6Q60)		
Number of magnets	2	
Gradient at E_{des}	2.52	T/m
Pole tip field at E_{des}	0.201	T
QFI5 injection straight (6Q60)		
Number of magnets	2	
Gradient at E_{des}	3.14	T/m
Pole tip field at E_{des}	0.251	T
QD6 interaction straight (4Q39)		
Number of magnets	2	
Gradient at E_{des}	5.16	T/m
Pole tip field at E_{des}	0.258	T
QF7 interaction straight (4Q39)		
Number of magnets	2	
Gradient at E_{des}	4.04	T/m
Pole tip field at E_{des}	0.202	T

TABLE A–12

Main Low Energy Ring Cell Quadrupole Parameters

Parameter	Symbol	Value	Units
Magnet designation		4Q20	
Number of magnets	N_Q	264	
Gradient at E_{des}	G_Q	2.50	T/m
Pole tip field at E_{des}	B_Q	0.1250	T
Gradient length product at E_{des}		1.362	T
Inscribed radius	r_Q	1.968	in
Minimum gap	h_Q	1.457	in
Core length	$L_{\text{core}\,Q}$	20.00	in
Magnetic length	L_Q	21.457	in
Lamination height	$h_{\ell\,Q}$	10.50	in
Lamination width	$w_{\ell\,Q}$	10.50	in
Packing factor (minimum)		98	%
Core weight	$m_{\text{core}\,Q}$	1800	lb
Ampere-turns per pole at E_{des}		2484	A-turns
Turns/pole		37	
Pancakes/pole		1	
Conductor width		0.50	in
Conductor height		0.50	in
Cooling hole diameter		0.25	in
Conductor cross section area		0.197	in^2
Current at E_{des}	I_Q	67	A
Resistance	R_Q	52.60	mΩ
Power at E_{des}	P_Q	0.24	kW
Voltage drop at E_{des}	V_Q	3.53	V
Coil weight	$m_{\text{coil}\,Q}$	151	lb
Number of water circuits		1	
Water flow rate		0.5	gpm
Water pressure drop		150	psi
Temperature rise		1.8	°C

TABLE A–13

Miscellaneous LER Quadrupole Parameters

Parameter	Value	Units
Interaction straight		
Magnet designation	4Q13	
Number of magnets	4	
Gradient at E_{des}	10.34	T/m
Pole tip field at E_{des}	0.517	T
Interaction straight		
Magnet designation	4Q28	
Number of magnets	4	
Gradient at E_{des}	8.98	T/m
Pole tip field at E_{des}	0.449	T
Interaction straight		
Magnet designation	4Q40	
Number of magnets	6	
Gradient at E_{des}	8.98	T/m
Pole tip field at E_{des}	0.449	T
Interaction straight		
Magnet designation	4Q21	
Number of magnets	12	
Gradient at E_{des}	11.35	T/m
Pole tip field at E_{des}	0.568	T
Interaction straight		
Magnet designation	4Q21	
Number of magnets	4	
Gradient at E_{des}	3.41	T/m
Pole tip field at E_{des}	0.171	T
Wiggler straight		
Magnet designation	4Q21	
Number of magnets	6	
Gradient at E_{des}	4.50	T/m
Pole tip field at E_{des}	0.225	T

TABLE A–14

High Energy Ring Sextupole Parameters

Parameter	Value						Units
Magnet designation	4.5S10						
Principal function	D	F	D1	F1	D2	F2	
Number of main sextupoles	56	64	8	4	8	4	
Gradient at E_{des}	73.04	44.67	104.41	66.57	33.61	22.81	T/m^2
Pole tip field at E_{des}	0.131	0.080	0.188	0.120	0.060	0.041	T
Integrated strength @ E_{des}	18.63	11.39	26.63	16.98	8.57	5.817	T/m
Inscribed radius	2.362	2.362	2.362	2.362	2.362	2.362	in
Core length	8.071	8.071	8.071	8.071	8.071	8.071	in
Magnetic length	10.041	10.041	10.041	10.041	10.041	10.041	in
Core weight	170	170	170	170	170	170	lb
Ampere-turns per pole at E_{des}	2081	1273	2974	1896	957	650	A-turns
Turns/pole	24	24	24	24	24	24	
Pancakes/pole	1	1	1	1	1	1	
Conductor width	0.375	0.375	0.375	0.375	0.375	0.375	in
Conductor height	0.375	0.375	0.375	0.375	0.375	0.375	in
Cooling hole diameter	0.125	0.125	0.125	0.125	0.125	0.125	in
Conductor cross section area	0.127	0.127	0.127	0.127	0.127	0.127	in^2
Current at E_{des}	86.7	53.0	123.9	79.0	39.9	27.1	A
Resistance	44.3	44.3	44.3	44.3	44.3	44.3	mΩ
Power at E_{des}	0.33	0.12	0.68	0.28	0.07	0.03	kW
Voltage drop at E_{des}	3.84	2.35	5.48	3.50	1.77	1.20	V
Coil weight	200	200	200	200	200	200	lb
Number of water circuits	2	2	2	2	2	2	
Water flow rate	0.25	0.25	0.25	0.25	0.25	0.25	gpm
Water pressure drop	150	150	150	150	150	150	psi
Temperature rise	5.1	1.9	10.3	4.2	1.1	0.5	°C

TABLE A–15

Low Energy Ring Sextupole Parameters

Parameter	Symbol	Value	Units
Magnet designation		4.5S10	
Number of main sextupoles	N_S	144	
Gradient at E_{des}		36.07	T/m^2
Pole tip field at E_{des}	B_S	0.0650	T
Integrated strength @ E_{des}		9.20	T/m
Inscribed radius		2.362	in
Core length	$L_{core\,S}$	8.071	in
Magnetic length	L_S	10.041	in
Core weight	$m_{core\,S}$	170	lb
Ampere-turns per pole at E_{des}		1027.6	A-turns
Turns/pole		24	
Pancakes/pole		2	
Conductor width		0.375	in
Conductor height		0.375	in
Cooling hole diameter		0.125	in
Conductor cross section area		0.127	in^2
Current at E_{des}	I_S	42.8	A
Resistance	R_S	62.0	mΩ
Power at E_{des}	P_S	0.11	kW
Voltage drop at E_{des}	V_S	2.65	V
Coil weight	$m_{coil\,S}$	200	lb
Number of water circuits		2	
Water flow rate		0.25	gpm
Water pressure drop		150	psi
Temperature rise		1.8	°C

TABLE A–16

IR Permanent Magnet Parameters

Parameter	Symbol	Value	Units
Magnetic material	Sm_2Co_{17} – R26HS		
Remanent field	B_r	1.050	T
Temperature dependence	$\frac{dB_r}{dT}$	−0.03	$\%/°C$
Curie point	T_C	1093	K
Density	ρ	8.4	g/cm^3

B1 H: First separation dipole			
Parameter	Symbol	Value	Units
Field at E_{des}	B_{B1}	0.750	T
Length	L_{B1}	0.160	m
Inner diameter	ID_{B1}	0.048	m
Outer diameter	OD_{B1}	0.106	m
Magnet weight	W_{B1}	21	lb
Trim range (air core coil)		±4	%

IR Permanent magnet quadrupoles					
Parameter	Symbol	Value			Units
Function		Q1 D	Q2 F	Q3 D	
Gradient at E_{des}	G_Q	38.84	30.70	14.04	T/m
Pole tip field at E_{des}	B_Q	1.474	1.351	0.969	T
Length	L_Q	0.642	0.516	0.240	m
Inner diameter	ID_Q	0.076	0.088	0.138	m
Outer diameter	OD_Q	0.302	0.280	0.272	m
Magnet weight	W_Q	798	530	192	lb
Trim range (air core coil)		±4	±4	±4	%

TABLE A–17

IR Septum Quadrupole (Q4)

Parameter	Symbol	High energy beam	Low energy beam	Units
Technology	superconducting			
Number of magnets	N_{Q4}	2		
Distance from IP	d_{Q4}	3.960		m
Beam-beam separation at d_{Q4}		6.46		cm
Magnetic length	L_{Q4}	0.80		m
Gradient	G_{Q4}	15.18		T/m
Bore tube inner radius		4.5	2.5	cm
Beam offset in tube		1.9	0.0	cm

TABLE A-18

Wiggler Parameters (Low energy ring)

Parameter	Symbol	Value	Units
Number of wiggler arrays	N_W	2	
Wiggle plane	Horizontal		
Total length of wigglers	L_W	48	m
Energy loss/turn at E_{des}	$U_{0,W}$	0.95	MeV
Wiggler segments per array	N_S	4	
Segment length	L_S	6	m
Dipole length		0.20	m
Dipole field	B_W	1.63	T
Drift space		0.133	m
Fill factor		60	%
Effective wiggler period		0.666	m

TABLE A–19
Injection Parameters

Parameter	Symbol	High energy ring	Low energy ring	Units
Injection energy	E	9.000	3.109	GeV
Injection energy range		8–10	2.8–4	GeV
Number of populated bunches	n_b	1658	1658	
Number of empty bunches	n_b(gap)	88	88	
Bunch spacing	t_b	4.202		ns
Revolution frequency	f_0	136.312	136.312	kHz
Circulating current	I	1.479	2.140	A
Number of particles/bunch	N_b	4.084×10^{10}	5.911×10^{10}	
Horizontal emittance	ϵ_x	48.24	96.48	nm−rad
Horizontal damping time	τ_x	37.2	36.5	ms
Linac repetition rate		60 or 120		s^{-1}
Linac current ($e^{\pm}$/bunch/pulse)		$(0.2 - 1.0) \times 10^{10}$		
Linac invariant emittance	$\epsilon_{N\,\mathrm{linac}}$	5.0×10^{-5}		m–rad
Ring kicker pulse length	t_{kick}	≤ 1500		ns
Injection top-off time from 80%		3.0		min
Injection time from zero		6.0		min
Magnet standardization time		15		min
Fractional energy tolerance	$\delta E/E$	0.002		
Injection timing tolerance	δt	100		ps
Injection transverse tolerance	δr	10.0		mm

TABLE A–20

Linac Bypass Lines

Parameter	Electron	Positron	Units
Energy range	8–10	2.8–4	GeV
Linac exit sector	7	3	
Bypass line length	2.2	2.6	km
Extraction plane (from vertical)	35	51	deg
e^+ extraction H magnet bend	–	1.25	deg
e^- extraction pulsed magnets	2	–	
Total bend angle	0.55	–	deg
Matching quadrupoles	24	24	
Bypass drift quadrupoles	44	52	
Pole tip field	1.0	0.4	T
Bore	1.085	1.085	in
Spacing	50	50	m
Steering correctors	56	64	
Beam position monitors	56	64	
Readouts	28	32	
Profile monitors	2	2	
Bypass drift ion pumps	23	29	
Pump capacity	120	120	L/s

TABLE A–21

Parameters Relevant to Experiment Design

Parameter	Symbol	High energy ring	Low energy ring	Units
Horizontal spot size at IP	σ_x^*	190	190	μm
Vertical spot size at IP	σ_y^*	7.6	7.6	μm
Natural bunch length	σ_ℓ	1.00	1.00	cm
Beam cross half-angle	θ_x	0.0		mrad
Natural energy spread	σ_E	5.50	2.97	MeV
Natural CM energy spread	$\sigma_{E_{\rm c.m.}}$	5.992		MeV
Beam pipe inner radius at IP	r^*	2.50		cm
IP to first magnet distance	d_f	0.200		m
Detector solenoid field	$B_{\rm sol}$	1.00		T
Detector solenoid length	$L_{\rm sol}$	4.00		m
Beam pipe thickness	$X_{0;\rm pipe}$	0.0053		X_0
Support tube ID	$\rm ID_{tube}$	31.19		cm
Support tube OD	$\rm OD_{tube}$	35.00		cm
Support tube thickness at IP	$X_{0;\rm tube}$	0.0047		X_0
Support tube length	$\rm L_{tube}$	4.35		m
Minimum acceptance angle	$\theta_{\rm min}$	0.300	0.300	rad
cos(min. acceptance angle in C.M.)	$\cos\theta^*_{\rm min}$	0.876	0.984	

APPENDIX B:
FUTURE UPGRADES

B.1 FUTURE LUMINOSITY IMPROVEMENTS

Increasing the luminosity of the B Factory over the lifetime of the machine is a highly desirable goal, and the machine design is such that future upgrades can be accommodated. However, the factors limiting the luminosity are difficult to predict so far ahead, so it is important that the machine be designed with sufficient flexibility to maximize its performance under a variety of operating conditions.

In its simplest form (see Section 4.4) the luminosity can be written as:

$$\mathscr{L} = 2.17 \times 10^{34} (1 + r) \xi \left(\frac{IE}{\beta_y^*} \right)_{+,-} \qquad \text{(B-1)}$$

where I is the total current (in A), E is the beam energy (in GeV), and β_y^* is the vertical beta function (in cm). In this equation, most of the parameters are limited by other effects and allow little possibility for improving the luminosity. This was discussed in Chapter 3.

The minimum beta value at the interaction point (IP) is limited by chromatic aberrations, and it seems unlikely that a considerable improvement can be obtained over the values reached in other storage rings. The vertical beta values are also bounded by the bunch length, so a value less than about 1 cm seems unlikely. Should it prove possible to reduce the beta functions at the IP, most of the other parameters of the machine would be unaffected. The major impact would be on the background, owing to the increased angular divergence. If it can be shown that the machine can operate well with the decreased beta values, it is probable that a new masking scheme would need to be installed, profiting from the operational experience acquired.

If the beam-beam tune shift is higher than 0.03 in the vertical dimension, a common occurrence in many storage rings, the vertical beam height can be reduced by lowering the coupling with the installed skew quadrupoles. In this case, the luminosity will increase in proportion to $\xi_y^{1/2}$. It is therefore important to design the interaction region for a conservative value of the emittance ratio, to be certain that higher vertical tune shifts can be fully exploited. We have taken a ratio of 25:1 for the nominal design, comfortably below the 40:1 routinely attained in PEP.

If the beam-beam tune shift were higher than 0.03 in both planes (as it always is in PEP), then the emittance will need to be reduced or the number of bunches decreased for the same total current. In this case, the luminosity will increase as $\xi_y^{1/2}\xi_x^{1/2}$. If the same bunch spacing is maintained, and if the beam-beam tune shift were 0.06 in each beam in each plane—a factor of two above nominal, but a value that has been regularly obtained in PEP at higher energies—then the uncoupled horizontal emittance required is 25 nm·rad in the HER and 50 nm·rad in the LER. These values would require increasing the phase

advance per cell in the HER, for which there is sufficient flexibility, and reducing the dispersion in the LER wiggler sections, again a straightforward operation. If the bunch spacing were halved, the bunch current would double while the emittance could remain at the nominal value. The bunch current would still remain below the turbulent bunch lengthening threshold.

B.1.1 Increased Current Scenarios

The currents are limited by the amount of RF power available and by the ability to absorb the synchrotron radiation produced. The B Factory has been designed for maximum currents of 3 A in each ring. Although this capability will not be available initially, all distributed components that would be difficult to upgrade without complete replacement will be designed for the eventual maximum current. Those components that can be upgraded easily are designed for the nominal currents.

Components and systems that are already dimensioned for the maximum current include

- The radiation shielding
- The vacuum chambers of both rings
- The LCW cooling water distribution system in the tunnel

Components that would require upgrading or replacing to go to higher currents are discussed below.

B.1.1.1 RF System. The number of RF modules will be increased to a total of 22 in the two rings. This would require an increase in the site electrical power and an extension of one of the RF support buildings. The RF parameters for this case are shown in Table B-1. Because of the modularity of the system, practically all the installed RF components will accept the higher currents without modification. The main exception is that the higher-order-mode losses in the cavities are proportional to the square of the current, so the loads in the damping waveguides may need upgrading.

B.1.1.2 Vacuum Chamber Pumping. Additional pump ports are provided on the chambers so that additional lumped vacuum pumps can be added as necessary. The exact requirements will depend critically on the long-term beam conditioning of the chambers, which is very difficult to predict.

B.1.1.3 Electrical Power Distribution System. Additional feeders must be run to IR-12, where the new RF stations would be installed. The existing duct banks have spare space for these feeders, so no new civil engineering will be required.

Table B-1. Upgraded RF system parameters.

	HER	LER
Frequency [MHz]	476.0	476.0
Harmonic number	3492	3492
Maximum circulating current [A]	3.0	3.0
Number of klystrons	15	7
Power per klystron [MW]	1.0	1.0
Number of cavities	30	14
Shunt impedance per cavity [MΩ]	3.5	3.5
Total shunt impedance [MΩ]	105	49
Field gradient [MeV/m]	2.8	3.0
Synchrotron radiation loss per turn [MeV]	3.58	1.24
HOM energy loss per turn [MeV]	0.79	0.64
Peak cavity voltage [MV]	18.5	9.5
Total RF power [MW]	15.0	7.0
Fundamental cavity dissipation [MW]	1.6	0.9
Synchrotron radiation loss [MW]	10.8	3.7
Power loss to parasitic modes [MW]	2.4	1.9

B.1.1.4 Cooling Capacity. The capacity of the cooling tower would need to be increased by the addition of another cell to the present tower. The existing headers for the cooling tower water are capable of carrying the extra water, but an additional pump would be needed. At IR-12, an additional heat exchanger would be needed, but the other required changes are relatively minor, as the existing low-conductivity water headers can take the increased flow.

B.1.1.5 Collimators and Scrapers. The masking scheme will probably require modification in the light of operational experience (this has been the case with practically every detector ever installed on a collider). Therefore, the masks and collimators are only dimensioned for the nominal current and would be replaced or upgraded as necessary.

B.1.1.6 Feedback Systems. It is likely that the feedback system will need upgrading. The exact requirements will only be determined as the performance limitations of the system become understood. Since the present design is modular, there would be no problem in upgrading the power. If the number of bunches were to be increased, then the rise time of the system might be insufficient and the front-end might need improvements. There is every reason to believe that the faster low-level electronics required for this purpose would be available at the appropriate time. Indeed, similar systems for a 500-MHz bunch repetition rate are now being designed for the ALS.

B.1.2 Exploiting Increased Current

There are three different scenarios for exploiting the increased current, and flexibility is provided for all three. The easiest of the three follows if the tune shift can be increased above the nominal value adopted. In this case, no other changes would be required. The second alternative is to increase the emittance. The vacuum chambers have been dimensioned to accept twice the nominal emittance (that is, to accommodate 100 nm·rad in the HER and 200 nm·rad in the LER), and the techniques for increasing the emittance have already been discussed in Section 4.1. The interaction region masking would need modifying, as discussed above. The final alternative is to increase the number of bunches. This would require an upgrade of the feedback system and, more importantly, would require modifying the interaction region layout. The most likely configuration would be the crab-crossing scheme, which is discussed in Section B.2 of this appendix.

B.1.3 Summary

The design of the B Factory presented in this document incorporates considerable flexibility, which would allow future upgrades of luminosity. Where necessary, provision has been made for the increase in current that will become possible when resources are available for upgrading the RF system and associated services.

B.2 CRAB CROSSING

The present B Factory lattice (see Section 4.1), with head-on collisions, is designed to avoid the excitation of synchrobetatron resonances, which result when beams collide with a nonzero crossing angle [Piwinski, 1977]. However, the use of a head-on collision scheme requires us to deal with the following issues:

- The two beams must go through common magnetic elements near the interaction region (IR); designing masks to shield the detector from the synchrotron radiation produced by the beams passing through these magnetic elements is difficult.
- The longitudinal spacing of the bunches must be chosen such that the transverse separation of the beams away from the interaction point (IP) is sufficient to reduce the long-range beam-beam effect between bunches in the opposing beams; this limits the total number of beam bunches in each ring.

For the design luminosity of 3×10^{33} cm^{-2} s^{-1}, satisfactory solutions have been found for these problems. However, to upgrade the luminosity to significantly higher values, solutions of this type become ever more difficult to obtain.

A configuration that utilizes a crossing angle would allow the longitudinal spacing between bunches to be reduced and would reduce the problem of lost particles from elsewhere in the ring being swept into the detector beam pipe by the separation dipoles (required for head-on collisions) near the IP. Either or both of these advantages may be necessary for a luminosity upgrade. Fortunately, a new idea, the so-called "crab crossing" scheme, allows a nonzero crossing angle at the collision point while avoiding the excitation of synchrobetatron resonances. In this scheme, shown schematically in Fig. B-1, the bunches still collide head-on, but in a transversely moving reference frame.

The bunches are tilted before the collision by an angle equal to half of the total crossing angle and then tilted back to their original direction after collision. Figure B-2 shows a layout of an IR with a crab-crossing configuration. Because we anticipate modifying the head-on crossing to a crab-crossing layout as a machine upgrade, great

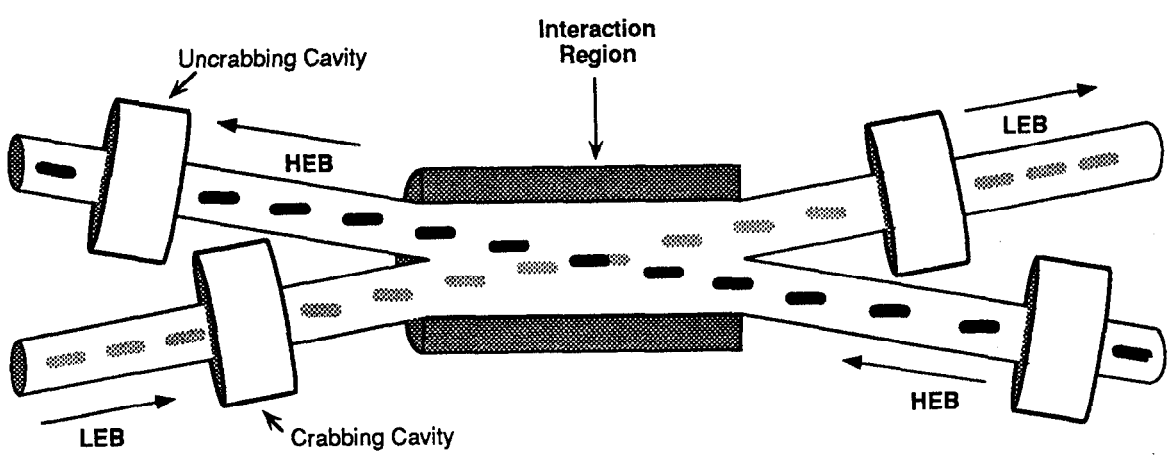

Fig. B-1. Schematic of crab-crossing concept.

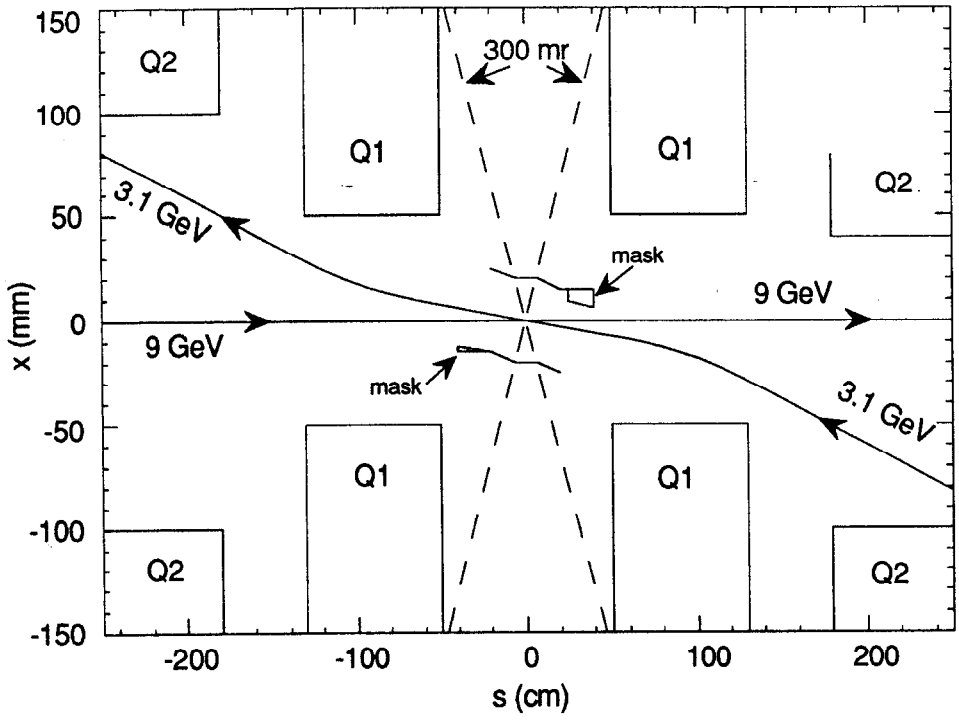

Fig. B-2. Example of a crab-crossing geometry. The total synchrotron power for this geometry, 7.1 kW, is much lower than for the head-on crossing design described in Chapter 4.

care has been taken in all the design choices to ensure the greatest possible compatibility between the two configurations. For example, one of the reasons for the selection of the S-bend geometry of the head-on crossing was that it can be easily converted into a crab-crossing layout. A comparison of the synchrotron radiation power for the head-on and crab-crossing collision scenarios is given in Table B-2. The total synchrotron power is more than an order of magnitude lower in the case of the crab crossing, as might be expected from the discussion above. This is the prime reason for the interest in pursuing this direction.

Crab crossing with transversely deflecting cavities was first proposed as a way to increase the luminosity in linear colliders [Palmer, 1988] and was subsequently proposed for storage rings [Oide and Yokoya, 1989] to suppress synchrobetatron resonances. For the storage ring case, this scheme requires transversely deflecting cavities at locations of $\pm 90°$ in betatron phase advance away from the IP. The crab-crossing scheme has not yet been tested, and it is difficult to estimate how successful it will ultimately turn out to be. In particular, the tolerances on the various elements used for crab crossing need to be studied both theoretically and experimentally, and the effect on the feedback system to combat coupled-bunch instabilities (due to the additional impedance of the crab cavities) must be assessed. In this section, we report on computer simulations that have been used to address some of the tolerance issues.

There is a second method to produce a tilt of the bunches at the IP that uses *longitudinally* accelerating cavities in a region with a large dispersion [Jackson, 1990]. In

Table B-2. Comparison of synchrotron radiation power near the IP for a head-on and a nonzero-crossing-angle geometry.

Magnet	Fan power from head-on design (kW)	Fan power from crossing angle design (kW)
LEB:		
Upstream Q3	0.84	0.0
Upstream Q1	0.83	3.53
Upstream B1	2.39	—
Downstream B1	2.39	—
Downstream Q1	0.96	3.53
Downstream Q3	0.91	0.0
Subtotal	8.3	7.1
HEB:		
Upstream Q2	28.3	0.0
Upstream Q1	2.3	0.0
Upstream B1	13.8	—
Downstream B1	13.8	—
Downstream Q1	1.1	0.0
Downstream Q2	26.1	0.0
Subtotal	85.4	0.0
Total	93.7	7.1

this case, the phase of the dispersion must satisfy the condition that the derivative of $D_x/\sqrt{\beta_x}$ vanish at a distance of 180° from the IP [Piwinski, 1991]. The position of the cavity is then arbitrary within the straight section, and one can use several cavities distributed over a larger region of betatron phase.

A disadvantage of the longitudinal crab-crossing scheme is that the required longitudinal gradient is larger by an order of magnitude than that needed for the transverse case. The longitudinal and transverse gradients differ by a factor of $\sqrt{\beta_{xct}\beta_{xl}}/D_{xl}$, where D_{xl} is the dispersion at a position where the above-mentioned derivative vanishes, and t and l refer to the transverse and longitudinal cases, respectively. There would be potential advantages to this scheme if the acceleration cavities could be used for the compensation. On the other hand, the disadvantage of a coupling between synchrotron and betatron oscillations is then still present in the longitudinal scheme, due to the large dispersion at the accelerating cavities (which cannot be compensated completely and which can excite all satellite resonances of the integer). Insofar as a solution to this problem is not clear, we focus here on the more commonly considered transversely deflecting cavities.

B.2.1 Simulation Studies

In the double-ring DORIS-I, it was found that a crossing angle excites synchrobetatron resonances that are characterized by

$$k\nu_\beta + m\nu_s = n \tag{B-2}$$

where k, m, and n are integers, and ν_β and ν_s are the betatron tune (in the plane of the crossing angle) and the synchrotron tune, respectively. These resonances are spread over the whole tune diagram and cause beam loss [Piwinski, 1977]. With a crab-crossing scheme, the synchrobetatron coupling vanishes completely. The horizontal kick $\delta x_c'$ given to a particle in a crab cavity must be proportional to its longitudinal position s. The kick causes a displacement at the IP given by

$$\delta x^* = \delta x_c' \sqrt{\beta_{xc}\beta_x^*} \tag{B-3}$$

where β_{xc} and β_x^* are the betatron functions at the crab cavity and at the IP, respectively. The tilt angle $\delta x^*/s$ must be equal to half the crossing angle ϕ in order to get parallel bunches at the IP. The amplitude of the required sinusoidally varying transverse kick is then given by

$$A_{\delta x'} = \frac{\phi\lambda}{2\pi\sqrt{\beta_{xc}\beta_x^*}} \tag{B-4}$$

where λ is the wavelength of the transverse crab-cavity voltage waveform; this should not be smaller than the wavelength of the accelerating voltage in order to avoid deviations from a linear tilt [Piwinski, 1990]. With β_{xc} = 15 m (15 m), β_x^* = 75 cm (37.5 cm), and λ = 63 cm, one obtains a maximum transverse momentum change of 3.6 MeV (1.8 MeV) per cavity for the HER (LER).

Because crab crossing has not yet been verified in an existing storage ring it was initially studied by means of computer simulations for round beams [Piwinski, 1990]. In particular, errors in the strength of the crab cavities and in the betatron phase advance between the cavities and the IP were simulated in order to determine the tolerances for these parameters. Numerical estimates were also made by Kheifets et al. [1989]. For the upgraded B Factory, we have carried out simulations for flat beams with an aspect ratio of 25:1. The coordinate changes due to the crab cavity were calculated from

$$\delta x' = \frac{x\phi\Delta V}{\sqrt{\beta_{xc}\beta_x^*}} \tag{B-5}$$

$$\frac{\delta E}{E} = \frac{x\phi\Delta V}{\sqrt{\beta_{xc}\beta_x^*}} \tag{B-6}$$

where $\Delta V = V/V_0 \neq 1$ describes the deviation from the correct value. The changes of the betatron angles, and of the energy, due to the beam-beam interaction are given by

$$\delta x' = 4\pi\xi_x f_x(x + s\phi, y) \tag{B-7}$$

$$\delta y' = 4\pi\xi_y f_y(x + s\phi, y) \tag{B-8}$$

$$\delta E = \phi E \delta x' \tag{B-9}$$

where ξ_x and ξ_y are the beam-beam space-charge parameters and the functions f_x and f_y are integrals that cannot be expressed by elementary functions but are solved numerically, tabulated, and interpolated linearly for each passage of a particle. As in the rest of the ring, the coordinates between the crab cavities and the IP are transformed linearly. Quantum fluctuations and damping are neglected, because the rise times on a resonance are typically shorter than the damping time. Also, the betatron phase variation seen by a particle due to its longitudinal motion is neglected; that is, it is assumed that the ratio σ_ℓ/β_x^* is small (it is 0.013 and 0.027 for the HER and LER, respectively). This is the worst case, because, for a greater bunch length, the space-charge forces are distributed over a larger betatron phase and the excitation of higher-order resonances will be partially suppressed [Sagan et al., 1990]. Most of the simulations were done for 3000 revolutions and with 98 particles. The synchrotron tune ν_s is 0.06, and ν_y (which has no influence on the horizontal synchrobetatron resonances) is 0.23. The total crossing angle is $2\phi = 15$ mrad, and the normalized crossing angle ϕ (σ_ℓ/σ_x) is 0.41.

As measurements with DORIS-I and our simulations have shown, the incoherent resonances described by Eq. B-2 influence mainly the beam lifetime and not the beam size and the luminosity. For this reason, many of the present simulations were done for large amplitudes, $6\sigma_x$ and $6\sigma_\ell$. Particles at these amplitudes must remain stable in order to obtain sufficient lifetime. Figure B-3 shows the increase of the horizontal amplitude as a function of the horizontal betatron tune. For perfect compensation (lower curve) the synchrobetatron resonances vanish completely. The remaining resonances are the quarter-integer resonance and some others that are excited by the nonlinear beam-beam forces.

Figure B-3 also shows that there are some tune regions that give a relatively small increase of amplitude, for example, that between 0.03 and 0.05. Particles in these tune regions will not be lost if the aperture of the ring is larger than $8\sigma_x$.

Figure B-4 shows, in contrast to Fig. B-3, that the beam size, that is, the rms value of 1200 particles having an initially Gaussian distribution, does not blow up at many resonances. Only at the first satellite of the integer and the two lowest satellites of the

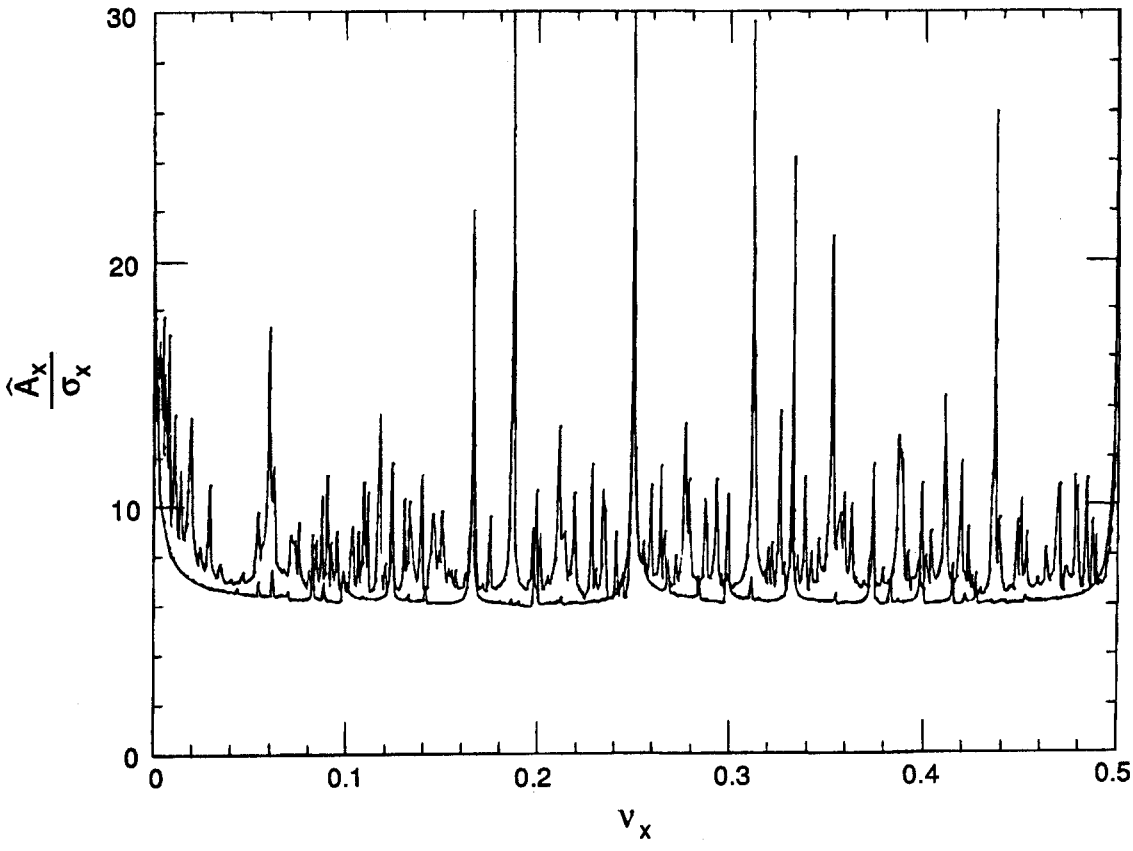

Fig. B-3. Increase of horizontal amplitude as a function of the horizontal betatron tune.

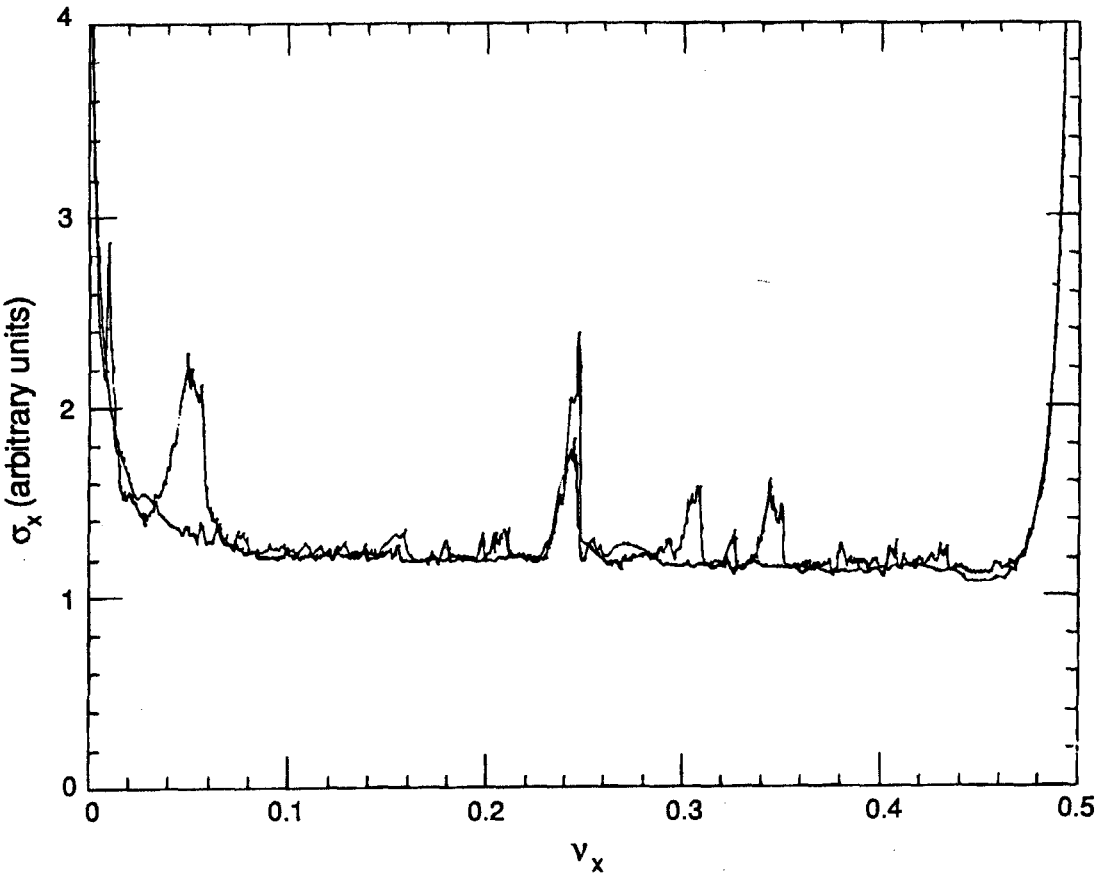

Fig. B-4. The rms value of 120 particles (having an initially Gaussian distribution) vs horizontal tune.

third-order resonance, $\nu_x = (1 \pm \nu_s)/3$ does the beam size increase noticeably. The reason for this behavior is that there are always particles with increasing amplitude and those with decreasing amplitude, depending on the phase between betatron and synchrotron oscillations. For small excitations, the increase and the decrease tend to compensate each other.

Figure B-5 shows the dependence of the maximum amplitude on the voltage error $\Delta V = V/V_0$, at the resonance $3\nu_x - \nu_s = 1$. It was assumed in this calculation that both cavities have the same error, in which case there is a residual angle at the IP whose value is equal to the crossing angle times the relative voltage error. If only one cavity has an error, the residual angle is smaller [Piwinski, 1990], but in this case, a tilt (on the order of the crossing angle times the relative error) will oscillate around the ring. The initial amplitudes for the two curves in Fig. B-5 are $3\sigma_x$ and $6\sigma_x$, respectively. Not surprisingly, the simulation shows that the dependence on the voltage error is stronger for the larger amplitude.

The dependence on phase errors between cavity and IP is shown in Fig. B-6. Here again, equal errors on both sides of the IP was assumed. If the two cavities have position errors, the beams will not only cross at a small angle, but a small tilt angle will also oscillate around the ring. In principle, the error of the tilt at the IP can be compensated by varying the strength of the two cavities; this, however, increases the oscillation of the tilt

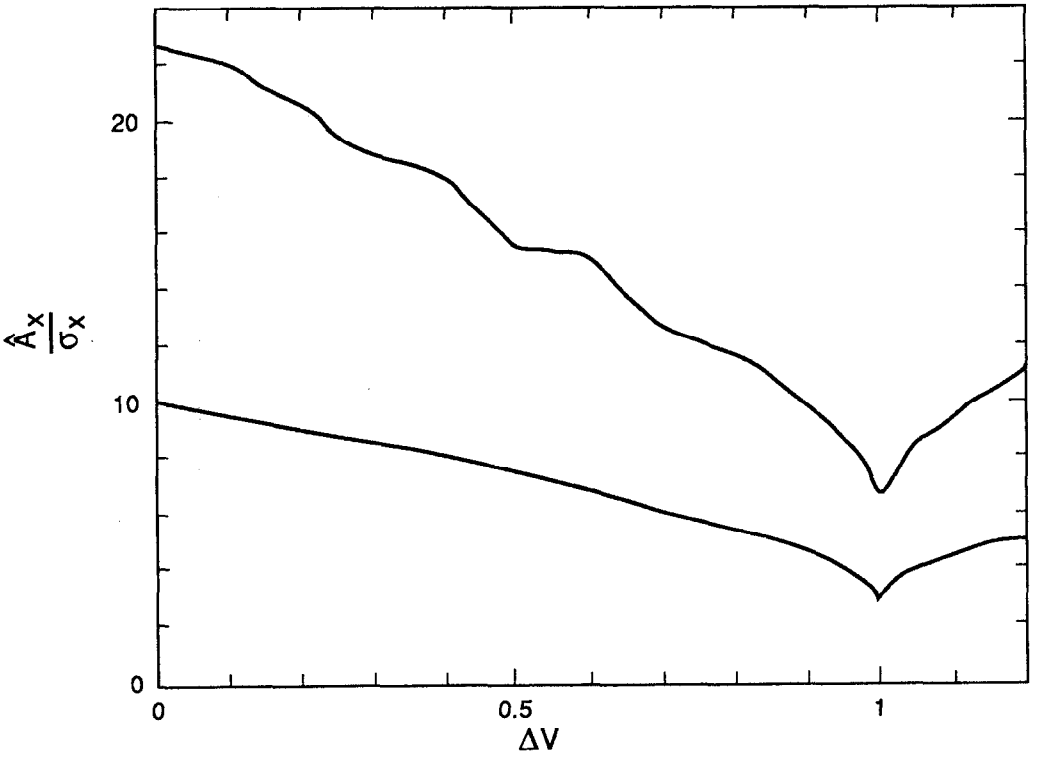

Fig. B-5. Dependence of the maximum amplitude on the voltage error $\Delta V = V/V_0$, at the resonance $3\nu_x - \nu_s = 1$.

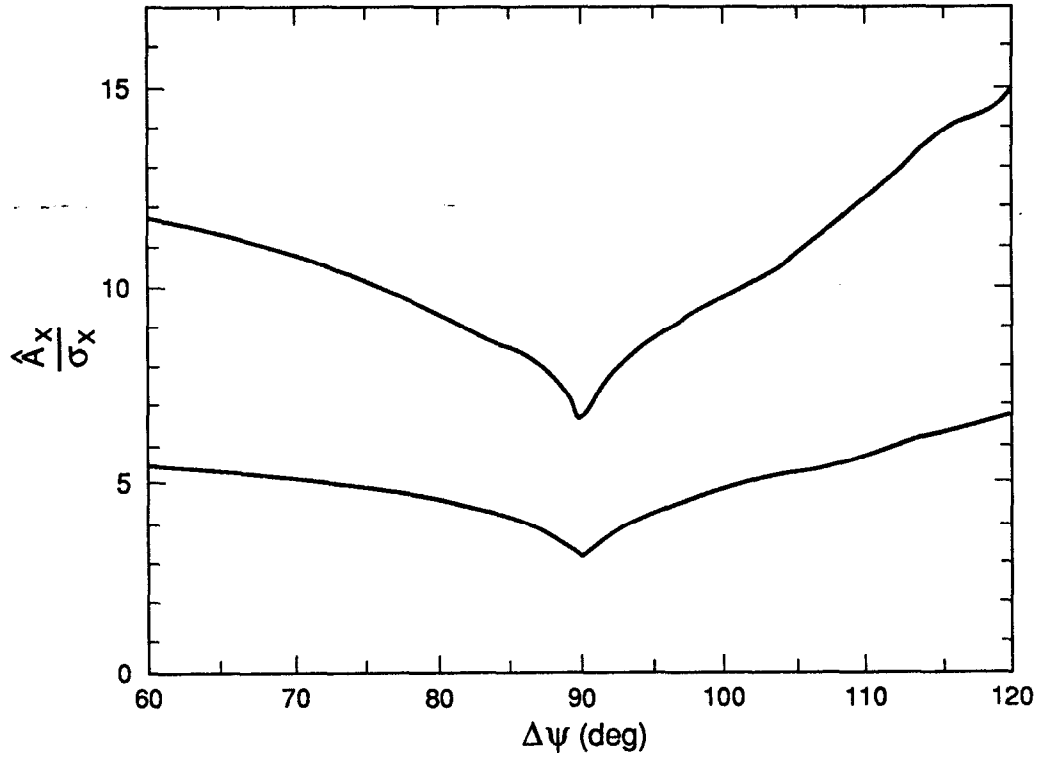

Fig. B-6. Dependence of maximum amplitude on phase errors between crab cavity and IP.

around the ring. Table B-3 shows the tolerable errors of the cavity strength and the phase advance for two synchrobetatron resonances.

Close to the second resonance, $\nu_x = (1 + 2\nu_s)/6 = 0.1866$, there are a number of other resonances, $\nu_x = (1 - \nu_s)/5 = 0.1880$, $\nu_x = (1 + 5\nu_s)/7 = 0.1857$, $\nu_x = 1/8 + \nu_s = 0.1850$, as well as some higher-order resonances. At those frequencies where several resonances are very close to each other, it is difficult to compensate them; these few frequencies must be avoided.

Phase errors of the crab voltage produce orbit displacements of the whole bunch around the ring with an amplitude

$$\Delta x = (\lambda/2\pi)\sqrt{\frac{\beta_{xc}\beta_x^*}{2\sin \pi\nu_x}}(dx'/ds)\,\Delta\psi \qquad \text{(B-10)}$$

At the IP, the displacement is given by $(\lambda/4\pi)\phi\,\Delta\psi$ if the voltage in only one cavity has a phase error $\Delta\psi$. To keep the displacement smaller than $\sigma_x^*/10$, $\Delta\psi$ must be smaller than 2.8°.

Table B-3. Increase of amplitudes for different errors of the cavity voltage $\Delta V = V/V_0$ and the phase advance $\Delta\psi$ on two resonances: (a) $3\nu_x - \nu_s = 1$, and (b) $6\nu_x - 2\nu_s = 1$.

$\Delta\hat{x}$	(a)	(b)	(a)	(b)	(a)	(b)
	10%		50%		100%	
ΔV [%]	2.5	0.5	11	4	35	10
$\Delta\psi$ [deg]	1.5	0.4	2.5	1.5	25	2.5

Dispersion in a crab cavity can give an additional synchrobetatron coupling if it is produced by an error between the crab cavities. If the dispersion is produced outside the crab cavity region, the kicks in the two cavities will compensate each other (because the dispersion oscillates with the betatron phase advance). If a bend between the cavities produces a dispersion of a few centimeters, its effect must be compared with that from the dispersion in the main accelerating cavities (where a spurious dispersion of a few centimeters usually cannot be avoided). Because the synchrobetatron resonance excitation is approximately proportional to the dispersion and to the voltage gradient [Piwinski and Wrulich, 1976], the excitation in the accelerating cavities will be larger than that in the crab cavities by an order of magnitude. In either case, the first satellite of the integer must be avoided.

B.2.2 Summary

The excitation of synchrobetatron resonances causes mainly a reduction in beam lifetime, but it does not generally give rise to beam size blowup or to a loss in luminosity. Three parameters are important: The lifetime is determined by the normalized crossing angle $\phi(\sigma_\ell/\sigma_x)$, by the beam-beam space charge parameter ξ_x, and by the physical aperture or the dynamical acceptance of the ring. If the first two parameters are not too large ($\phi\sigma_l/\sigma_x \leq 0.5$, $\xi_x \leq 0.03$), and if the acceptance is large enough ($A_x > 15\sigma_x$), it should be possible to avoid beam loss from almost all synchrobetatron resonances with reasonable tolerances for the crab cavities. For some very limited regions in the tune diagram, it may even be possible to operate the machine with a nonzero crossing angle *without* crab cavities. However, more studies must be done for this last possibility to ensure its viability.

☆ U.S. GOVERNMENT PRINTING OFFICE 1991-586-603 991-586-603